A theory of genetic analysis using transcriptomic phenotypes

Thesis by
David Angeles-Albores

In Partial Fulfillment of the Requirements for the
degree of
Doctor of Philosophy

CALIFORNIA INSTITUTE OF TECHNOLOGY
Pasadena, California

[Year Degree Conferred]
Defended [Exact Date]

David Angeles-Albores
ORCID: 0000–0001–5497–8264

ACKNOWLEDGEMENTS

[Add acknowledgements here. If you do not wish to add any to your thesis, you may simply add a blank titled Acknowledgements page.]

ABSTRACT

[This abstract must provide a succinct and informative condensation of your work. Candidates are welcome to prepare a lengthier abstract for inclusion in the dissertation, and provide a shorter one in the CaltechTHESIS record.]

PUBLISHED CONTENT AND CONTRIBUTIONS

[Include a bibliography of published articles or other material that are included as part of the thesis. Describe your role with the each article and its contents. Citations must include DOIs or publisher URLs if available electronically.

If you are incorporating any third-party material in the thesis, including works that you have authored/co-authored but for which you have transferred copyright, you must indicate that permission has been secured to use the material. For example: "Fig. 2 reprinted with permission from the copyright holder, holder name"

Add the option `iknowwhattodo` to this environment to dismiss this message.]

Cahn, J. K. B., A. Baumschlager, et al. (2016). "Mutations in adenine-binding pockets enhance catalytic properties of NAD (P) H-dependent enzymes". In: *Protein Engineering Design and Selection* 19.1, pp. 31–38. DOI: 10.1093/protein/gzv057.
J.K.B.C participated in the conception of the project, solved and analyzed the crystal structures, prepared the data, and participated in the writing of the manuscript.

Cahn, J. K. B., S. Brinkmann-Chen, et al. (2015). "Cofactor specificity motifs and the induced fit mechanism in class I ketol-acid reductoisomerases". In: *Biochemical Journal* 468.3, pp. 475–484. DOI: 10.1042/BJ20150183.
J.K.B.C participated in the conception of the project, solved and analyzed the crystal structures, prepared the data, and participated in the writing of the manuscript.

TABLE OF CONTENTS

Acknowledgements . . . iii
Abstract . . . iv
Published Content and Contributions . . . v
Table of Contents . . . vi
List of Illustrations . . . vii
List of Tables . . . xvii
Nomenclature . . . xviii
Chapter I: Introduction . . . 1
Chapter II: Genetic analysis of a metazoan pathway using transcriptomic phenotypes . . . 2
Chapter III: Transcriptomic description of an endogenous female state in *C. elegans* . . . 41
Chapter IV: Understanding the SynMuv phenotype from a transcriptomic perspective . . . 62
Chapter V: Qualitative or quantitative allelic series . . . 63
Chapter VI: A study of dosage response in *C. elegans* using transcriptome profiling . . . 64
Chapter VII: Structural genes have transcriptional consequences . . . 65
Chapter VIII: Genetic analysis of a pathway using transcriptomic trans-phenotypes . . . 66
Chapter IX: Tissue enrichment analysis for *C. elegans* genomics . . . 67
Chapter X: Phenotype and gene ontology enrichment as guides for disease modeling in *C. elegans* . . . 87
Chapter XI: An automated framework for transcriptional profiling . . . 108
Appendix A: Questionnaire . . . 109
Appendix B: Consent Form . . . 110

LIST OF ILLUSTRATIONS

Number *Page*

2.1 Genetic and biochemical representation of the hypoxia pathway in *C. elegans*. Red arrows are arrows that lead to inhibition of HIF-1, and blue arrows are arrows that increase HIF-1 activity or are the result of HIF-1 activity. EGL-9 is known to exert *vhl-1*-dependent and independent repression on HIF-1 as shown in the genetic diagram. The *vhl-1*-independent repression of HIF-1 by EGL-9 is denoted by a dashed line and is not dependent on the hydroxylating activity of EGL-9. Technically, RHY-1 inhibits CYSL-1, which in turn inhibits EGL-9, but this interaction was abbreviated in the genetic diagram for clarity. 5

2.2 Principal component analysis of various *C. elegans* mutants. Genotypes that have an activated hypoxia response (*i.e*, *egl-9(lf)*, *vhl-1(lf)*, and *rhy-1(lf)*) cluster far from *hif-1(lf)*. *hif-1(lf)* clusters with the suppressed *egl-9(lf) hif-1(lf)* double mutant. The *fog-2(lf)* transcriptome, used as an outgroup, is far away from either cluster. 8

2.3 Strong transcriptional correlations can be identified between genes that share a positive regulatory connection. We took the *egl-9(lf)* and the *rhy-1(lf)* transcriptomes, identified differentially expressed genes common to both transcriptomes and ranked each gene according to its differential expression coefficient β. We plotted the rank of each gene in *rhy-1(lf)* versus the rank of the same gene in the *egl-9(lf)* transcriptome. The result is an almost perfect correlation. Green, transparent large points mark inliers to the primary regressions (blue lines); red squares mark outliers to the primary regressions. 9

2.4 **A**. Heatmap showing pairwise regression values between all single mutants. **B**. Correlation network drawn from **A**. Edge width is proportional to the logarithm of the magnitude of the weighted correlation between two nodes divided by absolute value of the weighted correlation value of smallest magnitude. Edges are also colored according to the heatmap in **A**. Inhibitors of *hif-1* are tightly correlated and form a control module; *hif-1* is positively correlated to its inhibitors, albeit weakly; and *fog-2*, a gene that is not reported to interact with the hypoxia pathway, has the smallest, negative correlation to any gene. . 10

2.5 **Top**: Observed β values of select genes. We selected four genes (*rhy-1*, *egl-9*, *nhr-57* and *lam-3*, shown on the x-axis) and plotted their regression coefficients, β, as measured for every genotype (represented by one of six colors) to study the epistatic relationships between each gene. Asterisks above a bar represent a regression coefficient statistically significantly different from 0 ($q < 10^{-1}$) relative to a wild-type control. Error bars show standard error of the mean value of β. *nhr-57* is an expression reporter that has been used previously to identify *hif-1* regulators (Shen, Shao, and Powell-Coffman, 2006; Shao, Zhang, and Powell-Coffman, 2009). *lam-3* is shown here as a negative control that should not be altered by mutations in this pathway. We measured modest increases in the levels of *rhy-1* mRNA when *hif-1(lf)* is knocked out. 11

2.6 (**A**) Schematic diagram of an epistasis plot. The X-axis on an epistasis plot is the expected coefficient for a double mutant under an additive model (null model). The Y-axis plots deviations from this model. Double mutants that deviate in a systematic manner from the null model exhibit transcriptome-wide epistasis (s). To measure s, we perform a linear regression on the data. The slope of the line of best fit is s. This coefficient is related to genetic architectures. Genes that act additively on a phenotype **(Ph)** will have $s = 0$ (orange line); whereas genes that act along an unbranched pathway will have $s = -1/2$ (blue line). Strong repression is reflected by $s = -1$ (red line). Cases where $s > 0$ correspond to synthetic interactions (purple line), and in the limit as $s \to \infty$, the synthetic interaction must be an OR-gate. Cases where $0 < s < -1/2$ correspond to circuits that have multiple positive branches; whereas cases where $-1/2 < s < -1$ correspond to cases where the branches have different valence. Cases where $s < -1$ represent inhibitory branches. (**B**) Epistasis plot showing that the *egl-9(lf);vhl-1(lf)* transcriptome deviates significantly from a null additive. Points are colored qualitatively according to density (purple—low, yellow—high) and size is inversely proportional to the standard error (S.E.) of the y-axis (larger points, higher accuracy). The purple line is the line of best fit from an orthogonal distance regression. (**C**) Comparison of simulated epistatic coefficients against the observed coefficient. Green curve shows the bootstrapped observed transcriptome-wide epistasis coefficient for *egl-9* and *vhl-1*. Dashed green line shows the mean value of the data. Using the single mutants, we simulated coefficient distributions for a linear model (light blue, centered at −0.5); an additive model (orange, centered at 0); a model where either *egl-9* or *vhl-1* masks the other phenotype (dark blue and black, respectively) and a complete suppression epistasis model (red, centered at −1). The observed coefficient overlaps the predicted epistasis curve for *egl-9(lf);vhl-1(lf)* = *egl-9(lf)* (green and dark blue). 15

2.7 Theoretically, transcriptomes can be used to order genes in a pathway under certain assumptions. Arrows in the diagrams above are intended to show the direction of flow, and do not indicate valence. **A**. A linear pathway in which *rhy-1* is the only gene controlling *egl-9*, which in turn controls *hif-1* does not contain information to infer the order between genes. **B**. If *rhy-1* and *egl-9* have transcriptomic effects that are separable from *hif-1*, then the *rhy-1* transcriptome should contain contributions from *egl-9*, *hif-1* and *egl-9*- and *hif-1*-independent pathways. This pathway contains enough information to infer order. **C**. If a pathway is branched both upstream and downstream, transcriptomes will show even faster decorrelation. Nodes that are separated by many edges may begin to behave almost independently of each other with marginal transcriptomic overlap or correlation. **D**. The hypoxia pathway can be ordered. We hypothesize the rapid decay in correlation is due to a mixture of upstream and downstream branching that happens along this pathway. Bars show the standard error of the weighted coefficient from the Monte Carlo Markov Chain computations. 17

2.8 A feedback loop can generate transcriptomes that are both correlated and anti-correlated. The *vhl-1(lf)/rhy-1(lf)* STP shows a cross-pattern. Green large points are inliers to the first regression. Red squares are outliers to the first regression. Only the red small points were used for the secondary regression. Blue lines are representative samples of the primary bootstrapped regression lines. Orange lines are representative samples of the secondary bootstrapped regression lines. 18

2.9 Gene ontology enrichment analysis of genes associated with the main hypoxia response. A number of terms reflecting catabolism and bioenergetics are enriched. 20

2.10 **A**. 27 genes in *C. elegans* exhibit non-classical epistasis in the hypoxia pathway, characterized by opposite effects on gene expression, relative to the wild-type, of of the *vhl-1(lf)* compared to *egl-9(lf)* (or *rhy-1(lf)*) mutants. Shown are a random selection of 15 the 27 genes for illustrative purposes. **B**. Representative genes showing that non-canonical epistasis shows a consistent pattern. *vhl-1(lf)* mutants have an opposite effect to *egl-9(lf)*, but *egl-9* remains epistatic to *vhl-1* and loss-of-function mutations in *hif-1* suppress the *egl-9(lf)* phenotype. Asterisks show β values significantly different from 0 relative to wild-type ($q < 10^{-1}$). 22

2.11 A graphic summary of the genome-wide effects of HIF-1 from our RNA-seq data. 23

2.12 A hypothetical model showing a mechanism where HIF-1-hydroxyl antagonises HIF-1. **A**. Diagram showing that RHY-1 activates EGL-9. EGL-9 hydroxylates HIF-1 in an oxygen dependent fashion. Under normoxia, HIF-1 is rapidly hydroxylated and only slowly does hydroxylated HIF-1 return to its original state. EGL-9 can also inhibit HIF-1 in an oxygen-independent fashion. HIF-1 hydroxyl is rapidly degraded in a VHL-1 dependent fashion. In our model, HIF-1 and HIF-1 hydroxyl have opposing effects on transcription. The width of the arrows represents the rates under normoxic conditions. **B**. Table showing the effects of loss-of-function mutations on HIF-1 and HIF-1 hydroxyl activity, showing how this can potentially explain the behavior of *ftn-1* in each case. S.S = Steady-state. 26

3.1 Experimental design to identify genes associated with sperm loss and with aging. Studying the wild-type worm alone would measure time- and sperm-related changes at the same time, without allowing us to separate these changes. Studying the wild-type worm and a *fog-2(lf)* mutant would enable us to measure sperm-related changes but not time-related changes. By mixing both designs, we can measure and separate both modules. 44

3.2 **A** We identified a common aging transcriptome between N2 and *fog-2(lf)* animals, consisting of 6,193 differentially expressed isoforms totaling 5,592 genes. The volcano plot is randomly downsampled 30% for ease of viewing. Each point represents an individual isoform. β_{Aging} is the regression coefficient. Larger magnitudes of β indicate a larger log-fold change. The y-axis shows the negative logarithm of the q-values for each point. Green points are differentially expressed isoforms; orange points are differentially expressed isoforms of predicted transcription factor genes (Reece-Hoyes et al., 2005). An interactive version of this graph can be found on our website. **B** Tissue Enrichment Analysis (Angeles-Albores, N. Lee, et al., 2016) showed that genes associated with muscle tissues and the nervous system are enriched in aging-related genes. Only statistically significantly enriched tissues are shown. Enrichment Fold Change is defined as $Observed/Expected$. hmc stands for head mesodermal cell. 47

3.3 **A**. A linear regression with two variables, age and genotype. The expression level of a gene increases by the same amount as worms age regardless of genotype. However, *fog-2(lf)* has more mRNA than the wild-type at all stages (blue arrow). **B**. A linear regression with two variables and an interaction term. In this example, the expression level of this hypothetical gene is different between wild-type worms and *fog-2(lf)* (blue arrow). Although the expression level of this gene increases with age, the slope is different between wild-type and *fog-2(lf)*. The difference in the slope can be accounted for through an interaction coefficient (red arrow). 48

3.4 *fog-2(lf)* partially phenocopies early aging in *C. elegans*. The β in each axes is the regression coefficient from the GLM, and can be loosely interpreted as an estimator of the log-fold change. Feminization by loss of *fog-2(lf)* is associated with a transcriptomic phenotype involving 1,881 genes. 1,040/1,881 of these genes are also altered in wild-type worms as they progress from young adulthood to old adulthood, and 905 change in the same direction. However, progression from young to old adulthood in a *fog-2(lf)* background results in no change in the expression level of these genes. **A** We identified genes that change similarly during feminization and aging. The correlation between feminization and aging is almost 1:1. **B** Epistasis plot of aging versus feminization. Epistasis plots indicate whether two genes (or perturbations) act on the same pathway. When two effects act on the same pathway, this is reflected by a slope of −0.5. The measured slope was -0.51 ± 0.01. 52

3.5 Phenotype and GO enrichment of genes involved in the female state. **A**. Phenotype Enrichment Analysis. **B**. Gene Ontology Enrichment Analysis. Most of the terms enriched in PEA reflect the abundance of ribosomal subunits present in this gene set. 54

3.6 **A**. A substrate model showing how *fog-2* promotes sperm generation, whereas aging promotes sperm depletion, leading to entry to the female state. Such a model can explain why *fog-2* and aging appear epistatic to each other. **B**. The complete *C. elegans* life cycle. Recognized stages of *C. elegans* are marked by black arrows. States are marked by red arrows to emphasize that at the end of a state, the worm returns to the developmental timepoint it was at before entering the state. The L2d state is an exception. It is the only stage that does not return to the same developmental timepoint; rather, the L2d state is a permissive state that allows entry into either dauer or the L3 stage. We have presented evidence of a female state in *C. elegans*. At this point, it is unclear whether the difference between hermaphrodites and females is reversible by males. Therefore, it remains unclear whether it is a stage or a true state. 56

9.1 Schematic representation of trimming filters for an acyclical ontology. **a.** The parent node (green) contains at least as many annotations as the union of the two sisters. These two sisters share annotations extensively, as expressed by the overlap in the Venn diagram, so they qualify for removal. **b.** Nodes with less than a threshold number of genes are trimmed (red) and discarded from the dictionary. Here, the example threshold is 25 genes. Nodes ϵ, ζ, η, shown in red are removed. **c.** Parent nodes are removed recursively, starting from the root, if all their daughter nodes have more than the threshold number of annotations. Nodes in grey (ϵ, ζ, η) were removed in the previous step. Nodes α, β shown in red are trimmed because each one has a complete daughter set. Only nodes γ and δ will be used to generate the static dictionary. 80

9.2 Screenshot of results from the web GUI. After inputting a gene-list, the user is provided with the results. An HTML table is output with hyperlinks to the ontology terms. A publication-ready graph is provided below, which can be saved by dragging to the desktop. The graph is colored for better visualization; color is not intended to convey information. The graph and the table show anatomy terms in human-readable format, followed by their unique WBbt ID. Finally, lists of the genes used and discarded for the analysis are also presented. 81

9.3 TEA Workflow. The complete ontology is annotated continuously by WormBase curators. After each update, the ontology is processed to remove uninformative terms, and the remaining terms are used for statistical testing. Users can select a gene list and input it into our tool using our WormBase portal. The gene list is tested for enrichment using the trimmed ontology, and results are output in tabular and graphic formats for analysis. 82

9.4 Kernel density estimates (KDE) for 30 gold standard datasets. We ran TEA on 30 datasets we believed to be enriched in particular tissues and pooled all the results to observe the distribution of q-values. The mode of the distribution for dictionaries with annotation cut-offs of 100 and 50 genes are very similar; however, when the cut-off is lowered to 25 genes, the mode of the distribution shifts to the left, potentially signalling a decrease in measurement power. 82

9.5 Independently derived gene sets show similar results when tested with the same dictionary. **Set 1.** GABAergic gene set from Watson (Watson et al., 2008). **Set 2.** GABAergic gene set from Spencer (Spencer et al., 2011). Arrowheads highlight identical terms between both analyses. All terms refer to neurons or neuronal tissues and are GABA-associated. Dictionary with cutoff: 33; threshold: 0.95; method: 'any'. 83

9.6 *D. coniospora* Gene Enrichment Analysis and Tissue Enrichment Analysis results. We compared and contrasted the results from a gene enrichment analysis program, pantherDB, with TEA by analyzing genes that were significantly down-regulated when *C. elegans* was exposed to *D. coniospora* in a previously published dataset by Engelmann *et al* (Engelmann et al., 2011) with both tools. **a.** pantherDB screenshot of results, sorted by p-value. Only top hits shown. **b.** TEA results, sorted by q-value (lowest on top) and fold-change. Both pantherDB and TEA identify terms associated with neurons (red square). The two analyses provide complementary, not redundant, information. 84

10.1 Experimental design for human-nematode phenologue identification. We used GWAS candidates from the EBI-NHGRI catalog to identify disease associated genes, then used DIOPT to identify candidate orthologs in *C. elegans*. Orthologs were used to run phenotype, gene and tissue ontology enrichment analyses to identify disease phenologues. 91

10.2 Phenologue identification for systemic lupus erythematosus. **A** Phenotype Enrichment Analysis. **B** GO Enrichment Analysis. **C** Lupus in *C. elegans* may be best represented by a combination of three phenotypes: Cell proliferation possibly accompanied by aneuploidy; cell fate transformations that may lead to dysmorphias; and a molecular phenotype involving impairment of the Nonsense-Mediated Decay (NMD) pathway. 93

10.3 PEA shows that the ciliary transcriptome is enriched in phenotypes related to cell division. Although this could reflect enrichment of microtubules and microtubule-related genes, the enrichment is at least partially driven by cell-cycle and DNA repair genes. 97

10.4 The Egl phenotype is a complex phenotype that is the result of interactions between many tissues. To dissect the contributions of individual tissues to generating an Egl phenotype, we obtained all genes annotated with with an Egl term. **A** We used TEA on the set of Egl genes to identify enriched tissues. **B** Anatomic diagram showing the tissues that are most enriched in the Egl gene set. Color coding shows the qualitative ordering of enrichment (red-Most enriched, yellow-least enriched). For clarity, not all cells are shown. All vm1 (4 cells) and vm2 (4 cells) muscles are symmetrical arranged around the vulva, but only 2 cells are shown for each. There are two seam cells on the left and right side of the vulva, but only cell on the right is shown. Only terminally differentiated cells are shown. 100

LIST OF TABLES

Number *Page*

2.1 Number of differentially expressed genes in each mutant. 6

9.1 Parameter specifications and number of tissues for all dictionaries. The 'Method' column refers to the trimming criterion for the similarity metric. We used two such criteria, 'any' and 'avg'.'any': For a given sister set, if any sister had a similarity exceeding the corresponding threshold, all sisters were removed from the final dictionary. 'avg': For a given sister set, if the average similarity across all the sisters in the set was greater than the corresponding threshold, all sisters were removed from the final dictionary. 79

9.2 Comparison of results for a GABAergic neuronal-enriched gene set from Watson (Watson et al., 2008) showing that results are similar regardless of annotation cutoff. We ran the same gene list on a dictionary with a minimum annotation cutoff of 50, similarity threshold of 0.95 and similarity method 'any' versus another with a minimum annotation cutoff of 33, similarity threshold of 0.95 and similarity method 'any'. In the table, columns are abeled with their significance value (Q-value) or enrichment fold change followed by a hyphen and a number which indicates which the cutoff for the dictionary that was used for testing. Not all tissues are present in either dictionary. Hyphens denote not-applicable values, which occurs when a particular tissue is not present in both dictionaries. 79

10.1 Conditional probabilities for various tissues. The first column shows the conditional probability that a gene has an Egl phenotype given that it has expression in tissue X (given by the row). The second column shows the conditional probability that a gene has expression in the anatomy term X given that it has an Egl phenotype. The first 9 terms are the terms for which $P(\text{Egl}|X)$ is maximized. The last three terms are the terms which have the highest $P(X|\text{Egl})$. For clarity, the Pn.p cells are not shown even though $P(\text{Egl}|\text{Pn.p}) \sim 0.24$. 101

NOMENCLATURE

Asteroid. A very small planet ranging from 1,000 km to less than one km in diameter. Asteroids are found commonly around other larger planets.

Galaxy. A system of stars independent from all other systems.

Chapter 1

INTRODUCTION

Prologue

A short history of genetic analysis

Epistasis and genetic interactions

Birth of genomics

Genetical genomics

Overview of the problem

Chapter 2

GENETIC ANALYSIS OF A METAZOAN PATHWAY USING TRANSCRIPTOMIC PHENOTYPES

Abstract

RNA-seq is commonly used to identify genetic modules that respond to perturbations. In single cells, transcriptomes have been used as phenotypes, but this concept has not been applied to whole-organism RNA-seq. Linear models can quantify expression effects of individual mutants and identify epistatic effects in double mutants. However, interpreting these high-dimensional measurements is unintuitive. We developed a single coefficient to quantify transcriptome-wide epistasis which accurately reflects the underlying interactions. To demonstrate the power of our approach, we sequenced four single and two double C. elegans mutants. From these mutants, we successfully reconstructed the known hypoxia pathway. Using this approach, we uncovered a class of 31 genes that have opposing changes in expression in *egl-9(lf)* and *vhl-1(lf)* but the *egl-9(lf);vhl-1(lf)* mutant phenocopies *egl-9(lf)*. These changes violate the classical model of HIF-1 regulation, but can be explained by postulating a role of hydroxylated HIF-1 in transcriptional control.

Introduction

Genetic analysis of molecular pathways has traditionally been performed through epistatis analysis. Generalized epistasis indicates that two genes interact functionally; such interaction can involve the direct interaction of their products or the interaction of any consequence of their function (small molecules, physiological or behavioral effects) (L. S. Huang and Paul W Sternberg, 2006). If two genes interact, and the mutants of these genes have a quantifiable phenotype, the double mutant of interacting genes will have a phenotype that is not the sum of the phenotypes of the single mutants that make up its genotype. Epistasis analysis remains a cornerstone of genetics today (Phillips, 2008).

Recently, biological studies have shifted in focus from studying single genes to studying all genes in parallel. In particular, RNA-seq (Mortazavi et al., 2008) enables

biologists to identify genes that change expression in response to a perturbation. Gene expression profiling using RNA-seq has become much more sensitive thanks to deeper and more frequent sequencing due to lower sequencing costs (Metzker, 2010), better and faster abundance quantification (Patro, Mount, and Kingsford, 2014; Bray et al., 2016; Patro, Duggal, et al., 2016), and improved differential expression analysis methods (Pimentel et al., 2016; Trapnell et al., 2013). RNA-seq has been successfully used to identify genetic modules involved in a variety of processes, including T-cell regulation (Singer et al., 2016; Shalek et al., 2013), the *Caenorhabditis elegans* (*C. elegans*) linker cell migration (Schwarz, Kato, and Paul W. Sternberg, 2012), and planarian stem cell maintenance (Van Wolfswinkel, Wagner, and Reddien, 2014; Scimone et al., 2014). For the most part, the role of transcriptional profiling has been restricted to target gene identification.

Although transcriptional profiling has been primarily used for descriptive purposes, transcriptomic phenotypes have previously been used to make genetic inferences. Microarray analyses in *S. cerevisiae* and *D. discoideum* were used to show that transcriptomes can be interpreted to infer genetic relationships in simple eukaryotes (Hughes et al., 2000; Van Driessche et al., 2005). eQTL studies in many organisms, from yeast to humans, have established the usefulness of transcriptomic phenotypes for population genetics studies (Brem et al., 2002; Schadt et al., 2003; Li et al., 2006; King et al., 2014). In cell culture, single-cell RNA-seq has seen significant progress towards using transcriptomes as phenotypes with which to test genetic interactions (Adamson et al., 2016; Dixit et al., 2016). More recently, we have identified a new developmental state of *C. elegans* using whole-organism transcriptome profiling (Angeles-Albores, Leighton, et al., 2016). To investigate the ability of whole-organism transcriptomes to serve as quantitative phenotypes for epistasis analysis in metazoans, we sequenced the transcriptomes of of four well-characterized loss of function mutants in the *C. elegans* hypoxia pathway (Epstein et al., 2001; Shen, Shao, and Powell-Coffman, 2006; Shao, Zhang, and Powell-Coffman, 2009; H. Jiang, Guo, and Powell-Coffman, 2001).

Metazoans depend on the presence of oxygen in sufficient concentrations to support aerobic metabolism. Genetic pathways evolved to rapidly respond to any acute or chronic changes in oxygen levels at the cellular or organismal level. Biochemical and genetic approaches identified the Hypoxia Inducible Factors (HIFs) as an important group of oxygen-responsive genes that are involved in a broad range of human pathologies (Gregg L. Semenza, 2012).

Hypoxia Inducible Factors are highly conserved in metazoans (Loenarz et al., 2011). A common mechanism for hypoxia-response induction is heterodimerization between a HIFα and a HIFβ subunit; the heterodimer then initiates transcription of target genes (B. H. Jiang et al., 1996). The number and complexity of HIFs varies throughout metazoans, with humans having three HIFα subunits and two HIFβ subunits, whereas in the roundworm *C. elegans* there is a single HIFα gene, *hif-1* (H. Jiang, Guo, and Powell-Coffman, 2001) and a single HIFβ gene, *ahr-1* (Powell-Coffman, Bradfield, and Wood, 1998). HIF target genes have been implicated in a wide variety of cellular and extracellular processes including glycolysis, extracellular matrix modification, autophagy and immunity (G L Semenza et al., 1994; Bishop et al., 2004; Shen, Nettleton, et al., 2005; Bellier et al., 2009; Gregg L. Semenza, 2012).

Levels of HIFα proteins tend to be tightly regulated. Under conditions of normoxia, HIF-1α exists in the cytoplasm and partakes in a futile cycle of continuous protein production and rapid degradation (L. E. Huang et al., 1996). HIF-1α is hydroxylated by three proline hydroxylases in humans (PHD1, PHD2 and PHD3) but is only hydroxylated by one proline hydroxylase (EGL-9) in *C. elegans* (Kaelin and Ratcliffe, 2008). HIF-1 hydroxylation increases its binding affinity to Von Hippel Lindau Tumor Suppressor 1 (VHL-1), which allows ubiquitination of HIF-1 leading to its subsequent degradation. In *C. elegans*, EGL-9 activity is inhibited by binding of CYSL-1, a homolog of sulfhydrylases/cysteine synthases, and CYSL-1 activity is in turn inhibited at the protein level by RHY-1, which is a putative transmembrane O-acyltransferase, possibly by post-translational modifications to CYSL-1 (Ma et al., 2012) (see Fig. 2.1).

Here, we show that transcriptomes contain robust signals that can be used to infer relationships between genes in complex metazoans by reconstructing the hypoxia pathway in *C. elegans* using RNA-seq. Furthermore, we show that the phenomenon of phenotypic epistasis, a hallmark of genetic interaction, holds at the molecular systems level. We also demonstrate that transcriptomes contain sufficient information, under certain circumstances, to order genes in a pathway using only single mutants. Finally, we were able to identify genes that appear to be downstream of *egl-9* and *vhl-1*, but do not appear to be targets of *hif-1*. Using a single set of genome-wide measurements, we were able to observe and quantitatively assess significant fraction of the known transcriptional effects of *hif-1* in *C. elegans*. A complete version of the analysis, with ample documentation, is available at

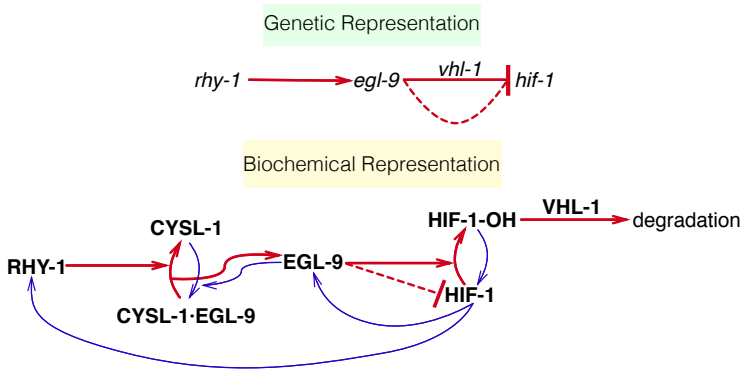

Figure 2.1: Genetic and biochemical representation of the hypoxia pathway in *C. elegans*. Red arrows are arrows that lead to inhibition of HIF-1, and blue arrows are arrows that increase HIF-1 activity or are the result of HIF-1 activity. EGL-9 is known to exert *vhl-1*-dependent and independent repression on HIF-1 as shown in the genetic diagram. The *vhl-1*-independent repression of HIF-1 by EGL-9 is denoted by a dashed line and is not dependent on the hydroxylating activity of EGL-9. Technically, RHY-1 inhibits CYSL-1, which in turn inhibits EGL-9, but this interaction was abbreviated in the genetic diagram for clarity.

https://wormlabcaltech.github.io/mprsq.

Results

The hypoxia pathway controls thousands of genes in *C. elegans*

We selected four single mutants within the hypoxia pathway for expression profiling: *egl-9(lf)* (*sa307*), *rhy-1(lf)* (*ok1402*), *vhl-1(lf)* (*ok161*), *hif-1(lf)* (*ia4*). We also sequenced the transcriptomes of two double mutants, *egl-9(lf);vhl-1(lf)* (*sa307*, *ok161*) and *egl-9(lf) hif-1(lf)* (*sa307*, *ia4*) as well as wild-type N2 as a control sample. Each genotype was sequenced in triplicate at a depth of 15 million reads. We performed whole-animal RNA-seq of these mutants at a moderate sequencing depth ($\sim$ 7 million mapped reads for each individual replicate) under normoxic conditions. For single samples, we identified around 22,000 different isoforms per sample, which allowed us to measure differential expression of 18,344 isoforms across all replicates and genotypes (this constitutes ~70% of the protein coding isoforms in *C. elegans*). We also included in our analysis a *fog-2(lf)* (*q71*) mutant which we have previously studied (Angeles-Albores, Leighton, et al., 2016), because *fog-2* is not reported to interact with the hypoxia pathway. We analyzed our data using a general linear model on logarithm-transformed counts. Changes in gene expression are reflected in the regression coefficient, β which is specific to each isoform within a genotype. Statistical significance is achieved when the q-values

for each β (p-values adjusted for multiple testing) are less than 0.1. Genes that are significantly altered between wild-type and a given mutant have β values that are statistically significantly different from 0. These coefficients are not equal to the average log-fold change per gene, although they are loosely related to this quantity. Larger magnitudes of β correspond to larger perturbations. Negative values of β indicate an isoform has been downregulated in a mutant relative to a wild-type control, whereas positive values of β indicate the isoform was upregulated. These coefficients can be used to study the RNA-seq data in question.

In spite of the moderate sequencing depth, transcriptome profiling of the hypoxia pathway revealed that this pathway controls thousands of genes in *C. elegans*. The *egl-9(lf)* transcriptome showed differential expression of 1,806 genes. Similarly, 2,103 genes were differentially expressed in *rhy-1(lf)* mutants. The *vhl-1(lf)* transcriptome showed considerably fewer differentially expressed genes (689), possibly because it is a weaker controller of *hif-1(lf)* than *egl-9(lf)* (Shao, Zhang, and Powell-Coffman, 2009). The *egl-9(lf);vhl-1(lf)* double mutant transcriptome showed 2,376 differentially expressed genes. The *hif-1(lf)* mutant also showed a transcriptomic phenotype involving 546 genes. The *egl-9(lf) hif-1(lf)* double mutant showed a similar number of genes with altered expression (404 genes, see Table 2.1).

Genotype	Differentially Expressed Genes
egl-9(lf)	1,806
rhy-1(lf)	2,103
vhl-1(lf)	689
hif-1(lf)	546
egl-9(lf);vhl-1(lf)	2,376
egl-9(lf) hif-1(lf)	404
fog-2(lf)	2,090

Table 2.1: Number of differentially expressed genes in each mutant.

Principal Component Analysis visualizes epistatic relationships between genotypes

Principal Component Analysis (PCA) is a well-known technique in bioinformatics that is used to identify relationships between high dimensional data points (Yeung and Ruzzo, 2001). We performed PCA on our data to examine whether each genotype clustered in a biologically relevant manner. PCA identifies the vector that can explain most of the variation in the data;this is called the first PCA dimension.

Using PCA, one can identify the first n dimensions that can explain more than 95% of the variation in the data. Sample clustering in these n dimensions often indicates biological relationships between the data, although interpreting PCA dimensions can be difficult.

After applying PCA, we expected *hif-1(lf)* to cluster near *egl-9(lf) hif-1(lf)*, because *hif-1(lf)* exhibits no phenotypic defects under normoxic conditions, in contrast to *egl-9(lf)*, which exhibits an egg-laying (Egl) phenotype in the same environment. In *egl-9(lf) hif-1(lf)* mutants the Egl phenotype of *egl-9(lf)* mutants is suppressed and instead the grossly wild-type phenotype of *hif-1(lf)* is observed. On the other hand, we expected *egl-9(lf)*, *rhy-1(lf)*, *vhl-1(lf)* and *egl-9(lf);vhl-1(lf)* to form a separate cluster since each of these genotypes is Egl and has a constitutive hypoxic response. Finally, we included as a negative control a *fog-2(lf)* mutant we have analyzed previously (Angeles-Albores, Leighton, et al., 2016). This data was obtained at a different time from the other genotypes, so we included a batch-normalization term in our equations to account for this. Since *fog-2* has not been described to interact with the hypoxia pathway, we expected that it should appear far away from either cluster.

The first dimension of the PCA analysis was able to discriminate between mutants that have constitutive high levels of HIF-1 and mutants that have no HIF-1, whereas the second dimension was able to discriminate between mutants within the hypoxia pathway and outside the hypoxia pathway (see Fig. 2.2). Therefore expression profiling measures enough signal to cluster genes in a meaningful manner in complex metazoans.

Reconstruction of the hypoxia pathway from first genetic principles

Having shown that the signal in the mutants we selected was sufficient to cluster mutants using the values of the regression coefficients β, we set out to reconstruct the hypoxia pathway from genetic first principles. In general, to reconstruct a pathway, we must first assess whether two genes act on the same phenotype. If they do not act on the same phenotype, these mutants are independent. If they are not independent, then we must measure whether these genes act additively or epistatically on the phenotype of interest; if there is epistasis we must measure whether it is positive or negative, in order to assess whether the epistatic relationship is a genetic suppression or a synthetic interaction. To allow coherent comparisons of different mutant transcriptomes (the phenotype we are studying here), we define

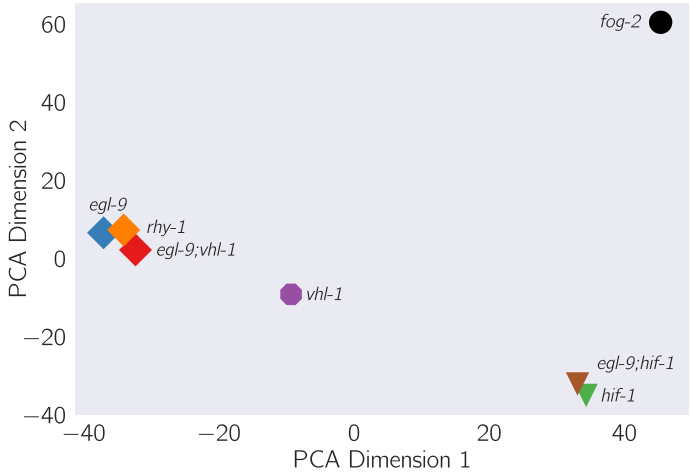

Figure 2.2: Principal component analysis of various *C. elegans* mutants. Genotypes that have an activated hypoxia response (*i.e*, *egl-9(lf)*, *vhl-1(lf)*, and *rhy-1(lf)*) cluster far from *hif-1(lf)*. *hif-1(lf)* clusters with the suppressed *egl-9(lf) hif-1(lf)* double mutant. The *fog-2(lf)* transcriptome, used as an outgroup, is far away from either cluster.

the shared transcriptomic phenotype (STP) as the set of genes or isoforms that are differentially expressed in two mutants being compared, regardless of the direction of change.

Genes in the hypoxia mutant act on the same transcriptional phenotype

We observed that all the hypoxia mutants had a significant STP (fraction of the transcriptomes that was shared between mutants ranged from a minimum of 6.8% shared between *hif-1(lf)* and *egl-9(lf);vhl-1(lf)* to a maximum of 31% shared genes between *egl-9(lf)* and *egl-9(lf);vhl-1(lf)*). For comparison, we also analyzed a previously published *fog-2(lf)* transcriptome (Angeles-Albores, Leighton, et al., 2016). The *fog-2* gene is involved in masculinization of the *C. elegans* germline, which enables sperm formation, and is not known to be involved in the hypoxia pathway. The hypoxia pathway mutants and the *fog-2(lf)* mutant also showed shared transcriptomic phenotypes (3.6%–12% genes), but correlations between expression level changes were considerably weaker (see below), suggesting that there is minor cross-talk between these pathways.

We wanted to know whether it was informative to look at quantitative agreement within STPs. For each mutant pair, we rank-transformed the regression coefficients β of each isoform within the STP, and calculated lines of best fit using Bayesian

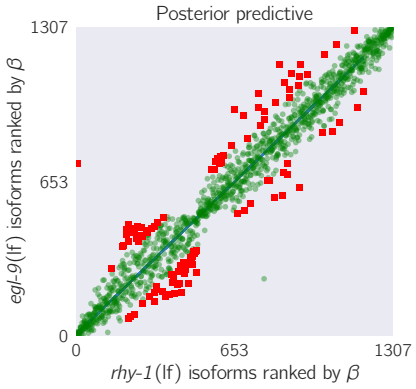

Figure 2.3: Strong transcriptional correlations can be identified between genes that share a positive regulatory connection. We took the *egl-9(lf)* and the *rhy-1(lf)* transcriptomes, identified differentially expressed genes common to both transcriptomes and ranked each gene according to its differential expression coefficient β. We plotted the rank of each gene in *rhy-1(lf)* versus the rank of the same gene in the *egl-9(lf)* transcriptome. The result is an almost perfect correlation. Green, transparent large points mark inliers to the primary regressions (blue lines); red squares mark outliers to the primary regressions.

regression with a Student-T distribution to mitigate noise from outliers and plotted the results in a rank plot (see Fig 2.3). For transcriptomes associated with the hypoxia pathway, we found that these correlations tended to have values higher than 0.9 with a tight distribution around the line of best fit. The correlations for mutants from the hypoxia pathway with the *fog-2(lf)* mutant were considerably weaker, with magnitudes between 0.6–0.85 and greater variance around the line of best fit. Although *hif-1* is known to be genetically repressed by *egl-9*, *rhy-1* and *vhl-1* (Epstein et al., 2001; Shen, Shao, and Powell-Coffman, 2006), all the correlations between mutants of these genes and *hif-1(lf)* were positive.

After we calculated the pairwise correlation within each STP, we weighted the result of each regression by the number of isoforms within the STP and divided by the total number of differentially expressed isoforms present in the two mutant transcriptomes that contributed to that specific STP, $N_{\text{overlap}}/N_{\text{g1}\cup\text{g2}}$. The weighted regressions recapitulated a module network (see Fig. 2.4). We identified a strong positive interaction between *egl-9(lf)* and *rhy-1(lf)*. The magnitude of this weighted correlation derives from the number of genes that are differentially expressed for these mutants (1,806 and 2,103 differentially expressed genes respectively) and the size of their STP, which makes the weighting factor considerably larger than other pairs. The weak correlation between *hif-1(lf)* and *egl-9(lf)* results from the large

effect size of the *egl-9(lf)* transcriptome coupled with the small STP between both mutants.

The fine-grained nature of transcriptional phenotypes means that these weighted correlations between transcriptomes of single mutants are predictive of genetic interaction.

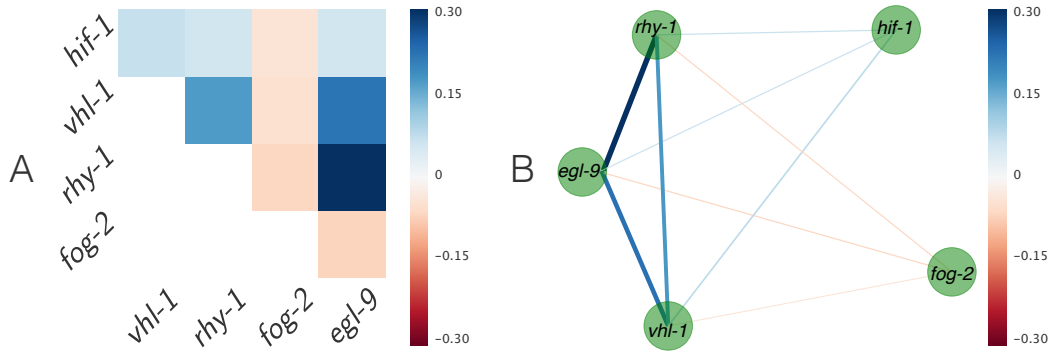

Figure 2.4: **A**. Heatmap showing pairwise regression values between all single mutants. **B**. Correlation network drawn from **A**. Edge width is proportional to the logarithm of the magnitude of the weighted correlation between two nodes divided by absolute value of the weighted correlation value of smallest magnitude. Edges are also colored according to the heatmap in **A**. Inhibitors of *hif-1* are tightly correlated and form a control module; *hif-1* is positively correlated to its inhibitors, albeit weakly; and *fog-2*, a gene that is not reported to interact with the hypoxia pathway, has the smallest, negative correlation to any gene.

A quality check of the transcriptomic data reveals excellent agreement with the literature

One way to establish whether genes are acting additively or epistatically to each other is to perform qPCR of a reporter gene in the single and double mutants. This approach was used to successfully map the relationships within the hypoxia pathway (see, for example (Shao, Zhang, and Powell-Coffman, 2009; Shen, Shao, and Powell-Coffman, 2006)). A commonly used hypoxia reporter gene is *nhr-57*, which is known to exhibit a several-fold increase in mRNA expression when HIF-1 accumulates (Shen, Shao, and Powell-Coffman, 2006; Shen, Nettleton, et al., 2005; Park et al., 2012). Likewise, increased HIF-1 function is known to cause increased transcription of *rhy-1* and *egl-9* (Powell-Coffman, 2010).

We can selectively look at the expression of a few genes at a time. Therefore, we queried the changes in expression of *rhy-1*, *egl-9*, and *nhr-57*. We included the

nuclear laminin gene *lam-3* as a representative negative control not believed to be responsive to alterations in the hypoxia pathway. *nhr-57* was upregulated in *egl-9(lf)*, *rhy-1(lf)* and *vhl-1(lf)*, but remains unchanged in *hif-1(lf)*. *egl-9(lf);vhl-1(lf)* had an expression level similar to *egl-9(lf)*; whereas the *egl-9(lf) hif-1(lf)* mutant showed wild-type levels of the reporter expression, as reported previously (Shen, Shao, and Powell-Coffman, 2006) (see Fig. 2.5).

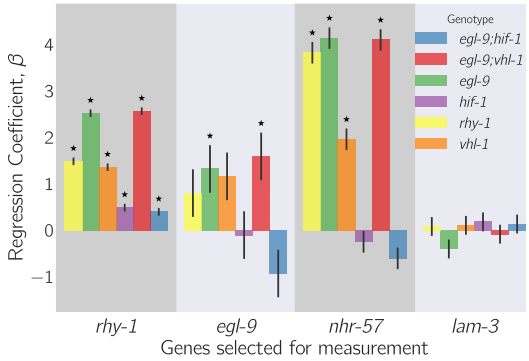

Figure 2.5: **Top**: Observed β values of select genes. We selected four genes (*rhy-1*, *egl-9*, *nhr-57* and *lam-3*, shown on the x-axis) and plotted their regression coefficients, β, as measured for every genotype (represented by one of six colors) to study the epistatic relationships between each gene. Asterisks above a bar represent a regression coefficient statistically significantly different from 0 ($q < 10^{-1}$) relative to a wild-type control. Error bars show standard error of the mean value of β. *nhr-57* is an expression reporter that has been used previously to identify *hif-1* regulators (Shen, Shao, and Powell-Coffman, 2006; Shao, Zhang, and Powell-Coffman, 2009). *lam-3* is shown here as a negative control that should not be altered by mutations in this pathway. We measured modest increases in the levels of *rhy-1* mRNA when *hif-1(lf)* is knocked out.

We observed changes in *rhy-1(lf)* expression consistent with previous literature (Shen, Shao, and Powell-Coffman, 2006) when HIF-1 accumulates. We also observed increases in *egl-9* expression in *egl-9(lf)*. *egl-9* is known as a hypoxia responsive gene (Powell-Coffman, 2010). Although changes in *egl-9* expression were not statistically significantly different from the wild-type in *rhy-1(lf)* and *vhl-1(lf)* mutants, the mRNA levels of *egl-9* still trended towards increased expression in these genotypes. As with *nhr-57*, *egl-9* and *rhy-1* expression were wild-type in *egl-9(lf) hif-1(lf)* and *egl-9(lf);vhl-1(lf)* mutant showed expression phenotypes identical to *egl-9(lf)*. This dataset also showed that knockout of *hif-1* resulted in a modest increase in the levels of *rhy-1*. This suggests that *hif-1*, in addition to being a positive regulator of *rhy-1*, also inhibits it, which constitutes a novel observation. Using a single reporter we would have been able to reconstruct an important fraction of the genetic relation-

ships between the genes in the hypoxia pathway—-but would likely fail to observe yet other genetic interactions, such as the evidence for *hif-1* negatively regulating *rhy-1* transcript levels.

Transcriptome-wide epistasis

Ideally, any measurement of transcriptome-wide epistasis should conform to certain expectations. First, it should make use of the regression coefficients of as many genes as possible. Second, it should be summarizable in a single, well-defined number. Third, it should have an intuitive behavior, such that special values of the statistic should each have an unambiguous interpretation.

One way of displaying transcriptome-wide epistasis is to plot transcriptome data onto an epistasis plot (see Fig 2.6). In an epistasis plot, the X-axis represents the expected expression of a double mutant a^-b^- if a and b interact additively. In other words, each individual isoform's x-coordinate is the sum of the regression coefficients from the single mutants a^- and b^-. The Y-axis represents the deviations from the additive (null) model, and can be calculated as the difference between the observed regression coefficient and the predicted regression coefficient. Only genes that are differentially expressed in all three genotypes are plotted. Assuming that the two genes interact via a simple phenotype (for example, if both genes affect a transcription factor that generates the entire transcriptome), these plots will generate specific patterns that can be described through linear regressions. The slope of these lines, $s_{a,b}$, is the transcriptome-wide epistasis coefficient.

Epistasis plots can be understood intuitively for simple cases of genetic interactions. If two genes act additively on the same set of differentially expressed isoforms then all the plotted points will fall along the line $y = 0$. If two genes act positively in an unbranched pathway, then a^- and b^- should have identical phenotypes for a^-, b^- and a^-b^-, if all the genotypes are homozygous for genetic null alleles (L. S. Huang and Paul W Sternberg, 2006). It follows that the data points should fall along a line with slope equal to $-\frac{1}{2}$. On the other hand, in the limit of complete inhibition of a by b in an unbranched pathway, the plots should show a line of best fit with slope equal to -1[1]. Genes that interact synthetically (*i.e.*, through an OR-gate) will fall along lines with slopes > 0. When there is epistasis of one gene over another, the points will fall along a line of best fit with slope $s_{ab=b}$ or $s_{ab=a}$. This slope must be determined from the single-mutant data. From this information, we can use the

[1] Specifically, this follows from assuming that b^- is wild-type under the conditions assayed; and a^-b^- = b^- = wild-type

single mutant data to predict the distribution of slopes that results for each case stated above, as well as for each epistatic combination ($a^-b^- = a^-$ or $a^-b^- = b^-$). The transcriptome-wide epistasis coefficient ($s_{a,b}$), emerges as a powerful way to quantify epistasis because it integrates information from many different genes or isoforms into a single number (see Fig. 2.6).

In our experiment, we studied two double mutants, *egl-9(lf) hif-1(lf)* and *egl-9(lf);vhl-1(lf)*. We wanted to understand how well an epistasis analysis based on transcriptome-wide coefficients agreed with the epistasis results reported in the literature, which were based on qPCR of single genes. Therefore, we performed orthogonal distance regression on the two gene combinations we studied (*egl-9* and *vhl-1*; and *egl-9* and *hif-1*) to determine the epistasis coefficient for each gene pair. We also generated models for the special cases mentioned above (additivity, $a^-b^- = a^-$, strong suppression, etc. . .) using the single mutant data. For every simulation, as well as for the observed data, we used bootstraps to generate probability distributions of the epistasis coefficients.

When we compared the predictions for the transcriptome-wide epistasis coefficient, $s_{egl-9,vhl-1}$ under different assumptions with the observed slope (−0.42). We observed that the predicted slope matched the simulated slope for the case where *egl-9* is epistatic over *vhl-1* (*egl-9(lf)* = *egl-9(lf);vhl-1(lf)*, see Fig. 2.6) and did not overlap with any other prediction. Next, we predicted the distribution of $s_{egl-9,hif-1}$ for different pathways and contrasted with the observed slope. In this case, we saw that the uncertainty in the observed coefficient overlapped significantly with the strong suppression model, where EGL-9 strongly suppresses HIF-1, and also with the model where *hif-1(lf)* = *egl-9(lf) hif-1(lf)*. In this case, both models are reasonable—HIF-1 is strongly suppressed by EGL-9, and we know from previous literature that the epistatic relationship, *hif-1(lf)* = *egl-9(lf) hif-1(lf)*, is true for these mutants. In fact, as the repression of HIF-1 by EGL-9 becomes stronger, the epistatic model should converge on the limit of strong repression (see Epistasis).

Another way to test which model best explains the epistatic relationship between *egl-9* and *vhl-1* is to use Bayesian model selection to calculate an odds ratio between two models to explain the observed data. Models can be placed into two categories: parameter-free and fit. Parameter free models are ‘simpler’ because their parameter space is smaller (0 parameters) than the fit models (n parameters). By Occam’s razor, simpler models should be preferred to more complicated models. However, simple models suffer from the drawback that systematic deviations from them cannot be

explained or accomodated, whereas more complicated models can alter the fit values to maximize their explanatory power. In this sense, more complicated models should be preferred when the data shows systematic deviations from the simple model. Odds-ratio selection gives us a way to quantify the trade-off between simplicity and explanatory power.

We reasoned that comparing a fit model ($y = \alpha \cdot x$, where α is the slope of best fit) against a parameter-free model ($y = \gamma \cdot x$, where γ is a single number) constituted a conservative approach towards selecting which theoretical model (if any) best explained the data. In particular, this approach will tend to strongly favor the line of best fit over simpler model for all but very small, non-systematic deviations. We decided that we would reject the theoretical models only if the line of best-fit was 10^3 times more likely than the theoretical models (odds ratio, OR $> 10^3$). Comparing the odds-ratio between the line of best fit and the different pathway models for *egl-9* and *vhl-1* showed similar results to the simulation. Only the theoretical model *egl-9(lf)* = *egl-9(lf);vhl-1(lf)* could not be rejected (OR = 0.46), whereas all other models were significantly less likely than the line of best fit (OR $> 10^{44}$). Therefore, *egl-9* is epistatic to *vhl-1*. Moreover, since $s_{egl-9,vhl-1}$ is strictly between and not equal to 0 and -0.5, we conclude that *egl-9* acts on its transcriptomic phenotype in *vhl-1*-dependent and independent manners. A branched pathway that can lead to epistasis coefficients in this range is a pathway where *egl-9* interacts with its transcriptomic phenotype via branches that have the same valence (both positive or both negative) (Shao, Zhang, and Powell-Coffman, 2009). When we performed a similar analysis to establish the epistatic relationship between *egl-9* and *hif-1*, we observed that the best alternative to a free-fit model was a model where *hif-1* is epistatic over *egl-9* (OR= 2551), but the free-fit model was still preferred. All other models were strongly rejected (OR $> 10^{25}$).

Epistasis can be predicted

Given our success in measuring epistasis coefficients, we wanted to know whether we could predict the epistasis coefficient between *egl-9* and *vhl-1* in the absence of the *egl-9(lf)* genotype. Since RHY-1 indirectly activates EGL-9, the *rhy-1(lf)* transcriptome should contain more or less equivalent information to the *egl-9(lf)* transcriptome. Therefore, we generated predictions of the epistasis coefficient between *egl-9* and *vhl-1* by substituting in the *rhy-1(lf)* data. We predicted $s_{rhy-1,vhl-1} = -0.45$. Similarly, we used the *egl-9(lf);vhl-1(lf)* double mutant to measure the epistasis

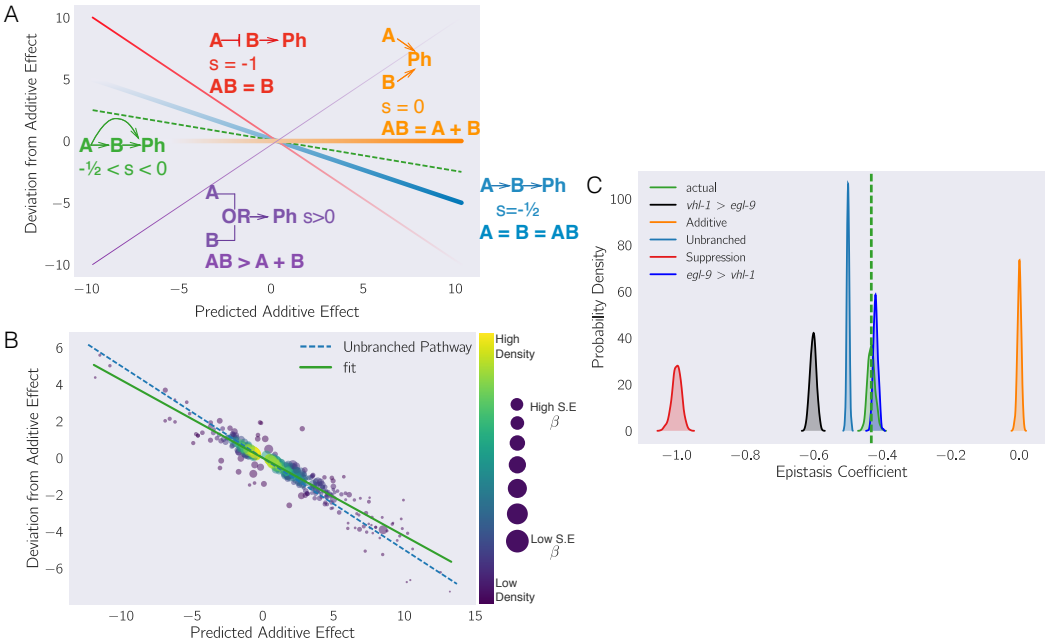

Figure 2.6: (**A**) Schematic diagram of an epistasis plot. The X-axis on an epistasis plot is the expected coefficient for a double mutant under an additive model (null model). The Y-axis plots deviations from this model. Double mutants that deviate in a systematic manner from the null model exhibit transcriptome-wide epistasis (s). To measure s, we perform a linear regression on the data. The slope of the line of best fit is s. This coefficient is related to genetic architectures. Genes that act additively on a phenotype **(Ph)** will have $s = 0$ (orange line); whereas genes that act along an unbranched pathway will have $s = -1/2$ (blue line). Strong repression is reflected by $s = -1$ (red line). Cases where $s > 0$ correspond to synthetic interactions (purple line), and in the limit as $s \to \infty$, the synthetic interaction must be an OR-gate. Cases where $0 < s < -1/2$ correspond to circuits that have multiple positive branches; whereas cases where $-1/2 < s < -1$ correspond to cases where the branches have different valence. Cases where $s < -1$ represent inhibitory branches. (**B**) Epistasis plot showing that the *egl-9(lf);vhl-1(lf)* transcriptome deviates significantly from a null additive. Points are colored qualitatively according to density (purple—low, yellow—high) and size is inversely proportional to the standard error (S.E.) of the y-axis (larger points, higher accuracy). The purple line is the line of best fit from an orthogonal distance regression. (**C**) Comparison of simulated epistatic coefficients against the observed coefficient. Green curve shows the bootstrapped observed transcriptome-wide epistasis coefficient for *egl-9* and *vhl-1*. Dashed green line shows the mean value of the data. Using the single mutants, we simulated coefficient distributions for a linear model (light blue, centered at -0.5); an additive model (orange, centered at 0); a model where either *egl-9* or *vhl-1* masks the other phenotype (dark blue and black, respectively) and a complete suppression epistasis model (red, centered at -1). The observed coefficient overlaps the predicted epistasis curve for *egl-9(lf);vhl-1(lf)* = *egl-9(lf)* (green and dark blue).

coefficient while replacing the *egl-9(lf)* dataset with the *rhy-1(lf)* dataset. We found that the epistasis coefficient using this substitution was −0.40. This coefficient was different from −0.50 (OR > 10^{62}), reflecting the same qualitative conclusion that the hypoxia pathway is branched. In conclusion, we were able to obtain a quantitatively close prediction of the epistasis coefficient for two mutants using the transcriptome of a related, upstream mutant. Finally, we showed that in the absence of a single mutant, an upstream locus can under some circumstances be used to estimate epistasis between two genes.

Transcriptomic decorrelation can be used to infer functional distance

So far, we have shown that RNA-seq can accurately measure genetic interactions. However, genetic interactions are far removed from biochemical interactions: Genetic interactions do not require two gene products to interact physically, nor even to be physically close to each other. RNA-seq cannot measure physical interactions between genes, but we wondered whether expression profiling contains sufficient information to order genes along a pathway.

Single genes are often regulated by multiple independent sources. The connection between two nodes can in theory be characterized by the strength of the edges connecting them (the thickness of the edge); the sources that regulate both nodes (the fraction of inputs common to both nodes); and the genes that are regulated by both nodes (the fraction of outputs that are common to both nodes). In other words, we expected that expression profiles associated with a pathway would respond quantitatively to quantitative changes in activity of the pathway. Targeting a pathway at multiple points would lead to expression profile divergence as we compare nodes that are separated by more degrees of freedom, reflecting the flux in information between them.

We investigated the possibility that transcriptomic signals do in fact contain relevant information about the degrees of separation by weighting the robust Bayesian regression between each pair of genotypes by the size of the shared transcriptomic phenotype of each pair divided by the total number of isoforms differentially expressed in either mutant ($N_{\text{Intersection}}/N_{\text{Union}}$). We plotted the weighted correlation of each gene pair, ordered by increasing functional distance (see Fig. 2.7). In every case, we see that the weighted correlation decreases monotonically due mainly, but not exclusively, to a smaller STP. We believe that this result is not due to random noise or insufficiently deep sequencing. Instead, we propose a framework in which

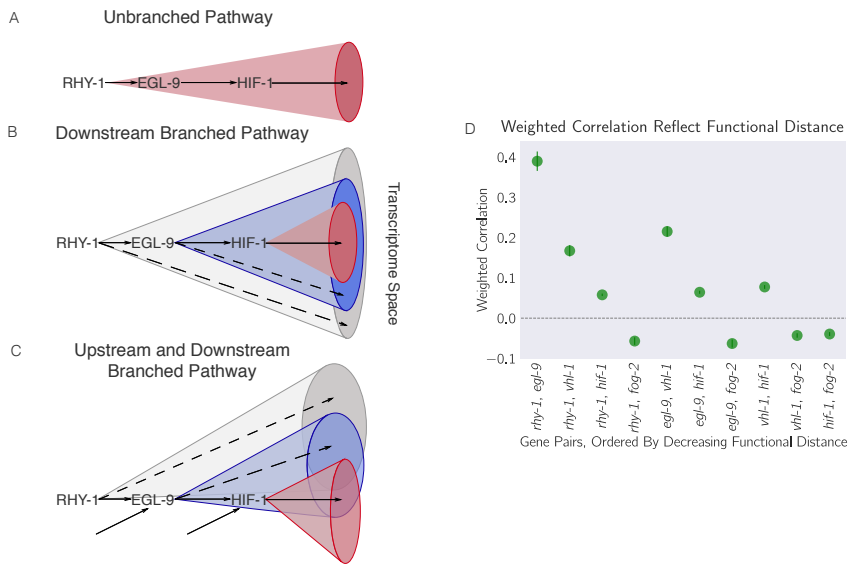

Figure 2.7: Theoretically, transcriptomes can be used to order genes in a pathway under certain assumptions. Arrows in the diagrams above are intended to show the direction of flow, and do not indicate valence. **A**. A linear pathway in which *rhy-1* is the only gene controlling *egl-9*, which in turn controls *hif-1* does not contain information to infer the order between genes. **B**. If *rhy-1* and *egl-9* have transcriptomic effects that are separable from *hif-1*, then the *rhy-1* transcriptome should contain contributions from *egl-9*, *hif-1* and *egl-9*- and *hif-1*-independent pathways. This pathway contains enough information to infer order. **C**. If a pathway is branched both upstream and downstream, transcriptomes will show even faster decorrelation. Nodes that are separated by many edges may begin to behave almost independently of each other with marginal transcriptomic overlap or correlation. **D**. The hypoxia pathway can be ordered. We hypothesize the rapid decay in correlation is due to a mixture of upstream and downstream branching that happens along this pathway. Bars show the standard error of the weighted coefficient from the Monte Carlo Markov Chain computations.

every gene is regulated by multiple different molecular species, which induces progressive decorrelation. This decorrelation in turn has two consequences. First, decorrelation within a pathway implies that two nodes may be almost independent of each other if the functional distance between them is large. Second, it may be possible to use decorrelation dynamics to infer gene order in a branching pathway, as we have done with the hypoxia pathway.

The circuit topology of the hypoxia pathway explains patterns in the data

We noticed that while some of the rank plots contained a clear positive correlation (see Fig. 2.3), other rank plots showed a discernible cross-pattern (see Fig. 2.8).

In particular, this cross-pattern emerged between *vhl-1(lf)* and *rhy-1(lf)* or between *vhl-1(lf)* and *egl-9(lf)*, even though genetically *vhl-1*, *rhy-1* and *egl-9* are all suppressors of *hif-1(lf)*. Such cross-patterns could be indicative of feedback loops or other complex interaction patterns.

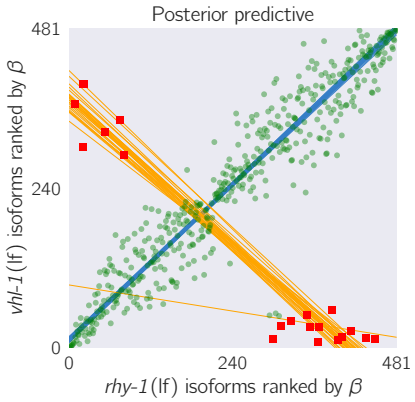

Figure 2.8: A feedback loop can generate transcriptomes that are both correlated and anti-correlated. The *vhl-1(lf)*/*rhy-1(lf)* STP shows a cross-pattern. Green large points are inliers to the first regression. Red squares are outliers to the first regression. Only the red small points were used for the secondary regression. Blue lines are representative samples of the primary bootstrapped regression lines. Orange lines are representative samples of the secondary bootstrapped regression lines.

If the above is correct, then it should be possible to identify *egl-9*-independent, *rhy-1*-dependent target genes in a logically consistent way. One erroneous way to identify these targets is via subtractive logic. Using subtractive logic, we would identify genes that are differentially expressed in *rhy-1(lf)* mutants but not in *egl-9(lf)* mutants. Such a gene set would consist of almost 700 genes. One major drawback of subtractive logic is that it cannot be applied when feedback loops exist between the genes in question. Another problem is that the set of identified genes are statistically indistinguishable from false positive and false negative hits because they have no distinguishing property beyond the condition that they should be differentially expressed in one mutant but not the other. In fact, this is exactly the behavior expected of false-positive hits—presence in one, but not multiple, mutants. We need to consider the relationship between two genes before we can begin to identify targets which expression is dependent on one gene and independent of the other.

rhy-1 and *egl-9* share a well-defined relationship. RHY-1 inhibits CYSL-1, which in turn inhibits EGL-9 (Ma et al., 2012). Therefore, loss of RHY-1 leads to inactivation

of EGL-9, which leads to increase in the cellular levels of HIF-1. HIF-1 in turn causes the mRNA levels of *rhy-1* and *egl-9* to increase, as they are involved in the *hif-1*-dependent hypoxia response. However, since *rhy-1* has been mutated, the observed transcriptome is RHY-1 'null'; EGL-9 'off'; HIF-1 'on'. The situation is similar for *egl-9(lf)*, except that RHY-1 is not inactive, and therefore the observed transcriptome is the result of RHY-1 'up'; EGL-9 'null'; and HIF-1 'on'. From this pattern, we conclude that the *egl-9(lf)* and *rhy-1(lf)* transcriptomes should exhibit a cross-pattern when plotted against each other: The positive arm of the cross is the result of the EGL-9 'off'/'null'; HIF-1 'on' dynamics; and the negative arm reflects the different direction of RHY-1 activity between transcriptomes. No negative arm is visible (with the exception of two outliers, which are annotated as pseudogenes in WormBase). Therefore, in this dataset we do not find genes that have *egl-9* independent, *rhy-1*-dependent expression patterns.

We also identified a main hypoxia response induced by disinhibiting *hif-1* (355 genes) by identifying genes that were commonly upregulated amongst *egl-9(lf)*, *rhy-1(lf)* and *vhl-1(lf)* mutants. Although the hypoxic response is likely to involve between three and seven times more genes (assuming the *rhy-1(lf)* transcriptome reflects the maximal hypoxic response), this is a conservative estimate that minimizes false positive results, since these changes were identified in four different genotypes with three replicates each. This response included five transcription factors (*W02D7.6*, *nhr-57*, *ztf-18*, *nhr-135* and *dmd-9*). The full list of genes associated with the hypoxia response (Supplementary Table 1)

hif-1-independent effects of *egl-9* have been reported previously (Park et al., 2012), which led us to question whether we could identify similar effects in our dataset. We have observed that *hif-1(lf)* displays a modest increase in the transcription of *rhy-1*, from which we speculated that EGL-9 would have increased activity in the *hif-1(lf)* mutant compared to the wild-type. Therefore, we searched for genes that were regulated in an opposite manner between *hif-1(lf)* and *egl-9(lf) hif-1(lf)*, and that were regulated in the same direction between all *egl-9(lf)* genotypes. We did not find any genes that met these conditions.

We also searched for genes with *hif-1* independent, *vhl-1*-dependent gene expression and found 45 genes, which can be found in the Supplementary Table 2. Finally, we searched for candidates directly regulated by *hif-1*. Initially, we searched for genes that had were significantly altered in *hif-1(lf)* genotypes in one direction, but altered in the opposite direction in mutants that activate the HIF-1 response. Only

two genes (*R08E5.3*, and *nit-1*) met these conditions. This could reflect the fact that HIF-1 exists at very low levels in *C. elegans*, so loss of function mutations in *hif-1* might only have mild effects on its transcriptional targets. We reasoned that genes that are overexpressed in mutants that induce the HIF-1 response would be enriched for genes that are direct candidates. We found 195 genes which have consistently increased expression in mutants with a constitutive hypoxic response (Supplementary Table 3).

Enrichment analysis of the hypoxia response

To validate that our transcriptomes were correct, and to understand how functionalities may vary between them, we subjected each decoupled response to enrichment analysis using the WormBase Enrichment Suite (Angeles-Albores, N. Lee, et al., 2016; Angeles-Albores, R. Y. Lee, et al., 2017).

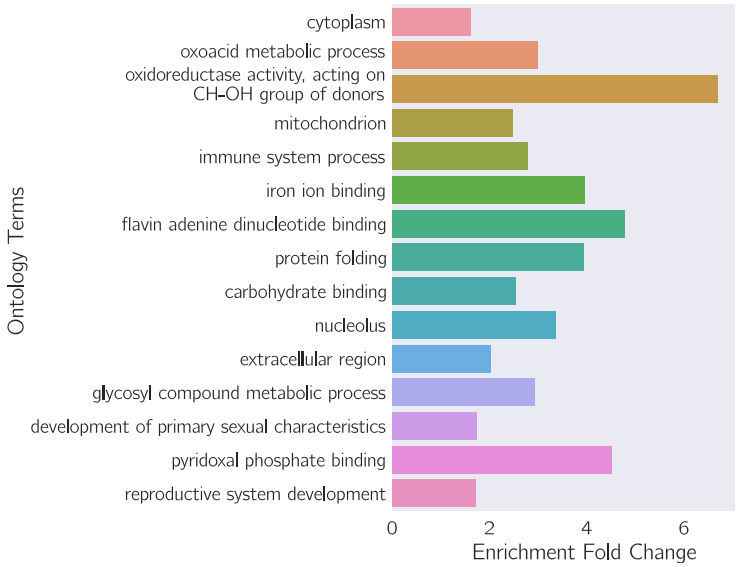

Figure 2.9: Gene ontology enrichment analysis of genes associated with the main hypoxia response. A number of terms reflecting catabolism and bioenergetics are enriched.

We used gene ontology enrichment analysis (GEA) on the main hypoxia response program. This showed that the terms 'oxoacid metabolic process' ($q < 10^{-4}$, 3.0 fold-change, 24 genes), 'iron ion binding' ($q < 10^{-2}$, 3.8 fold-change, 10 genes), and 'immune system process' ($q < 10^{-3}$, 2.9 fold-change, 20 genes) were significantly enriched. GEA also showed enrichment of the term 'mitochondrion' ($q < 10^{-3}$, 2.5 fold-change, 29 genes) (see Fig. 2.9). Indeed, *hif-1(lf)* has been implicated in all of these biological and molecular functions (Luhachack et al., 2012; Ackerman

and Gems, 2012; Romney et al., 2011; Gregg L. Semenza, 2011). As benchmark on the quality of our data, we selected a set of 22 genes known to be responsive to HIF-1 levels from the literature and asked whether these genes were present in our hypoxia response list. We found $8/22$ known genes, which constitutes a statistically significant result ($p < 10^{10}$). The small number of reporters found in this list probably reflects the conservative nature of our estimates. We studied the *hif-1*-independent, *vhl-1*-dependent gene set using enrichment analysis but no terms were significantly enriched.

Identification of non-classical epistatic interactions

hif-1(lf) has traditionally been viewed as existing in a genetic OFF state under normoxic conditions. However, our dataset indicates that 546 genes show altered expression when *hif-1* function is removed in normoxic conditions. Moreover, we observed positive correlations between *hif-1(lf)* β coefficients and *egl-9(lf)*, *vhl-1(lf)* and *rhy-1(lf)* β coefficients in spite of the negative regulatory relationships between these genes and *hif-1*. Such positive correlations could indicate a different relationship between these genes than has previously been reported, so we attempted to substantiate them through epistasis analyses.

To perform epistasis analyses, we first identified genes that exhibited violations of the canonical genetic model of the hypoxia pathway. To this end, we searched for genes that exhibited different behaviors between *egl-9(lf)* and *vhl-1(lf)*, or between *rhy-1(lf)* and *vhl-1(lf)* (we assume that all results from the *rhy-1(lf)* transcriptome reflect a complete loss of *egl-9* activity). We found 31 that satisfied this condition (see Fig. 2.10, Supplemental Table 4). Additionally, many of these genes exhibited a new kind of epistasis: *egl-9* was epistatic over *vhl-1*. Identification of a set of genes that have a consistent set of relationships between themselves suggests that we have identified a new aspect of the hypoxia pathway.

To illustrate this, we focused on three genes, *nlp-31*, *ftn-1* and *ftn-2*, which had epistasis patterns that we felt reflected the population well. *ftn-1* and *ftn-2* are both described in the literature as genes that are responsive to mutations in the hypoxia pathway. Moreover, these genes have been previously described to have aberrant behaviors (Ackerman and Gems, 2012; Romney et al., 2011), specifically the opposite effects of *egl-9(lf)* and *vhl-1(lf)*. These studies showed that loss of *vhl-1(lf)* decreases expression of *ftn-1* and *ftn-2* using both RNAi and alleles, which allays concerns of strain-specific interference. Moreover, Ackerman and Gems

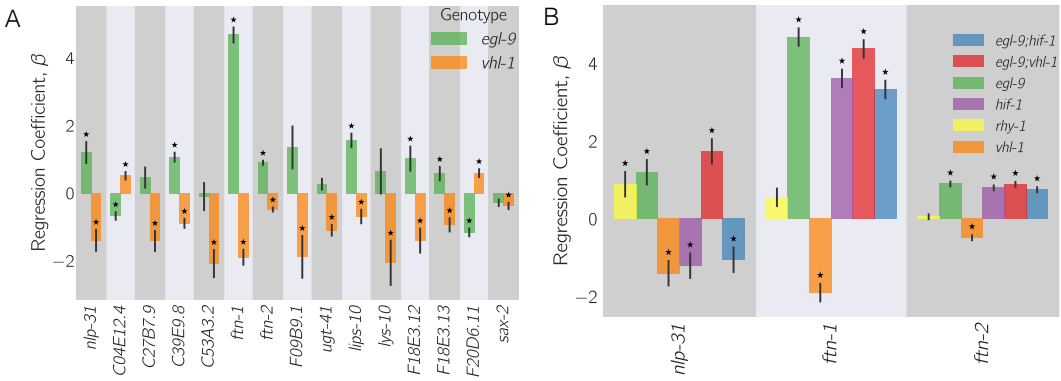

Figure 2.10: **A**. 27 genes in *C. elegans* exhibit non-classical epistasis in the hypoxia pathway, characterized by opposite effects on gene expression, relative to the wild-type, of of the *vhl-1(lf)* compared to *egl-9(lf)* (or *rhy-1(lf)*) mutants. Shown are a random selection of 15 the 27 genes for illustrative purposes. **B**. Representative genes showing that non-canonical epistasis shows a consistent pattern. *vhl-1(lf)* mutants have an opposite effect to *egl-9(lf)*, but *egl-9* remains epistatic to *vhl-1* and loss-of-function mutations in *hif-1* suppress the *egl-9(lf)* phenotype. Asterisks show β values significantly different from 0 relative to wild-type ($q < 10^{-1}$).

(2012) showed that *vhl-1* is epistatic to *hif-1* for the *ftn-1* expression phenotype, and that loss of HIF-1 is associated with increased expression of *ftn-1* and *ftn-2*. We observed that *hif-1* was epistatic to *egl-9*, and that *egl-9* and *hif-1* both promoted *ftn-1* and *ftn-2* expression.

Epistasis analysis of *ftn-1* and *ftn-2* expression reveals that *egl-9* is epistatic to *hif-1*; that *vhl-1* has opposite effects to *egl-9*, and that *vhl-1* is epistatic to *egl-9*. Analysis of *nlp-31* reveals similar relationships. *nlp-31* expression is decreased in *hif-1(lf)*, and increased in *egl-9(lf)*. However, *egl-9* is epistatic to *hif-1*. Like *ftn-1* and *ftn-2*, *vhl-1* has the opposite effect to *egl-9*, yet is epistatic to *egl-9*. We propose in the Discussion a model for how HIF-1 might regulate these targets.

HIF-1 in the cellular context

We identified the transcriptional changes associated with bioenergetic pathways in *C. elegans* by extracting from WormBase all genes associated with the tricarboxylic acid (TCA) cycle, the electron transport chain (ETC) and with the *C. elegans* GO term energy reserve. Previous research has described the effects of mitochondrial dysfunction in eliciting the hypoxia response (S. J. Lee, Hwang, and Kenyon, 2010), but transcriptional control of bioenergetic pathways by HIF-1 has not been studied as extensively in *C. elegans* as in vertebrates (see, for example (G L Semenza et al.,

1994; Gregg L. Semenza, 2012)). We also searched for the changes in ribosomal components and the proteasome, as well as for terms relating to immune response (see Fig 2.11).

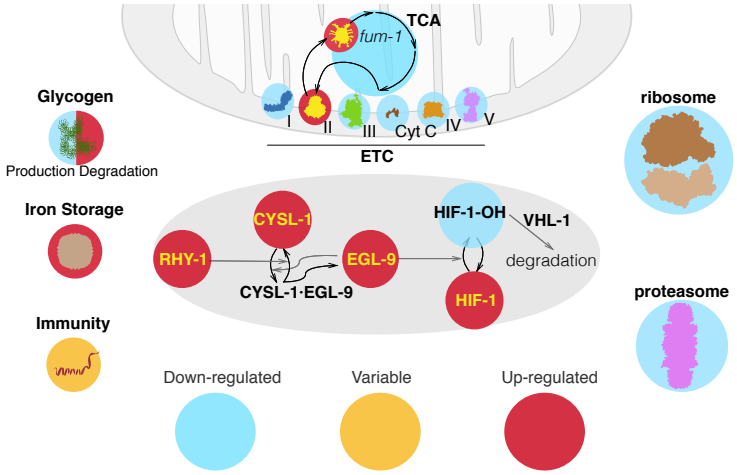

Figure 2.11: A graphic summary of the genome-wide effects of HIF-1 from our RNA-seq data.

Bioenergetic pathways

Our data shows that most of the enzymes involved in the TCA cycle and in the ETC are downregulated when HIF-1 is induced in agreement with the previous literature (Gregg L. Semenza, 2012). However, the fumarase gene *fum-1* and the mitochondrial complex II stood out as notable exceptions to the trend, as they were upregulated in every single genotype that causes deployment of the hypoxia response. FUM-1 catalyzes the reaction of fumarate into malate, and complex II catalyzes the reaction of succinate into fumarate. Complex II has been identified as a source of reserve respiratory capacity in neonatal rat cardiomyocytes previously (Pfleger, He, and Abdellatif, 2015). We found two energy reserve genes that were downregulated by HIF-1. *aagr-1* and *aagr-2*, which are predicted to function in glycogen catabolism (Sikora et al., 2010). Three distinct genes involved in energy reserve were upregulated. These genes were *ogt-1*, which encodes O-linked GlcNac Transferase gene; *T04A8.7*, encoding an ortholog of human glucosidase, acid beta (GBA); and *T22F3.3*, encoding ortholog of human glycogen phosphorylase isozyme in the muscle (PYGM).

Protein synthesis and degradation

hif-1(lf) is also known to inhibit protein synthesis and translation in varied ways. (Brugarolas et al., 2004). Most reported effects of HIF-1 on the translation machinery are posttranslational, and no reports to date show transcriptional control of the ribosomal machinery in *C. elegans* by HIF-1. We used the WormBase Enrichment Suite Gene Ontology dictionary (Angeles-Albores, R. Y. Lee, et al., 2017) to extract 143 protein-coding genes annotated as 'structural constituents of the ribosome' and we queried whether they were differentially expressed in our mutants. *egl-9(lf)*, *vhl-1(lf)*, *rhy-1(lf)* and *egl-9(lf)*;*vhl-1(lf)* showed differential expression of 91 distinct ribosomal constituents (not all constituents were detected in all genotypes). For every one of these genotypes, these genes were always downregulated. In contrast, *hif-1(lf)* showed upregulation of a single ribosomal constituent.

Next, we asked whether HIF-1 has any transcriptional effects on the proteasomal constituents; no such effects of HIF-1 on the proteasome have been reported in *C. elegans*. Out of 40 WormBase-annotated proteasomal constituents, we found 31 constituents that were differentially expressed in at least one of the four genotypes that induce a hypoxic response. Every gene we found was downregulated in at least two out of the four genotypes we studied.

Discussion

The *C. elegans* hypoxia pathway can be reconstructed entirely from RNA-seq data

In this paper, we have shown that whole-organism transcriptomic phenotypes can be used to reconstruct genetic pathways and to discern previously overlooked or uncharacterized genetic interactions. We successfully reconstructed the hypoxia pathway, and inferred order of action (*rhy-1* activates *egl-9*, *egl-9* and *vhl-1* inhibit *hif-1*), and we were able to infer from transcriptome-wide epistasis measurements that *egl-9* exerts *vhl-1*-dependent and independent inhibition on *hif-1*.

HIF-1 and the cellular environment

In addition to reconstructing the pathway, our dataset allowed us to observe a wide variety of physiologic changes that occur as a result of the HIF-1-dependent hypoxia response. In particular, we observed downregulation of most components of the TCA cycle and the mitochondrial electron transport chain with the exceptions of *fum-1* and the mitochondrial complex II. The mitochondrial complex II catalyzes

the reaction of succinate into fumarate. In mouse embryonic fibroblasts, fumarate has been shown to antagonize HIF-1 prolyl hydroxylase domain (PHD) enzymes, which are orthologs of EGL-9 (Sudarshan et al., 2009). If the inhibitory role of fumarate on PHD enzymes is conserved in *C. elegans*, upregulation of complex II by HIF-1 during hypoxia may increase intracellular levels of fumarate, which in turn could lead to artificially high levels of HIF-1 even after normoxia resumes. The increase in fumarate produced by the complex could be compensated by increasing expression of *fum-1*. Increased fumarate degradation allows *C. elegans* to maintain plasticity in the hypoxia pathway, keeping the pathway sensitive to oxygen levels.

Interpretation of the non-classical epistasis in the hypoxia pathway

The observation of almost 30 genes that exhibit a specific pattern of non-classical epistasis suggests the existence of previously undescribed aspects of the hypoxia pathway. Some of these non-classical epistases had been observed previously (Ackerman and Gems, 2012; Romney et al., 2011; Luhachack et al., 2012), but no satisfactory mechanism has been proposed to explain this biology. Romney et al. (2011) and Ackerman and Gems (2012) suggest that HIF-1 integrates information on iron concentration in the cell to bind to the *ftn-1* promoter, but could not definitively establish a mechanism. It is unclear why deletion of *hif-1* induces *ftn-1* expression, deletion of *egl-9* also causes induction of *ftn-1* expression, but deletion of *vhl-1* abolishes this induction. Moreover, Luhachack et al. (2012) have previously reported that certain genes important for the *C. elegans* immune response against pathogens reflect similar expression patterns. Their interpretation was that *swan-1*, which encodes a binding partner to EGL-9 (Shao, Zhang, Ye, et al., 2010), is important for modulating HIF-1 activity in some manner. The lack of a conclusive double mutant analysis in this work means the role of SWAN-1 in modulation of HIF-1 activity remains to be demonstrated. Nevertheless, mechanisms that call for additional transcriptional modulators become less likely given the number of genes with different biological functions that exhibit the same pattern.

One way to resolve this problem without invoking additional genes is to consider HIF-1 as a protein with both activating and inhibiting states. In fact, HIF-1 already exists in two states in *C. elegans*: unmodified HIF-1 and HIF-1-hydroxyl (HIF-1-OH). Under this model, HIF-1-hydroxyl antagonizes the effects of HIF-1 for certain genes like *ftn-1* or *nlp-31*. Loss of *vhl-1* stabilizes HIF-1-hydroxyl. A subset of genes that are sensitive to HIF-1-hydroxyl will be inhibited as a result of the increase in the amount of this species, in spite of loss of *vhl-1* function also increasing the

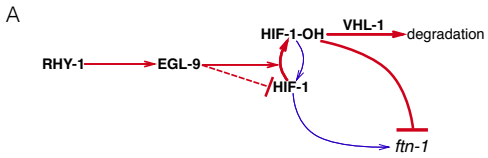

B

Genotype	Interpretation	
wild type	HIF-1 → *ftn-1* ⊣ HIF-1-OH	
egl-9	HIF-1 → *ftn-1*	HIF-1 activates/ HIF-1-OH represses
vhl-1	HIF-1 → *ftn-1* ⊣ HIF-1-OH	HIF-1-OH represses
hif-1	*ftn-1*	Depends on specific activities/ concentrations at S.S.
egl-9; hif-1	*ftn-1*	Depends on specific activities/ concentrations at S.S.
egl-9; vhl-1	HIF-1 → *ftn-1*	HIF-1 activates/ HIF-1-OH represses

Figure 2.12: A hypothetical model showing a mechanism where HIF-1-hydroxyl antagonises HIF-1. **A**. Diagram showing that RHY-1 activates EGL-9. EGL-9 hydroxylates HIF-1 in an oxygen dependent fashion. Under normoxia, HIF-1 is rapidly hydroxylated and only slowly does hydroxylated HIF-1 return to its original state. EGL-9 can also inhibit HIF-1 in an oxygen-independent fashion. HIF-1 hydroxyl is rapidly degraded in a VHL-1 dependent fashion. In our model, HIF-1 and HIF-1 hydroxyl have opposing effects on transcription. The width of the arrows represents the rates under normoxic conditions. **B**. Table showing the effects of loss-of-function mutations on HIF-1 and HIF-1 hydroxyl activity, showing how this can potentially explain the behavior of *ftn-1* in each case. S.S = Steady-state.

level of non-hydroxylated HIF-1. On the other hand, *egl-9(lf)* selectively removes all HIF-1-hydroxyl, stimulating accumulation of HIF-1 and promoting gene activity. Whether deletion of *hif-1(lf)* is overall activating or inhibiting will depend on the relative activity of each protein state under normoxia (see Fig. 2.12).

Multiple lines of circumstantial evidence that HIF-1-hydroxyl plays a role in the functionality of the hypoxia pathway. First, HIF-1-hydroxyl is challenging to study genetically because no mimetic mutations are available with which to study the pure hydroxylated HIF-1 species. Second, although mutations in the Von-Hippel Landau gene stabilize the hydroxyl species, they also increase the quantity of non-hydroxylated HIF-1 by mass action. Finally, since HIF-1 is detected low levels in cells under normoxic conditions (Wang and G L Semenza, 1993), total HIF-1 protein (unmodified HIF-1 plus HIF-1-hydroxyl) is often tacitly assumed to be vanishingly rare and therefore biologically inactive.

Our data show hundreds of genes that change expression in response to loss of *hif-1* under normoxic conditions. This establishes that there is sufficient total HIF-1 protein to be biologically active. Our analyses also revealed that *hif-1(lf)* shares

positive correlations with *egl-9(lf)*, *rhy-1(lf)* and *vhl-1(lf)*, and that each of these genotypes also shows a secondary negative rank-ordered expression correlation with each other. These cross-patterns between all loss of function of inhibitors of HIF-1 and *hif-1(lf)* can be most easily explained if HIF-1-hydroxyl is biologically active.

A homeostatic argument can be made in favor of the activity of HIF-1-hydroxyl. At any point in time, the cell must measure the levels of multiple metabolites at once. The *hif-1*-dependent hypoxia response integrates information from O_2, α-ketoglutarate (2-oxoglutarate) and iron concentrations in the cell. One way to integrate this information is by encoding it only in the effective hydroxylation rate of HIF-1 by EGL-9. Then the dynamics in this system will evolve exclusively as a result of the total amount of HIF-1 in the cell. Such a system can be sensitive to fluctuations in the absolute concentration of HIF-1 (Goentoro et al., 2009). Since the absolute levels of HIF-1 are low in normoxic conditions, small fluctuations in protein copy-number can represent a large fold-change in HIF-1 levels. These fluctuations would not be problematic for genes that must be turned on only under conditions of severe hypoxia—presumably, these genes would be associated with low affinity sites for HIF-1, so that they are only activated when HIF-1 levels are far above random fluctuations.

For yet other sets of genes that must change expression in response to the hypoxia pathway, it may not make as much sense to integrate metabolite information exclusively via EGL-9-dependent hydroxylation of HIF-1. In particular, genes that may function to increase survival in mild hypoxia may benefit from regulatory mechanisms that can sense minor changes in environmental conditions and which therefore benefit from robustness to transient changes in protein copy number. Likewise, genes that are involved in iron or α-ketoglutarate metabolism (such as *ftn-1*) may benefit from being able to sense, accurately, small and consistent deviations from basal concentrations of these metabolites. For these genes, the information may be better encoded by using HIF-1 and HIF-1-hydroxyl as an activator/repressor pair. Such circuits are known to possess distinct advantages for controlling output in a manner that is robust to transient fluctuations in the levels of their components (Hart, Antebi, et al., 2012; Hart and Alon, 2013).

Our RNA-seq data suggests that one of these atypical targets of HIF-1 may be RHY-1. Although *rhy-1* does not exhibit non-classical epistasis, *hif-1(lf)* and *egl-9(lf) hif-1(lf)* both had increased expression levels of *rhy-1*. We speculate that if *rhy-1* is controlled

by both HIF-1 and HIF-1-hydroxyl, then this might imply that HIF-1 regulates the expression of its pathway (and therefore itself) in a manner that is robust to total HIF-1 levels.

Insights into genetic interactions from vectorial phenotypes

Here, we have described a set of straightforward methods that can be in theory applied to any vectorial phenotype. Genome-wide methods afford a lot of information, but genome-wide interpretation of the results is often extremely challenging. Each method has its own advantages and disadvantages. We briefly discuss these methods, their uses and their drawbacks.

Principal component analysis is computationally tractable and clusters can often be visually detected with ease. However, PCA can be misleading, especially when the dimensions represented do not explain a very large fraction of the variance present in the data. In addition, principal dimensions are the product of a linear combination of vectors, and therefore must be interpreted with extreme care. In this case, the first principal dimension separated genotypes that increase HIF-1 protein levels from those that decrease it, but this dimension is a mix of vectors of change in gene expression. Although PCA showed that there is information hidden in these genotypes, it was not enough by itself to provide biological insight.

Whereas PCA operates on all genotypes simultaneously, correlation analysis is a pairwise procedure that measures how predictable the gene expression changes are in a mutant given the vector of expression changes in another. Like PCA, correlation analysis is easy and fast to perform. Unlike PCA, the product of a correlation analysis is a single number with a straightforward interpretation. However, correlation analysis is particularly sensitive to outliers. Although a common strategy is to rank-transform expression data to mitigate outliers, rank-transformations do not remove the cross-patterns that appear when feedback loops or other complex interactions are present between two genes. Such cross-patterns can still lead to vanishing correlations if both patterns are equally strong. Therefore, correlation analyses must take into account the possible existence of systematic outliers. Moreover, correlation values must be measured for both interactions in cross-patterned rank plots. Weighted correlations could be informative for ordering genes along pathways. A drawback of correlation analysis is that the number of pairwise comparisons that must be made increases combinatorially, though strategies could be used to decrease the total number of effective comparisons.

Epistasis plots are a novel way to visualize epistasis in vectorial phenotypes. Here, we have shown how an epistasis plot can be used to identify interactions between two single mutants and a double mutant. In reality, epistasis plots can be generated for any set of measurements involving a set of N mutants and an N-mutant genotype. Epistasis plots can accumulate an arbitrary number of points within them, possess a rich structure that can be visualized and have straightforward interpretations for special slope values.

Another way to analyze epistasis is via general linear models (GLMs) that include interaction terms between two or more genes. In this way, GLMs can quantify the epistatic effect of an interaction on single genes. We and others (Dixit et al., 2016; Angeles-Albores, Leighton, et al., 2016) have previously used GLMs to identify gene sets that are epistatically regulated by two or more inputs. While powerful, GLMs suffer from the multiple comparison problem. Correcting for false positives using well-known multiple comparison corrections such as FDR (Storey and Tibshirani, 2003) tends to increase false negative rates. Moreover, since GLMs attempt to estimate effect magnitudes for individual gene or isoform expression levels, they effectively treat each gene as an independent quantity, which prevents better estimation of the magnitude and direction of the epistasis between two genes.

Epistasis plots do not suffer from the multiple comparison problem because the number of tests performed is orders of magnitudes smaller than the number of tests performed by GLMs. Ideally, in an epistasis plot we need only perform 3 tests—rejection of additive, unbranched and suppressive null models—compared with the tens of thousands of tests that are performed in GLMs. Moreover, the magnitude of epistasis between two genes can be estimated using hundreds of genes, which greatly improves the statistical resolution of the epistatic coefficient. This increased resolution is important because the size and magnitude of the epistasis has specific consequences for the type of pathway that is expected.

Any quantitative use of genome-wide datasets requires a good experimental setup. Here, we have demonstrated that whole-organism RNA-seq can be used to dissect molecular pathways in exquisite detail when paired with experimental designs that are motivated by classical genetics. Much more research will be necessary to understand whether epistasis has different consequences in the microscopic realm of transcriptional phenotypes than in the macroscopic world that geneticists have explored previously. Our hope is that these tools, coupled with the classic genetics experimental designs, will reveal hitherto unknown aspects of genetics theory.

Methods

Nematode strains and culture

Strains used were N2 wild-type Bristol, CB5602 *vhl-1*(*ok161*), CB6088 *egl-9*(*sa307*) *hif-1*(*ia4*), CB6116 *egl-9*(*sa307*);*vhl-1*(*ok161*), JT307 *egl-9*(*sa307*), ZG31 *hif-1*(*ia4*), RB1297 *rhy-1*(*ok1402*). All lines were grown on standard nematode growth media (NGM) plates seeded with OP50 *E. coli* at 20°C (Brenner 1974).

RNA Isolation

Unsynchronized lines were grown on NGM plates at 20C and eggs harvested by sodium hypochlorite treatment. Eggs were plated on 6 to 9 6cm NGM plates with ample OP50 *E. coli* to avoid starvation and grown at 20°C. Worms were staged and harvested based on the time after plating, vulva morphology and the absence of eggs. Approximately 30–50 non-gravid young adults were picked and placed in 100μL of TE pH 8.0 at 4°C in 0.2mL PCR tubes. After settling and a brief spin in microcentrifuge approximately 80μL of TE (Ambion AM 9849) was removed from the top of the sample and individual replicates were snap frozen in liquid N2. These replicate samples were then digested with Proteinase K (Roche Lot No. 03115 838001 Recombinant Proteinase K PCR Grade) for 15min at 60° in the presence of 1% SDS and 1.25μL RNA Secure (Ambion AM 7005). RNA samples were then taken up in 5 Volumes of Trizol (Tri Reagent Zymo Research) and processed and treated with DNase I using Zymo MicroPrep RNA Kit (Zymo Research Quick-RNA MicroPrep R1050). RNA was eluted in RNase-free water and divided into aliquots and stored at -80°C. One aliquot of each replicate was analyzed using a NanoDrop (Thermo Fisher) for impurities, Qubit for concentration and then analyzed on an Agilent 2100 BioAnalyzer (Agilent Technologies). Replicates were selected that had RNA integrity numbers (RIN) equal or greater than 9.0 and showed no evidence of bacterial ribosomal bands, except for the ZG31 mutant where one of three replicates had a RIN of 8.3.

Library Preparation and Sequencing

10ng of quality checked total RNA from each sample was reverse-transcribed into cDNA using the Clontech SMARTer Ultra Low Input RNA for Sequencing v3 kit (catalog #634848) in the SMARTSeq2 protocol (Picelli et al., 2014). RNA was denatured at 70°C for 3 minutes in the presence of dNTPs, oligo dT primer and spiked-in quantitation standards (NIST/ERCC from Ambion, catalog #4456740). After chilling to 4°C, the first-strand reaction was assembled using the LNA TSO

primer described in Picelli et al. (2014), and run at 42°C for 90 minutes, followed by denaturation at 70°C for 10 minutes. The entire first strand reaction was then used as template for 13 cycles of PCR using the Clontech v3 kit. Reactions were cleaned up with 1.8X volume of Ampure XP SPRI beads (catalog #A63880) according to the manufacturer's protocol. After quantification using the Qubit High Sensitivity DNA assay, a 3ng aliquot of the amplified cDNA was run on the Agilent HS DNA chip to confirm the length distribution of the amplified fragments. The median value for the average cDNA lengths from all length distributions was 1076bp. Tagmentation of the full length cDNA for sequencing was performed using the Illumina/Nextera DNA library prep kit (catalog #FC-121–1030). Following Qubit quantitation and Agilent BioAnalyzer profiling, the tagmented libraries were sequenced. Libraries were sequenced on Illumina HiSeq2500 in single read mode with the read length of 50nt to an average depth of 15 million reads per sample following manufacturer's instructions. Base calls were performed with RTA 1.13.48.0 followed by conversion to FASTQ with bcl2fastq 1.8.4. Spearman correlation of the transcripts per million (TPM) for each genotype showed that every pairwise correlation within genotype was > 0.9.

Read Alignment and Differential Expression Analysis

We used Kallisto to perform read pseudo-alignment and performed differential analysis using Sleuth. We fit a general linear model for a transcript t in sample i:

$$y_{t,i} = \beta_{t,0} + \beta_{t,genotype} \cdot X_{t,i} + \beta_{t,batch} \cdot Y_{t,i} + \epsilon_{t,i} \tag{2.1}$$

where $y_{t,i}$ are the logarithm transformed counts; $\beta_{t,genotype}$ and $\beta_{t,batch}$ are parameters of the model, and which can be interpreted as biased estimators of the log-fold change; $X_{t,i}, Y_{t,i}$ are indicator variables describing the conditions of the sample; and $\epsilon_{t,i}$ is the noise associated with a particular measurement.

Genetic Analysis, Overview

Genetic analysis of the processed data was performed in Python 3.5. Our scripts made extensive use of the Pandas, Matplotlib, Scipy, Seaborn, Sklearn, Networkx, Bokeh, PyMC3, and TEA libraries (Bokeh Development Team, 2014; McKinney, 2011; Oliphant, 2007; Pedregosa et al., 2012; Salvatier, Wiecki, and Fonnesbeck, 2015; Van Der Walt, Colbert, and Varoquaux, 2011; Hunter, 2007; Angeles-Albores, N. Lee, et al., 2016; Waskom et al., 2016). Our analysis is available in a Jupyter

Notebook (Pérez and Granger, 2007). All code and required data (except the raw reads) are available at https://github.com/WormLabCaltech/mprsq along with version-control information. Our Jupyter Notebook and interactive graphs for this project can be found at https://wormlabcaltech.github.io/mprsq/. Raw reads were deposited in the Short Read Archive under the study accession number SRP100886.

Weighted Correlations

Pairwise correlations between transcriptomes where calculated by first identifying the set of differentially expressed genes (DEGs) common to both transcriptomes under analysis. DEGs were then rank-ordered according to their regression coefficient, β. Bayesian robust regressions were performed using a Student-T distribution. Bayesian analysis was performed using the PyMC3 library (Salvatier, Wiecki, and Fonnesbeck, 2015) (`pm.glm.families.StudenT` in Python). If the correlation has an average value > 1, the correlation coefficient was set to 1.

Weights were calculated as the proportion of genes that were < 1.5 standard deviations away from the primary regression out of the entire set of shared DEGs for each transcriptome.

Epistasis Analysis

For a double mutant X^-Y^-, we used the single mutants X^- and Y^- to find expected value of the coefficient for a double mutant under an additive model for each isoform i. Specifically,

$$\beta_{\text{Add},i} = \beta_{X,i} + \beta_{Y,i}. \tag{2.2}$$

Next, we find the difference, Δ_i, between the observed double mutant expression coefficient, $\beta_{XY,\text{Obs},i}$, and the predicted expression coefficient under an additive model for each isoform i.

To calculate the transcriptome-wide epistasis coefficient, we plotted $(\beta_{\text{Add},i}, \Delta_i)$ and found the line of best fit using orthogonal distance regression using the `scipy.odr` package in Python. We performed non-parametric bootstrap sampling of the ordered tuples with replacement using 5,000 iterations to generate a probability distribution of slopes of best fit.

There are as many models as epistatic relationships. For quantitative phenotypes,

epistatic relationships (except synthetic interactions) can be generally expressed as:

$$\beta_{XY} = \sum_{g \in G} \lambda_g \beta_g, \tag{2.3}$$

where P_i is the quantitative phenotype belonging to the genotype i; G is the set of single mutants $\{X, Y\}$ that make up the double mutant, XY; and λ_g is the contribution of the phenotype P_g to P_{XY}. Additive interactions between genes are the result of setting $\lambda_g = 1$. All other relationships correspond to setting $\lambda_X = 0$, $\lambda_Y = 1$ or $\lambda_X = 1$, $\lambda_Y = 0$.

A given epistatic interaction can be simulated by predicting the double mutant phenotype under that interaction and re-calculating the y-coordinates. The recalculated y-coordinates can then be used to predict the possible epistasis coefficients for the cases where X is epistatic over Y, and Y is epistatic over X.

To select between theoretical models, we implemented an approximate Bayesian Odds Ratio. We defined a free-fit model, M_1, that found the line of best fit for the data:

$$P(\alpha \mid M_1, D) \propto \prod_{(x_i, y_i, \sigma_i) \in D} \exp \frac{(y_i - \alpha \cdot x_i)^2}{2\sigma_i} \cdot (1 + \alpha^2)^{-3/2}, \tag{2.4}$$

where α is the slope of the model to be determined, x_i, y_i were the x- and y-coordinates of each point respectively, and σ_i was the standard error associated with the y-value. We minimized the negative logarithm of equation 2.4 to obtain the most likely slope given the data, D (`scipy.optimize.minimize` in Python). Finally, we approximated the odds ratio as:

$$OR = \frac{P(D \mid \alpha^*, M_1) \cdot (2\pi)^{1/2} \sigma_{\alpha^*}}{P(D \mid M_i)}, \tag{2.5}$$

where α^* is the slope found after minimization, σ^*_α is the standard deviation of the parameter at the point α^* and $P(D \mid M_i)$ is the probability of the data given the parameter-free model, M_i.

Enrichment Analysis

Tissue, Phenotype and Gene Ontology Enrichment Analysis were carried out using the WormBase Enrichment Suite for Python (Angeles-Albores, R. Y. Lee, et al., 2017; Angeles-Albores, N. Lee, et al., 2016).

Author Contributions:

This work was supported by HHMI with whom PWS is an investigator and by the Millard and Muriel Jacobs Genetics and Genomics Laboratory at California Institute of Technology. All strains were provided by the CGC, which is funded by NIH Office of Research Infrastructure Programs (P40 OD010440). This article was written with support of the Howard Hughes Medical Institute. This article wouldn't be possible without help from Dr._ Igor Antoshechkin who performed all sequencing. We thank Hillel Schwartz for all of his careful advice. We would like to thank Jonathan Liu, Han Wang, and Porfirio Quintero for helpful discussion.

References

Ackerman, Daniel and David Gems (2012). "Insulin/IGF-1 and hypoxia signaling act in concert to regulate iron homeostasis in *Caenorhabditis elegans*". In: *PLoS Genetics* 8.3. ISSN: 15537390. DOI: 10.1371/journal.pgen.1002498.

Adamson, Britt et al. (2016). "A Multiplexed Single-Cell CRISPR Screening Platform Enables Systematic Dissection of the Unfolded Protein Response". In: *Cell* 167.7, 1867–1882.e21. ISSN: 00928674. DOI: 10.1016/j.cell.2016.11.048.

Angeles-Albores, David, Raymond Y Lee, et al. (2017). "Phenotype and gene ontology enrichment as guides for disease modeling in C. elegans". In: *bioRxiv*. DOI: 10.1101/106369.

Angeles-Albores, David, Daniel H W Leighton, et al. (2016). "Transcriptomic Description of an Endogenous Female State in *C. elegans*". In: *bioRxiv*.

Angeles-Albores, David, Raymond Y. N. Lee, et al. (2016). "Tissue enrichment analysis for *C. elegans* genomics". In: *BMC Bioinformatics* 17.1, p. 366. ISSN: 1471-2105. DOI: 10.1186/s12859-016-1229-9.

Bellier, Audrey et al. (2009). "Hypoxia and the hypoxic response pathway protect against pore-forming toxins in *C. elegans*". In: *PLoS Pathogens* 5.12. ISSN: 15537366. DOI: 10.1371/journal.ppat.1000689.

Bishop, Tammie et al. (2004). "Genetic Analysis of Pathways Regulated by the von Hippel-Lindau Tumor Suppressor in *Caenorhabditis elegans*". In: *PLoS Biology* 2.10. ISSN: 15449173. DOI: 10.1371/journal.pbio.0020289.

Bokeh Development Team (2014). "Bokeh: Python library for interactive visualization". In:

Bray, Nicolas L et al. (2016). "Near-optimal probabilistic RNA-seq quantification." In: *Nature biotechnology* 34.5, pp. 525–7. ISSN: 1546-1696. DOI: 10.1038/nbt.3519.

Brem, Rachel B. et al. (2002). "Genetic Dissection of Transcriptional Regulation in Budding Yeast". In: *Science* 296.5568.

Brugarolas, James et al. (2004). "Regulation of mTOR function in response to hypoxia by REDD1 and the TSC1/TSC2 tumor suppressor complex". In: *Genes and Development* 18.23, pp. 1–12. ISSN: 08909369. DOI: 10.1101/gad.1256804.(mTOR).

Dixit, Atray et al. (2016). "Perturb-Seq: Dissecting Molecular Circuits with Scalable Single-Cell RNA Profiling of Pooled Genetic Screens". In: *Cell* 167.7, 1853–1866.e17. ISSN: 00928674. DOI: 10.1016/j.cell.2016.11.038.

Epstein, Andrew C. R. et al. (2001). "*C. elegans* EGL-9 and mammalian homologs define a family of dioxygenases that regulate HIF by prolyl hydroxylation". In: *Cell* 107.1, pp. 43–54. ISSN: 00928674. DOI: 10.1016/S0092-8674(01)00507-4.

Goentoro, Lea et al. (2009). "The Incoherent Feedforward Loop Can Provide Fold-Change Detection in Gene Regulation". In: *Molecular Cell* 36.5, pp. 894–899. ISSN: 10972765. DOI: 10.1016/j.molcel.2009.11.018.

Hart, Yuval and Uri Alon (2013). "The Utility of Paradoxical Components in Biological Circuits". In: *Molecular Cell* 49.2, pp. 213–221. ISSN: 10972765. DOI: 10.1016/j.molcel.2013.01.004.

Hart, Yuval, Yaron E Antebi, et al. (2012). "Design principles of cell circuits with paradoxical components". In: *Proceedings of the National Academy of Sciences of the United States of America* 109.21, pp. 8346–8351. ISSN: 0027-8424. DOI: 10.1073/pnas.1117475109.

Huang, L. Eric et al. (1996). "Activation of hypoxia-inducible transcription factor depends primarily upon redox-sensitive stabilization of its α subunit". In: *Journal of Biological Chemistry* 271.50, pp. 32253–32259. ISSN: 00219258. DOI: 10.1074/jbc.271.50.32253.

Huang, Linda S and Paul W Sternberg (2006). "Genetic dissection of developmental pathways." In: *WormBook : the online review of* C. elegans *biology* 1995, pp. 1–19. ISSN: 1551-8507. DOI: 10.1895/wormbook.1.88.2.

Hughes, Timothy R. et al. (2000). "Functional Discovery via a Compendium of Expression Profiles". In: *Cell* 102.1, pp. 109–126. ISSN: 00928674. DOI: 10.1016/S0092-8674(00)00015-5.

Hunter, John D. (2007). "Matplotlib: A 2D graphics environment". In: *Computing in Science and Engineering* 9.3, pp. 99–104. ISSN: 15219615. DOI: 10.1109/MCSE.2007.55.

Jiang, B H et al. (1996). "Dimerization, DNA binding, and transactivation properties of hypoxia-inducible factor 1." In: *The Journal of biological chemistry* 271.30, pp. 17771–17778. ISSN: 00219258. DOI: 10.1074/jbc.271.30.17771.

Jiang, Huaqi, Rong Guo, and Jo Anne Powell-Coffman (2001). "The *Caenorhabditis elegans* hif-1 gene encodes a bHLH-PAS protein that is required for adaptation to hypoxia." In: *Proceedings of the National Academy of Sciences of the United*

States of America 98.14, pp. 7916–7921. ISSN: 0027-8424. DOI: 10.1073/pnas.141234698.

Kaelin, William G. and Peter J. Ratcliffe (2008). "Oxygen Sensing by Metazoans: The Central Role of the HIF Hydroxylase Pathway". In: *Molecular Cell* 30.4, pp. 393–402. ISSN: 10972765. DOI: 10.1016/j.molcel.2008.04.009.

King, Elizabeth G. et al. (2014). "Genetic Dissection of the *Drosophila melanogaster* Female Head Transcriptome Reveals Widespread Allelic Heterogeneity". In: *PLoS Genetics* 10.5. Ed. by Greg Gibson, e1004322. ISSN: 1553-7404. DOI: 10.1371/journal.pgen.1004322.

Lee, Seung Jae, Ara B. Hwang, and Cynthia Kenyon (2010). "Inhibition of respiration extends *C. elegans* life span via reactive oxygen species that increase HIF-1 activity". In: *Current Biology* 20.23, pp. 2131–2136. ISSN: 09609822. DOI: 10.1016/j.cub.2010.10.057.

Li, Yang et al. (2006). "Mapping Determinants of Gene Expression Plasticity by Genetical Genomics in *C. elegans*". In: *PLoS Genetics* 2.12, e222. ISSN: 1553-7390. DOI: 10.1371/journal.pgen.0020222.

Loenarz, Christoph et al. (2011). "The hypoxia-inducible transcription factor pathway regulates oxygen sensing in the simplest animal, *Trichoplax adhaerens*". In: *EMBO reports* 12.1, pp. 63–70. ISSN: 1469-221X. DOI: 10.1038/embor.2010.170.

Luhachack, Lyly G. et al. (2012). "EGL-9 Controls *C. elegans* Host Defense Specificity through Prolyl Hydroxylation-Dependent and -Independent HIF-1 Pathways". In: *PLoS Pathogens* 8.7, p. 48. ISSN: 15537366. DOI: 10.1371/journal.ppat.1002798.

Ma, Dengke K. et al. (2012). "CYSL-1 Interacts with the O_2-Sensing Hydroxylase EGL-9 to Promote H_2S-Modulated Hypoxia-Induced Behavioral Plasticity in *C. elegans*". In: *Neuron* 73.5, pp. 925–940. ISSN: 08966273. DOI: 10.1016/j.neuron.2011.12.037.

McKinney, Wes (2011). "pandas: a Foundational Python Library for Data Analysis and Statistics". In: *Python for High Performance and Scientific Computing*, pp. 1–9.

Metzker, Michael L (2010). "Sequencing technologies - the next generation." In: *Nature reviews. Genetics* 11.1, pp. 31–46. ISSN: 1471-0056. DOI: 10.1038/nrg2626.

Mortazavi, Ali et al. (2008). "Mapping and quantifying mammalian transcriptomes by RNA-Seq". In: *Nature Methods* 5.7, pp. 621–628. ISSN: 1548-7091. DOI: 10.1038/nmeth.1226.

Oliphant, Travis E (2007). "SciPy: Open source scientific tools for Python". In: *Computing in Science and Engineering* 9, pp. 10–20. ISSN: 1521-9615. DOI: 10.1109/MCSE.2007.58.

Park, Eun Chan et al. (2012). "Hypoxia regulates glutamate receptor trafficking through an HIF-independent mechanism". In: *The EMBO Journal* 31.6, pp. 1618–1619. ISSN: 0261-4189. DOI: 10.1038/emboj.2012.44.

Patro, Rob, Geet Duggal, et al. (2016). "Salmon provides accurate, fast, and bias-aware transcript expression estimates using dual-phase inference". In: *bioRxiv*, p. 021592. DOI: 10.1101/021592.

Patro, Rob, Stephen M. Mount, and Carl Kingsford (2014). "Sailfish enables alignment-free isoform quantification from RNA-seq reads using lightweight algorithms". In: *Nature biotechnology* 32.5, pp. 462–464. ISSN: 1546-1696. DOI: 10.1038/nbt.2862.

Pedregosa, Fabian et al. (2012). "Scikit-learn: Machine Learning in Python". In: *Journal of Machine Learning Research* 12, pp. 2825–2830. ISSN: 15324435. DOI: 10.1007/s13398-014-0173-7.2.

Pérez, F. and B.E. Granger (2007). "IPython: A System for Interactive Scientific Computing Python: An Open and General- Purpose Environment". In: *Computing in Science and Engineering* 9.3, pp. 21–29. ISSN: 15219615. DOI: doi:10.1109/MCSE.2007.53..

Pfleger, J, M He, and M Abdellatif (2015). "Mitochondrial complex II is a source of the reserve respiratory capacity that is regulated by metabolic sensors and promotes cell survival". In: *Cell Death and Disease* 6.7, pp. 1–14. ISSN: 2041-4889. DOI: 10.1038/cddis.2015.202.

Phillips, Patrick C (2008). "Epistasis—the essential role of gene interactions in the structure and evolution of genetic systems". In: *Nat Rev Genet* 9.11, pp. 855–867. ISSN: 1471-0056. DOI: 10.1038/nrg2452.

Picelli, Simone et al. (2014). "Full-length RNA-seq from single cells using Smart-seq2." In: *Nature protocols* 9.1, pp. 171–81. ISSN: 1750-2799. DOI: 10.1038/nprot.2014.006.

Pimentel, Harold J et al. (2016). "Differential analysis of RNA-Seq incorporating quantification uncertainty". In: *bioRxiv*, p. 058164. DOI: 10.1101/058164.

Powell-Coffman, Jo Anne (2010). "Hypoxia signaling and resistance in *C. elegans*". In: *Trends in Endocrinology and Metabolism* 21.7, pp. 435–440. ISSN: 10432760. DOI: 10.1016/j.tem.2010.02.006.

Powell-Coffman, Jo Anne, Christopher A. Bradfield, and William B. Wood (1998). "*Caenorhabditis elegans* Orthologs of the Aryl Hydrocarbon Receptor and Its Heterodimerization Partner the Aryl Hydrocarbon Receptor Nuclear Translocator". In: *Proceedings of the National Academy of Sciences* 95.6, pp. 2844–2849. ISSN: 0027-8424. DOI: 10.1073/pnas.95.6.2844.

Romney, Steven Joshua et al. (2011). "HIF-1 regulates iron homeostasis in *Caenorhabditis elegans* by activation and inhibition of genes involved in iron uptake and storage". In: *PLoS Genetics* 7.12. ISSN: 15537390. DOI: 10.1371/journal.pgen.1002394.

Salvatier, John, Thomas Wiecki, and Christopher Fonnesbeck (2015). "Probabilistic Programming in Python using PyMC". In: *PeerJ Computer Science* 2.e55, pp. 1–24. ISSN: 2376-5992. DOI: 10.7717/peerj-cs.55.

Schadt, Eric E. et al. (2003). "Genetics of gene expression surveyed in maize, mouse and man". In: *Nature* 422.6929, pp. 297–302. ISSN: 00280836. DOI: 10.1038/nature01434.

Schwarz, Erich M., Mihoko Kato, and Paul W. Sternberg (2012). "Functional transcriptomics of a migrating cell in *Caenorhabditis elegans*." In: *Proceedings of the National Academy of Sciences of the United States of America* 109.40, pp. 16246–51. ISSN: 1091-6490. DOI: 10.1073/pnas.1203045109.

Scimone, M. Lucila et al. (2014). "Neoblast specialization in regeneration of the planarian *Schmidtea mediterranea*". In: *Stem Cell Reports* 3.2, pp. 339–352. ISSN: 22136711. DOI: 10.1016/j.stemcr.2014.06.001.

Semenza, G L et al. (1994). "Transcriptional regulation of genes encoding glycolytic enzymes by hypoxia-inducible factor 1." In: *The Journal of Biological Chemistry* 269.38, pp. 23757–63. ISSN: 0021-9258.

Semenza, Gregg L. (2011). "Hypoxia-inducible factor 1: Regulator of mitochondrial metabolism and mediator of ischemic preconditioning". In: *Biochimica et Biophysica Acta - Molecular Cell Research* 1813.7, pp. 1263–1268. ISSN: 01674889. DOI: 10.1016/j.bbamcr.2010.08.006.

– (2012). "Hypoxia-inducible factors in physiology and medicine". In: *Cell* 148.3, pp. 399–408. ISSN: 00928674. DOI: 10.1016/j.cell.2012.01.021.

Shalek, Alex K. et al. (2013). "Single-cell transcriptomics reveals bimodality in expression and splicing in immune cells". In: *Nature* 498.7453, pp. 236–40. ISSN: 1476-4687. DOI: 10.1038/nature12172.

Shao, Zhiyong, Yi Zhang, and Jo Anne Powell-Coffman (2009). "Two Distinct Roles for EGL-9 in the Regulation of HIF-1-mediated gene expression in *Caenorhabditis elegans*". In: *Genetics* 183.3, pp. 821–829. ISSN: 00166731. DOI: 10.1534/genetics.109.107284.

Shao, Zhiyong, Yi Zhang, Qi Ye, et al. (2010). "*C. elegans* SWAN-1 binds to EGL-9 and regulates HIF-1- mediated resistance to the bacterial pathogen *Pseudomonas aeruginosa* PAO1". In: *PLoS Pathogens* 6.8, pp. 91–92. ISSN: 15537366. DOI: 10.1371/journal.ppat.1001075.

Shen, Chuan, Daniel Nettleton, et al. (2005). "Roles of the HIF-1 hypoxia-inducible factor during hypoxia response in *Caenorhabditis elegans*". In: *Journal of Biological Chemistry* 280.21, pp. 20580–20588. ISSN: 00219258. DOI: 10.1074/jbc.M501894200.

Shen, Chuan, Zhiyong Shao, and Jo Anne Powell-Coffman (2006). "The *Caenorhabditis elegans rhy-1* Gene Inhibits HIF-1 Hypoxia-Inducible Factor Activity in a Negative Feedback Loop That Does Not Include *vhl-1*". In: *Genetics* 174.3, pp. 1205–1214. ISSN: 00166731. DOI: 10.1534/genetics.106.063594.

Sikora, Jakub et al. (2010). "Bioinformatic and biochemical studies point to AAGR-1 as the ortholog of human acid α-glucosidase in *Caenorhabditis elegans*". In: *Molecular and Cellular Biochemistry* 341.1-2, pp. 51–63. ISSN: 03008177. DOI: 10.1007/s11010-010-0436-3.

Singer, Meromit et al. (2016). "A Distinct Gene Module for Dysfunction Uncoupled from Activation in Tumor-Infiltrating T Cells". In: *Cell* 166.6, 1500–1511.e9. ISSN: 00928674. DOI: 10.1016/J.CELL.2016.08.052.

Storey, John D and Robert Tibshirani (2003). "Statistical significance for genomewide studies." In: *Proceedings of the National Academy of Sciences of the United States of America* 100.16, pp. 9440–5. ISSN: 0027-8424. DOI: 10.1073/pnas.1530509100.

Sudarshan, S. et al. (2009). "Fumarate hydratase deficiency in renal cancer induces glycolytic addiction and hypoxia-inducible transcription factor 1α stabilization by glucose-dependent generation of reactive oxygen species". In: *Mol Cell Biol* 29.15, pp. 4080–4090. ISSN: 0270-7306. DOI: 10.1128/MCB.00483-09.

Trapnell, Cole et al. (2013). "Differential analysis of gene regulation at transcript resolution with RNA-seq." In: *Nature biotechnology* 31.1, pp. 46–53. ISSN: 1546-1696. DOI: 10.1038/nbt.2450.

Van Der Walt, Stéfan, S. Chris Colbert, and Gaël Varoquaux (2011). "The NumPy array: A structure for efficient numerical computation". In: *Computing in Science and Engineering* 13.2, pp. 22–30. ISSN: 15219615. DOI: 10.1109/MCSE.2011.37.

Van Driessche, Nancy et al. (2005). "Epistasis analysis with global transcriptional phenotypes". In: *Nature Genetics* 37.5, pp. 471–477. ISSN: 1061-4036. DOI: 10.1038/ng1545.

Van Wolfswinkel, Josien C., Daniel E. Wagner, and Peter W. Reddien (2014). "Single-cell analysis reveals functionally distinct classes within the planarian stem cell compartment". In: *Cell Stem Cell* 15.3, pp. 326–339. ISSN: 18759777. DOI: 10.1016/j.stem.2014.06.007.

Wang, G L and G L Semenza (1993). "Characterization of hypoxia-inducible factor 1 and regulation of DNA binding activity by hypoxia." In: *The Journal of Biological Chemistry* 268.29, pp. 21513–8. ISSN: 0021-9258.

Waskom, Michael et al. (2016). “seaborn: v0.7.0 (January 2016)”. In: DOI: 10.5281/zenodo.45133.

Yeung, K. Y. and W. L. Ruzzo (2001). “Principal component analysis for clustering gene expression data.” In: *Bioinformatics (Oxford, England)* 17.9, pp. 763–774. ISSN: 1367-4803. DOI: 10.1093/bioinformatics/17.9.763.

Chapter 3

TRANSCRIPTOMIC DESCRIPTION OF AN ENDOGENOUS FEMALE STATE IN *C. ELEGANS*

Abstract

Understanding genome and gene function in a whole organism requires us to fully comprehend the life cycle and the physiology of the organism in question. Although *C. elegans* is traditionally thought of as a hermaphrodite, XX animals exhaust their sperm and become endogenous females after 3 days of egg-laying. The molecular physiology of this state has not been as intensely studied as other parts of the life cycle, despite documented changes in behavior and metabolism that occur at this stage. To study the female state of *C. elegans*, we measured the transcriptomes of 1st day adult hermaphrodites; endogenous, 6th day adult females; and at the same time points, mutant *fog-2(lf)* worms that have a feminized germline phenotype. At these time points, we could separate the effects of biological aging from the transition into the female state. *fog-2(lf)* mutants partially phenocopy 6 day adult wild-type animals and exhibit fewer differentially expressed genes as they age throughout these 6 days. Therefore, *fog-2* is epistatic to age as assessed by this transcriptomic phenotype, which indicates that both factors act on sperm status to mediate entry into the female state. These changes are enriched in transcription factors canonically associated with neuronal development and differentiation. Our data provide a high-quality picture of the changes that happen in global gene expression throughout the period of early aging in the worm.

Introduction

Transcriptome analysis by RNA-seq (Mortazavi et al., 2008) has allowed for in-depth analysis of gene expression changes between life stages and environmental conditions in many species (Gerstein et al., 2014; Blaxter et al., 2012). *Caenorhabditis elegans*, a genetic model nematode with extremely well defined and largely invariant development (Sulston and Horvitz, 1977; Sulston, Schierenberg, et al., 1983), has been subjected to extensive transcriptomic analysis across all stages of

larval development (Hillier et al., 2009; Boeck et al., 2016; Murray et al., 2012) and many stages of embryonic development (Boeck et al., 2016). Although RNA-seq was used to develop transcriptional profiles of the mammalian aging process soon after its invention (Magalhães, Finch, and Janssens, 2010), few such studies have been conducted in *C. elegans* past the entrance into adulthood.

A distinct challenge to the study of aging transcriptomes in *C. elegans* is the hermaphroditic lifestyle of wild-type individuals of this species. Young adult hermaphrodites are capable of self-fertilization (Sulston and Brenner, 1974; Corsi, Wightman, and Chalfie, 2015), and the resulting embryos will contribute RNA to whole-organism RNA extractions. Most previous attempts to study the *C. elegans* aging transcriptome have addressed the aging process only indirectly, or relied on the use of genetically or chemically sterilized animals to avoid this problem (Murphy et al., 2003; Halaschek-Wiener et al., 2005; Lund et al., 2002; McCormick et al., 2012; Eckley et al., 2013; Boeck et al., 2016; Rangaraju et al., 2015). In addition, most of these studies obtained transcriptomes using microarrays, which are less accurate than RNA-seq, especially for low-expressed genes (Wang et al., 2014).

Here, we investigate what we argue is a distinct state in the *C. elegans* life cycle, the endogenous female state. Although *C. elegans* hermaphrodites emerge into adulthood already replete with sperm, after about 3 days of egg-laying the animals become sperm-depleted and can only reproduce by mating, This marks a transition into what we define as the endogenous female state. This state is behaviorally distinguished by increased male-mating success (Garcia, LeBoeuf, and Koo, 2007), which may be due to an increased attractiveness to males (Morsci, Haas, and Barr, 2011). This increased attractiveness acts at least partially through production of volatile chemical cues (Leighton et al., 2014). These behavioral changes are also coincident with functional deterioration of the germline (Andux and Ellis, 2008), muscle (Herndon et al., 2002), intestine (McGee et al., 2011) and nervous system (Liu et al., 2013), changes traditionally attributed to the aging process (T. R. Golden and Melov, 2007).

To decouple the effects of aging and sperm-loss, we devised a two factor experiment. We examined wild-type XX animals at the beginning of adulthood (before worms contained embryos, referred to as 1st day adults) and after sperm depletion (6 days after the last molt, which we term 6th day adults). Second, we examined feminized XX animals that fail to produce sperm but are fully fertile if supplied sperm by mating with males (see Fig. 3.1). We used *fog-2(lf)* mutants to obtain feminized

animals. *fog-2* is involved in germ-cell sex determination in the hermaphrodite worm and is required for sperm production (Schedl and Kimble, 1988; Clifford et al., 2000).

C. elegans defective in sperm formation will never transition into or out of a hermaphroditic stage. As time moves forward, these spermless worms only exhibit changes related to biological aging. We also reasoned that we might be able to identify gene expression changes due to different life histories: whereas hermaphrodites lay almost 300 eggs over three days, spermless females do not lay a single one. The different life histories could affect gene expression.

Here, we show that we can detect a transcriptional signature associated both with loss of hermaphroditic sperm and entrance into the endogenous female state. We can also detect changes associated specifically with biological aging. Loss of sperm leads to increases in the expression levels of transcription factors that are canonically associated with development and cellular differentiation and enriched in neuronal functions. Biological aging causes transcriptomic changes consisting of 5,592 genes in *C. elegans*. 4,552 of these changes occur in both genotypes we studied, indicating they do not depend on life history or genotype. To facilitate exploration of the data, we have generated a website where we have deposited additional graphics, as well as all of the code used to generate these analyses: https://wormlabcaltech.github.io/Angeles_Leighton_2016/ .

Materials and Methods

Strains

Strains were grown at 20°C on NGM plates containing *E. coli* OP50. We used the laboratory *C. elegans* strain N2 as our wild-type strain (Sulston and Brenner, 1974). We also used the N2 mutant strain JK574, which contains the *fog-2(q71)* allele, for our experiments.

RNA extraction

Synchronized worms were grown to either young adulthood or the 6th day of adulthood prior to RNA extraction. Synchronization and aging were carried out according to protocols described previously (Leighton et al., 2014). 1,000–5,000 worms from each replicate were rinsed into a microcentrifuge tube in S basal (5.85g/L NaCl, 1g/L K_2HPO_4, 6g/L KH_2PO_4), and then spun down at 14,000rpm for 30s. The supernatant was removed and 1mL of TRIzol was added. Worms were lysed by vortexing for 30 s at room temperature and then 20 min at 4°. The

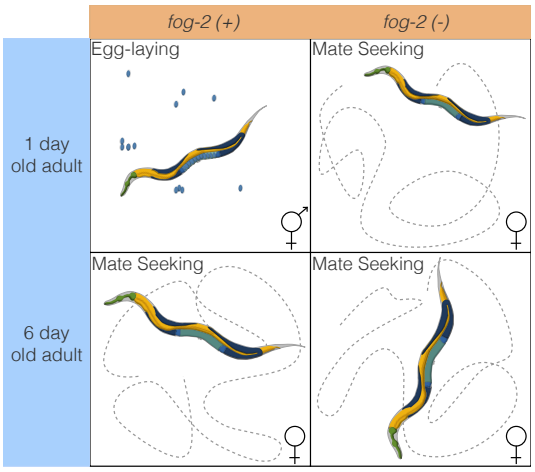

Figure 3.1: Experimental design to identify genes associated with sperm loss and with aging. Studying the wild-type worm alone would measure time- and sperm-related changes at the same time, without allowing us to separate these changes. Studying the wild-type worm and a *fog-2(lf)* mutant would enable us to measure sperm-related changes but not time-related changes. By mixing both designs, we can measure and separate both modules.

TRIzol lysate was then spun down at 14,000rpm for 10 min at 4°C to allow removal of insoluble materials. Thereafter the Ambion TRIzol protocol was followed to finish the RNA extraction (MAN0001271 Rev. Date: 13 Dec 2012). 3 biological replicates were obtained for each genotype and each time point.

RNA-Seq

RNA integrity was assessed using RNA 6000 Pico Kit for Bioanalyzer (Agilent Technologies #5067–1513) and mRNA was isolated using NEBNext Poly(A) mRNA Magnetic Isolation Module (New England Biolabs, NEB, #E7490). RNA-Seq libraries were constructed using NEBNext Ultra RNA Library Prep Kit for Illumina (NEB #E7530) following manufacturer's instructions. Briefly, mRNA isolated from $\sim 1\mu$g of total RNA was fragmented to the average size of 200nt by incubating at 94°C for 15 min in first strand buffer, cDNA was synthesized using random primers and ProtoScript II Reverse Transcriptase followed by second strand synthesis using Second Strand Synthesis Enzyme Mix (NEB). Resulting DNA fragments were end-repaired, dA tailed and ligated to NEBNext hairpin adaptors (NEB #E7335). After ligation, adaptors were converted to the 'Y' shape by treating with USER enzyme and DNA fragments were size selected using Agencourt AMPure XP beads (Beckman Coulter #A63880) to generate fragment sizes between 250 and 350 bp. Adaptor-ligated DNA was PCR amplified followed by AMPure XP bead clean

up. Libraries were quantified with Qubit dsDNA HS Kit (ThermoFisher Scientific #Q32854) and the size distribution was confirmed with High Sensitivity DNA Kit for Bioanalyzer (Agilent Technologies #5067–4626). Libraries were sequenced on Illumina HiSeq2500 in single read mode with the read length of 50nt following manufacturer's instructions. Base calls were performed with RTA 1.13.48.0 followed by conversion to FASTQ with bcl2fastq 1.8.4.

Statistical Analysis

RNA-Seq Analysis

RNA-Seq alignment was performed using Kallisto (Bray et al., 2016) with 200 bootstraps. The commands used for read-alignment are in the S.I. file 1. Differential expression analysis was performed using Sleuth (Pimentel et al., 2016). The following General Linear Model (GLM) was fit:

$$\begin{aligned}\log(y_i) =& \beta_{0,i} + \beta_{G,i}\dot{}G + \\ & \beta_{A,i}\dot{}A + \beta_{A::G,i}\dot{}A\ G,\end{aligned}$$

where y_i are the TPM counts for the ith gene; $\beta_{0,i}$ is the intercept for the ith gene, and $\beta_{X,i}$ is the regression coefficient for variable X for the ith gene; A is a binary age variable indicating 1st day adult (0) or 6th day adult (1) and G is the genotype variable indicating wild-type (0) or *fog-2(lf)* (1); $\beta_{A::G,i}$ refers to the regression coefficient accounting for the interaction between the age and genotype variables in the ith gene. Genes were called significant if the FDR-adjusted q-value for any regression coefficient was less than 0.1. Our script for differential analysis is available on GitHub.

Regression coefficients and TPM counts were processed using Python 3.5 in a Jupyter Notebook (Pérez and Granger, 2007). Data analysis was performed using the Pandas, NumPy and SciPy libraries (McKinney, 2011; Van Der Walt, Colbert, and Varoquaux, 2011; Oliphant, 2007). Graphics were created using the Matplotlib and Seaborn libraries (Waskom et al., 2016; Hunter, 2007). Interactive graphics were generated using Bokeh (Bokeh Development Team, 2014).

Tissue, Phenotype and Gene Ontology Enrichment Analyses (TEA, PEA and GEA, respectively) were performed using the WormBase Enrichment Suite for Python (Angeles-Albores, N. Lee, et al., 2016; Angeles-Albores, Lee, et al., 2017).

Data Availability

Strains are available from the *Caenorhabditis* Genetics Center. All of the data and scripts pertinent for this project except the raw reads can be found on our Github repository https://github.com/WormLabCaltech/Angeles_Leighton_2016. File S1 contains the list of genes that were altered in aging regardless of genotype. File S2 contains the list of genes and their associations with the *fog-2(lf)* phenotype. File S3 contains genes associated with the female state. Raw reads were deposited to the Sequence Read Archive under the accession code SUB2457229.

Results and Discussion

Decoupling time-dependent effects from sperm-status via general linear models

In order to decouple time-dependent effects from changes associated with loss of hermaphroditic sperm, we measured wild-type and *fog-2(lf)* adults at the 1st day adult stage (before visible embryos were present) and 6th day adult stage, when all wild-type hermaphrodites had laid all their eggs (see Fig 3.1), but mortality was still low (< 10%) (Stroustrup et al., 2013). We obtained 16–19 million reads mappable to the *C. elegans* genome per biological replicate, which enabled us to identify 14,702 individual genes totalling 21,143 isoforms (see Figure 3.2a).

One way to analyze the data from this two-factor design is by pairwise comparison of the distinct states. However, such an analysis would not make full use of all the statistical power afforded by this experiment. Another method that makes full use of the information in our experiment is to perform a linear regression in 3 dimensions (2 independent variables, age and genotype, and 1 output). A linear regression with 1 parameter (age, for example) would fit a line between expression data for young and old animals. When a second parameter is added to the linear regression, said parameter can be visualized as altering the y-intercept, but not the slope, of the first line in question (see Fig. 3.3a).

Although a simple linear model is oftentimes useful, sometimes it is not appropriate to assume that the two variables under study are entirely independent. For example, in our case, three out of the four timepoint-and-genotype combinations we studied did not have sperm, and sperm-status is associated with both the *fog-2(lf)* self-sterile phenotype and with biological age of the wild-type animal. One way to statistically model such correlation between variables is to add an interaction term to the linear regression. This interaction term allows extra flexibility in describing how changes occur between conditions. For example, suppose a given theoretical gene X has

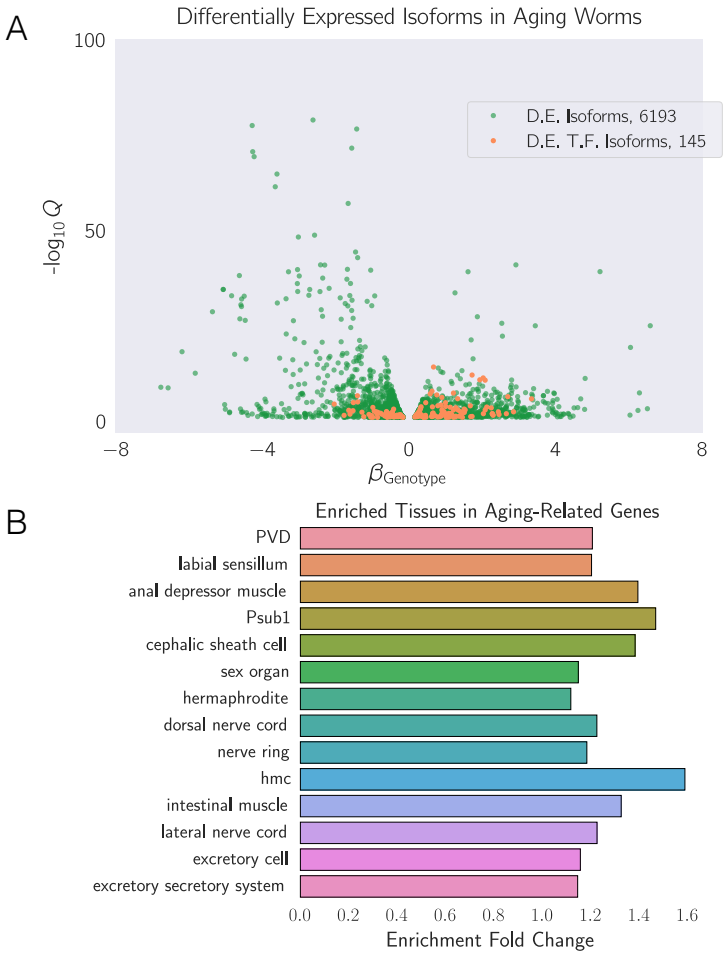

Figure 3.2: **A** We identified a common aging transcriptome between N2 and *fog-2(lf)* animals, consisting of 6,193 differentially expressed isoforms totaling 5,592 genes. The volcano plot is randomly down-sampled 30% for ease of viewing. Each point represents an individual isoform. β_{Aging} is the regression coefficient. Larger magnitudes of β indicate a larger log-fold change. The y-axis shows the negative logarithm of the q-values for each point. Green points are differentially expressed isoforms; orange points are differentially expressed isoforms of predicted transcription factor genes (Reece-Hoyes et al., 2005). An interactive version of this graph can be found on our website. **B** Tissue Enrichment Analysis (Angeles-Albores, N. Lee, et al., 2016) showed that genes associated with muscle tissues and the nervous system are enriched in aging-related genes. Only statistically significantly enriched tissues are shown. Enrichment Fold Change is defined as $Observed/Expected$. hmc stands for head mesodermal cell.

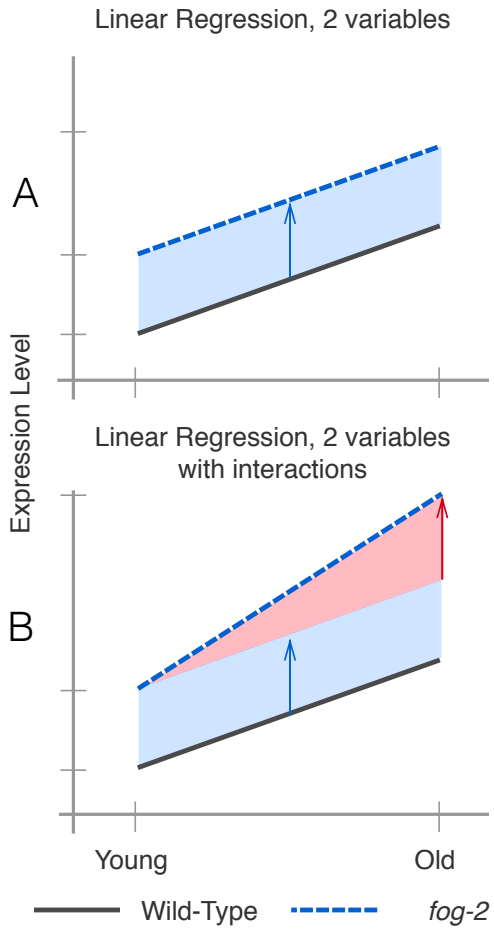

Figure 3.3: **A**. A linear regression with two variables, age and genotype. The expression level of a gene increases by the same amount as worms age regardless of genotype. However, *fog-2(lf)* has more mRNA than the wild-type at all stages (blue arrow). **B**. A linear regression with two variables and an interaction term. In this example, the expression level of this hypothetical gene is different between wild-type worms and *fog-2(lf)* (blue arrow). Although the expression level of this gene increases with age, the slope is different between wild-type and *fog-2(lf)*. The difference in the slope can be accounted for through an interaction coefficient (red arrow).

expression levels that increase in a *fog-2*-dependent manner, but also increases in an age-dependent manner. However, aged *fog-2(lf)* animals do not have expression levels of X that would be expected from adding the effect of the two perturbations; instead, the expression levels of X in this animal are considerably above what is expected. In this case, we could add a positive interaction coefficient to the model to explain the effect of genotype on the y-intercept as well as the slope (see Fig. 3.3b). When the two perturbations are loss-of-function mutations, such interactions are epistatic interactions.

For these reasons, we used a linear generalized model (see Statistical Analysis) with interactions to identify a transcriptomic profile associated with the *fog-2(lf)* genotype independently of age, as well as a transcriptomic profile of *C. elegans* aging common to both genotypes. The change associated with each variable is referred as β; this number, although related to the natural logarithm of the fold change, is not equal to it. However, it is true that larger magnitudes of β indicate greater change. Thus, for each gene we performed a linear regression, and we evaluated the whether the β values associated with each coefficient were significantly different from 0 via a Wald test corrected for multiple hypothesis testing. A coefficient was considered to be significantly different from 0 if the q-value associated with it was less than 0.1.

A quarter of all genes change expression between the 1st day of adulthood and the 6th day of adulthood in *C. elegans*.

We identified a transcriptomic signature consisting of 5,592 genes that were differentially expressed in 6th day adult animals of either genotype relative to 1st day adult animals (see SI file 2). This constitutes more than one quarter of the genes in *C. elegans*. Tissue Enrichment Analysis (TEA) (Angeles-Albores, N. Lee, et al., 2016) showed that nervous tissues including the 'nerve ring', 'dorsal nerve cord', 'PVD' and 'labial sensillum' were enriched in genes that become differentially expressed through aging. Likewise, certain muscle groups ('anal depressor muscle', 'intestinal muscle') were enriched. (see Figure 3.2b). Gene Enrichment Analysis (GEA) (Angeles-Albores, Lee, et al., 2017) revealed that genes that were differentially expressed during the course of aging were enriched in terms involving respiration ('respiratory chain', 'oxoacid metabolic process'); translation ('cytosolic large ribosomal subunit'); and nucleotide metabolism ('purine nucleotide', 'nucleoside phosphate' and 'ribose phosphate' metabolic process). Phenotype Enrichment Analysis (PEA) (Angeles-Albores, Lee, et al., 2017) showed enrichment of phenotypes that affect the *C. elegans* gonad, including 'gonad vesiculated', 'gonad small',

'oocytes lack nucleus' and 'rachis narrow'.

To verify the quality of our dataset, we generated a list of 1,056 golden standard genes expected to be altered in 6th day adult worms using previous literature reports including downstream genes of *daf-12*, *daf-16*, and aging and lifespan extension datasets (Murphy et al., 2003; Halaschek-Wiener et al., 2005; Lund et al., 2002; McCormick et al., 2012; Eckley et al., 2013). Out of 1,056 standard genes, we found 506 genes in our time-responsive dataset. This result was statistically significant with a p-value $< 10^{-38}$.

Next, we used a published compendium (Reece-Hoyes et al., 2005) to search for known or predicted transcription factors. We found 145 transcription factors in the set of genes with differential expression in aging nematodes. We subjected this list of transcription factors to TEA to understand their expression patterns. 6 of these transcription factors were expressed in the 'hermaphrodite specific neuron' (HSN), a neuron physiologically relevant for egg-laying (*hlh-14*, *sem-4*, *ceh-20*, *egl-46*, *ceh-13*, *hlh-3*), which represented a statistically significant 2-fold enrichment of this tissue ($q < 10^{-1}$). The term 'head muscle' was also overrepresented at twice the expected level ($q < 10^{-1}$, 13 genes). Many of these transcription factors have been associated with developmental processess, and it is unclear why they would change expression in adult animals.

The whole-organism *fog-2(lf)* transcriptome in *C. elegans*.

We identified 1,881 genes associated with the *fog-2(lf)* genotype, including 60 transcription factors (see SI file 3). TEA showed that the terms 'AB', 'midbody', 'uterine muscle', 'cephalic sheath cell', 'anal depressor muscle' and 'PVD' were enriched in this gene set. The terms 'AB' and 'midbody' likely reflect the impact of *fog-2(lf)* on the germline. Phenotype enrichment showed that only a single phenotype, 'spindle orientation variant' was enriched in the *fog-2(lf)* transcriptome ($q < 10^{-1}$, 38 genes, 2-fold enrichment). Most genes annotated as 'spindle orientation variant' were slightly upregulated, and therefore are unlikely to uniquely reflect reduced germline proliferation. GO term enrichment was very similar to the aging gene set and reflected enrichment in annotations pertaining to translation and respiration. Unlike the aging gene set, the *fog-2(lf)* transcriptome was significantly enriched in 'myofibril' and 'G-protein coupled receptor binding' ($q < 10^{-1}$). Enrichment of the term 'G-protein coupled receptor binding' was due to 14 genes: *cam-1*, *mom-2*, *dsh-1*, *spp-10*, *flp-6*, *flp-7*, *flp-9*, *flp-13*, *flp-14*, *flp-18*, *K02A11.4*, *nlp-12*, *nlp-13*, and

nlp-40. *dsh-1*, *mom-2* and *cam-1* are members of the Wnt signaling pathway. Most of these genes' expression levels were up-regulated, suggesting increased G-protein binding activity in *fog-2(lf)* mutants.

The *fog-2(lf)* transcriptome overlaps significantly with the aging transcriptome

Of the 1,881 genes that we identified in the *fog-2(lf)* transcriptome, 1,040 genes were also identified in our aging set. Moreover, of these 1,040 genes, 905 genes changed in the same direction in response either aging or germline feminization. The overlap between these transcriptomes suggests an interplay between sperm-status and age. The nature of the interplay should be captured by the interaction coefficients in our model. There are four possibilities. First, the *fog-2(lf)* worms may have a fast-aging phenotype, in which case the interaction coefficients should match the sign of the aging coefficient. Second, the *fog-2(lf)* worms may have a slow-aging phenotype, in which case the interaction coefficients should have an interaction coefficient that is of opposite sign, but not greater in magnitude than the aging coefficient (if a gene increases in aging in a wild-type worm, it should still increase in a *fog-2(lf)* worm, albeit less). Third, the *fog-2(lf)* worms exhibit a rejuvenation phenotype. If this is the case, then these genes should have an interaction coefficient that is of opposite sign and greater magnitude than their aging coefficient, such that the change of these genes in *fog-2(lf)* mutant worms is reversed relative to the wild-type. Finally, if these genes are indicative of a female state, then these genes should not change with age in *fog-2(lf)* animals, since these animals do not exit this state during the course of the experiment. Moreover, because wild-type worms become female as they age, a further requirement for a transcriptomic signature of the female state is that aging coefficients for genes in this signature should have genotype coefficients of equal sign and magnitude. In other words, entrance into the female state should be not be path-dependent.

To evaluate which of these possibilities was most likely, we selected the 1,040 genes that had aging, genotype and interaction coefficients significantly different from zero and we plotted their temporal coefficients against their genotype coefficients (see Fig. 3.4a). We observed that the aging coefficients were strongly predictive of the genotype coefficients. Most of these genes fell near the line $y = x$, suggesting that these genes define a female state. As a further test that these genes actually define a female state, we generated an epistasis plot using this gene set. We have previously used epistasis plots to measure transcriptome-wide epistasis between genes in a pathway (). Briefly, an epistasis plot plots the expected expression of

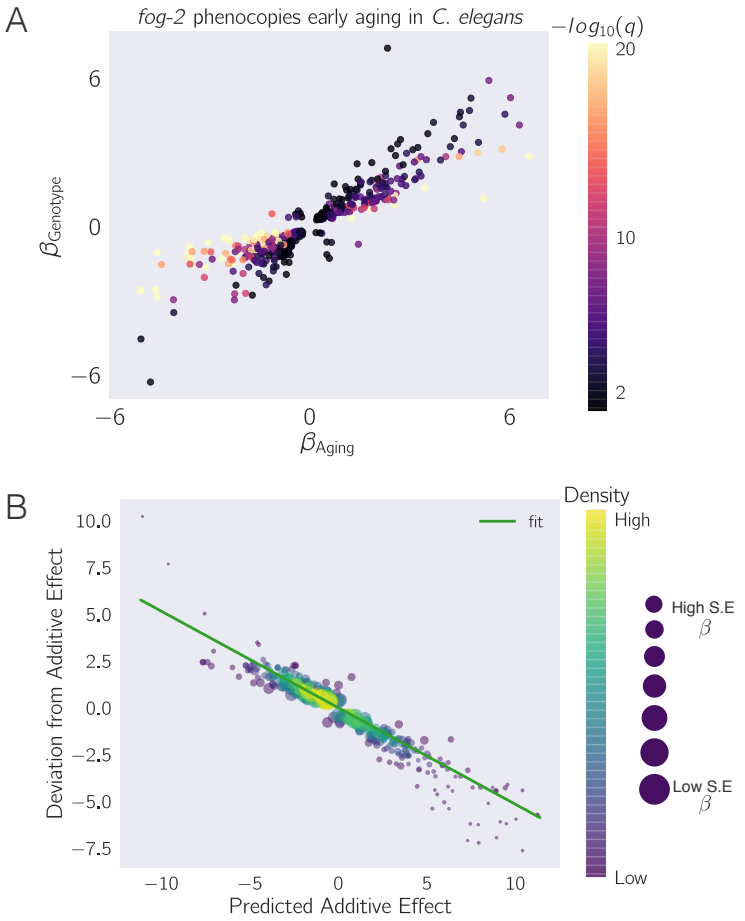

Figure 3.4: *fog-2(lf)* partially phenocopies early aging in *C. elegans*. The β in each axes is the regression coefficient from the GLM, and can be loosely interpreted as an estimator of the log-fold change. Feminization by loss of *fog-2(lf)* is associated with a transcriptomic phenotype involving 1,881 genes. 1,040/1,881 of these genes are also altered in wild-type worms as they progress from young adulthood to old adulthood, and 905 change in the same direction. However, progression from young to old adulthood in a *fog-2(lf)* background results in no change in the expression level of these genes. **A** We identified genes that change similarly during feminization and aging. The correlation between feminization and aging is almost 1:1. **B** Epistasis plot of aging versus feminization. Epistasis plots indicate whether two genes (or perturbations) act on the same pathway. When two effects act on the same pathway, this is reflected by a slope of -0.5. The measured slope was -0.51 ± 0.01.

a double perturbation under an additive model (null model) on the x-axis, and the deviation from this null model in the y-axis. In other words, we calculated the x-coordinates for each point by adding $\beta_{\text{Genotype}} + \beta_{\text{Aging}}$, and the y-coordinates are equal to $\beta_{Interaction}$ for each isoform. Previously we have shown that if two genes act in a linear pathway, an epistasis plot will generate a line with slope equal to -0.5. When we generated an epistasis plot and found the line of best fit, we observed a slope of -0.51 ± 0.01, which suggests that the *fog-2* gene and time are acting to generate a single transcriptomic phenotype along a single pathway. Overall, we identified 405 genes that increased in the same direction through age or mutation of the *fog-2(lf)* gene and that had an interaction coefficient of opposite sign to the aging or genotype coefficient (see SI file 4). Taken together, this information suggests that these 405 genes define a female state in *C. elegans*.

Analysis of the Female State Transcriptome

To better understand the changes that happen after sperm loss, we performed tissue enrichment, phenotype enrichment and gene ontology enrichment analyses on the set of 405 genes that we associated with the female state. TEA showed no tissue enrichment using this gene-set. GEA showed that this gene list was enriched in constituents of the ribosomal subunits almost four times above background ($q < 10^{-5}$, 17 genes). The enrichment of ribosomal constituents in this gene set in turn drives the enriched phenotypes: 'avoids bacterial lawn', 'diplotene absent during oogenesis', 'gonad vesiculated', 'pachytene progression during oogenesis variant', and 'rachis narrow'. The expression of most of these ribosomal subunits is down-regulated in aged animals or in *fog-2(lf)* mutants.

Discussion

Defining an Early Aging Phenotype

Our experimental design enables us to decouple the effects of egg-laying from aging. As a result, we identified a set of almost 4,000 genes that are altered similarly between wild-type and *fog-2(lf)* mutants. Due to the read depth of our transcriptomic data (20 million reads) and the number of samples measured (3 biological replicates for 4 different life stages/genotypes), this dataset constitutes a high-quality description of the transcriptomic changes that occur in aging populations of *C. elegans*. Although our data only capture $\sim 50\%$ of the expression changes reported in earlier aging transcriptome literature, this disagreement can be explained by a difference in methodology; earlier publications typically addressed the aging of fertile wild-type

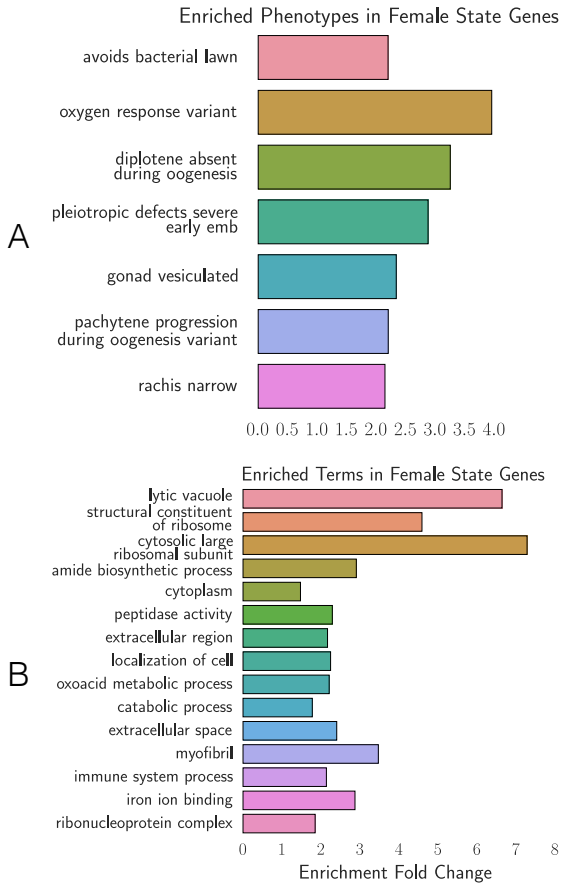

Figure 3.5: Phenotype and GO enrichment of genes involved in the female state. **A**. Phenotype Enrichment Analysis. **B**. Gene Ontology Enrichment Analysis. Most of the terms enriched in PEA reflect the abundance of ribosomal subunits present in this gene set.

hermaphrodites only indirectly, or queried aging animals at a much later stage of their life cycle.

Measurement of a female state is enabled by linear models

We set out to study the self-fertilizing (hermaphroditic) to self-sterile (female) transition by comparing wild-type animals with *fog-2(lf)* mutants as they aged. Our computational approach enabled us to separate between two biological processes that are correlated within samples. Because of this intra-sample correlation, identifying this state via pairwise comparisons would not have been straightforward. Although it is a favored method amongst biologists, such pairwise comparisons suffer from a number of drawbacks. First, pairwise comparisons are unable to draw on the full statistical power available to an experiment because they discard almost

all information except the samples being compared. Second, pairwise comparisons require a researcher to define *a priori* which comparisons are informative. For experiments with many variables, the number of pairwise combinations is explosively large. Indeed, even for this two-factor experiment, there are 6 possible pairwise comparisons. On the other hand, by specifying a linear regression model, each gene can be summarized with three variables, each of which can be analyzed and understood without the need to resort to further pairwise combinations.

Our explorations have shown that the loss of *fog-2(lf)* partially phenocopies the transcriptional events that occur naturally as *C. elegans* ages from the 1st day of adulthood to the 6th day of adulthood. Moreover, epistasis analysis of these perturbations suggest that they act on the same pathway, namely sperm generation and depletion (see Fig. 3.6). Sperm generation promotes a non-female states, whereas sperm depletion causes entry into the female state. Given the enrichment of neuronal transcription factors that are associated with sperm loss in our dataset, we believe this dataset should contain some of the transcriptomic modules that are involved in these pheromone production and behavioral pathways, although we have been unable to find these genes. Currently, we cannot judge how many of the changes induced by loss of hermaphroditic sperm are developmental (i.e., irreversible), and how many can be rescued by mating to a male. While an entertaining thought experiment, establishing whether these transcriptomic changes can be rescued by males is a daunting experimental task, given that the timescales for physiologic changes could reasonably be the same as the timescale of onset of embryonic transcription. All in all, our research supports the idea that wide-ranging transcriptomic effects of aging in various tissues can be observed well before onset of mortality, and that *C. elegans* continues to develop as it enters a new state of its life cycle.

The *C. elegans* life cycle, life stages and life states

C. elegans has a complicated life cycle, with two alternative developmental pathways that have multiple stages (larval development and dauer development), followed by reproductive adulthood. In addition to its developmental stages, researchers have recognized that *C. elegans* has numerous life states that it can enter into when given instructive environmental cues. One such state is the L1 arrest state, where development ceases entirely upon starvation (Johnson et al., 1984). More recently, researchers have described additional diapause states that the worm can access at the L3, L4 and young adult stages under conditions of low food (Angelo and Gilst, 2009; Seidel and Kimble, 2011; Schindler, Baugh, and Sherwood, 2014). Not all

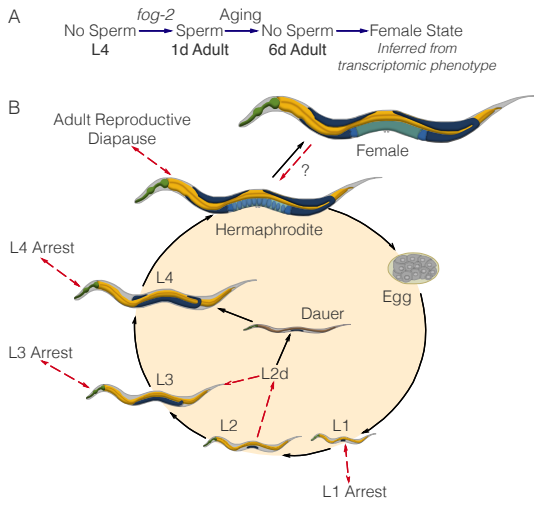

Figure 3.6: **A**. A substrate model showing how *fog-2* promotes sperm generation, whereas aging promotes sperm depletion, leading to entry to the female state. Such a model can explain why *fog-2* and aging appear epistatic to each other. **B**. The complete *C. elegans* life cycle. Recognized stages of *C. elegans* are marked by black arrows. States are marked by red arrows to emphasize that at the end of a state, the worm returns to the developmental timepoint it was at before entering the state. The L2d state is an exception. It is the only stage that does not return to the same developmental timepoint; rather, the L2d state is a permissive state that allows entry into either dauer or the L3 stage. We have presented evidence of a female state in *C. elegans*. At this point, it is unclear whether the difference between hermaphrodites and females is reversible by males. Therefore, it remains unclear whether it is a stage or a true state.

states of *C. elegans* are arrested, however (see Fig. 3.6). For example, the L2d state is induced by crowded and nutrient poor conditions (J. W. Golden and Riddle, 1984). While within this state, the worm is capable of entry into either dauer or the L3 larval stage, depending on environmental conditions. Thus, the L2d state is a permissive state, and marks the point at which the nematode development is committed to a single developmental pathway.

Identification of the *C. elegans* life states has often been performed by morphological studies (as in the course of L4 arrest or L2d) or via timecourses (L1 arrest). However, not all states may be visually identifiable, or even if they are, the morphological changes may be very subtle, making positive identification difficult. However, the detailed information afforded by a transcriptome should in theory provide sufficient information to definitively identify a state, since transcriptomic information underlies morphology. Moreover, transcriptomics can provide an informative description into the physiology of complex metazoan life state's via measurements of global

gene expression. By identifying differentially expressed genes and using ontology enrichment analyses to identify gene functions, sites of expression or phenotypes that are enriched in a given gene set, researchers can obtain a clearer picture of the changes that occur in the worm in a less biased manner than by identifying gross morphological changes. RNA-seq is emerging as a powerful technology that has been used successfully in the past as a qualitative tool for target acquisition. More recent work has successfully used RNA-seq to establish genetic interactions between genes (Dixit et al., 2016; Adamson et al., 2016). In this work, we have shown that whole-organism RNA-seq data can also be analyzed via a similar formalism to successfully identify internal states in a multi-cellular organism.

References

Adamson, Britt et al. (2016). "A Multiplexed Single-Cell CRISPR Screening Platform Enables Systematic Dissection of the Unfolded Protein Response". In: *Cell* 167.7, 1867–1882.e21. ISSN: 00928674. DOI: 10.1016/j.cell.2016.11.048.

Andux, Sara and Ronald E. Ellis (2008). "Apoptosis maintains oocyte quality in aging Caenorhabditis elegans females". In: *PLoS Genetics* 4.12. ISSN: 15537390. DOI: 10.1371/journal.pgen.1000295.

Angeles-Albores, David, Raymond Y Lee, et al. (2017). "Phenotype and gene ontology enrichment as guides for disease modeling in C. elegans". In: *bioRxiv*. DOI: 10.1101/106369. URL: http://biorxiv.org/content/early/2017/02/07/106369.

Angeles-Albores, David, Raymond Y. N. Lee, et al. (2016). "Tissue enrichment analysis for *C. elegans* genomics". In: *BMC Bioinformatics* 17.1, p. 366. ISSN: 1471-2105. DOI: 10.1186/s12859-016-1229-9.

Angelo, Giana and Marc R Van Gilst (2009). "Cells and Extends Reproductive". In: *Science* 326.November, pp. 954–958.

Blaxter, M. et al. (2012). "Genomics and transcriptomics across the diversity of the Nematoda". In: *Parasite Immunology* 34.2-3, pp. 108–120. ISSN: 01419838. DOI: 10.1111/j.1365-3024.2011.01342.x.

Boeck, Max E et al. (2016). "The time-resolved transcriptome of C . elegans". In: *Genome Research*, pp. 1–10. ISSN: 15495469. DOI: 10.1101/gr.202663.115.Freely.

Bokeh Development Team (2014). "Bokeh: Python library for interactive visualization". In:

Bray, Nicolas L et al. (2016). "Near-optimal probabilistic RNA-seq quantification." In: *Nature biotechnology* 34.5, pp. 525–7. ISSN: 1546-1696. DOI: 10.1038/nbt.3519.

Clifford, Robert et al. (2000). "FOG-2, a novel F-box containing protein, associates with the GLD-1 RNA binding protein and directs male sex determination in the C. elegans hermaphrodite germline." In: *Development (Cambridge, England)* 127.24, pp. 5265–5276. ISSN: 0950-1991.

Corsi, Ann K., Bruce Wightman, and Martin Chalfie (2015). "A transparent window into biology: A primer on Caenorhabditis elegans". In: *Genetics* 200.2, pp. 387–407. ISSN: 19432631. DOI: 10.1534/genetics.115.176099.

Dixit, Atray et al. (2016). "Perturb-Seq: Dissecting Molecular Circuits with Scalable Single-Cell RNA Profiling of Pooled Genetic Screens". In: *Cell* 167.7, 1853–1866.e17. ISSN: 00928674. DOI: 10.1016/j.cell.2016.11.038.

Eckley, D. Mark et al. (2013). "Molecular characterization of the transition to mid-life in Caenorhabditis elegans". In: *Age* 35.3, pp. 689–703. ISSN: 01619152. DOI: 10.1007/s11357-012-9401-2.

Garcia, L. Rene, Brigitte LeBoeuf, and Pamela Koo (2007). "Diversity in mating behavior of hermaphroditic and male-female Caenorhabditis nematodes". In: *Genetics* 175.4, pp. 1761–1771. ISSN: 00166731. DOI: 10.1534/genetics.106.068304.

Gerstein, Mark B. et al. (2014). "Comparative analysis of the transcriptome across distant species". In: *Nature* 512, pp. 445–448. ISSN: 0028-0836. DOI: 10.1038/nature13424. arXiv: NIHMS150003. URL: http://www.nature.com/doifinder/10.1038/nature13424%7B%5C%%7D5Cnhttp://dx.doi.org/10.1038/nature13424.

Golden, James W. and Donald L. Riddle (1984). "The Caenorhabditis elegans dauer larva: Developmental effects of pheromone, food, and temperature". In: *Developmental Biology* 102.2, pp. 368–378. ISSN: 00121606. DOI: 10.1016/0012-1606(84)90201-X.

Golden, Tamara R and Simon Melov (2007). "Gene expression changes associated with aging in C. elegans." In: *WormBook : the online review of C. elegans biology*, pp. 1–12. ISSN: 1551-8507. DOI: 10.1895/wormbook.1.127.2.

Halaschek-Wiener, Julius et al. (2005). "Analysis of long-lived C. elegans daf-2 mutants using serial analysis of gene expression". In: *Genome Research*, pp. 603–615. DOI: 10.1101/gr.3274805..

Herndon, Laura a et al. (2002). "Stochastic and genetic factors influence tissue-specific decline in ageing C. elegans." In: *Nature* 419.6909, pp. 808–814. ISSN: 0028-0836. DOI: 10.1038/nature01135.

Hillier, Ladeana W. et al. (2009). "Massively parallel sequencing of the polyadenylated transcriptome of C. elegans". In: *Genome Research* 19.4, pp. 657–666. ISSN: 10889051. DOI: 10.1101/gr.088112.108.

Hunter, John D. (2007). "Matplotlib: A 2D graphics environment". In: *Computing in Science and Engineering* 9.3, pp. 99–104. ISSN: 15219615. DOI: 10.1109/MCSE.2007.55.

Johnson, Thomas E. et al. (1984). "Arresting development arrests aging in the nematode Caenorhabditis elegans". In: *Mechanisms of Ageing and Development* 28.1, pp. 23–40. ISSN: 00476374. DOI: 10.1016/0047-6374(84)90150-7.

Leighton, Daniel H. W. et al. (2014). "Communication between oocytes and somatic cells regulates volatile pheromone production in Caenorhabditis elegans". In: *Proceedings of the National Academy of Sciences* 111.50, pp. 17905–17910. ISSN: 1091-6490. DOI: 10.1073/pnas.1420439111. URL: http://www.pnas.org/content/111/50/17905.abstract.

Liu, Jie et al. (2013). "Functional aging in the nervous system contributes to age-dependent motor activity decline in C. elegans". In: *Cell Metabolism* 18.3, pp. 392–402. ISSN: 15504131. DOI: 10.1016/j.cmet.2013.08.007. arXiv: NIHMS150003. URL: http://dx.doi.org/10.1016/j.cmet.2013.08.007.

Lund, James et al. (2002). "Transcriptional profile of aging in C. elegans". In: *Current Biology* 12.18, pp. 1566–1573. ISSN: 09609822. DOI: 10.1016/S0960-9822(02)01146-6.

Magalhães, Jp De, Ce Finch, and G Janssens (2010). "Next-generation sequencing in aging research: emerging applications, problems, pitfalls and possible solutions". In: *Ageing research reviews* 9.3, pp. 315–323. ISSN: 1872-9649. DOI: 10.1016/j.arr.2009.10.006.Next-generation.

McCormick, Mark et al. (2012). "New genes that extend Caenorhabditis elegans' lifespan in response to reproductive signals". In: *Aging Cell* 11.2, pp. 192–202. ISSN: 14749718. DOI: 10.1111/j.1474-9726.2011.00768.x. arXiv: NIHMS150003.

McGee, Matthew D. et al. (2011). "Loss of intestinal nuclei and intestinal integrity in aging C. elegans". In: *Aging Cell* 10.4, pp. 699–710. ISSN: 14749718. DOI: 10.1111/j.1474-9726.2011.00713.x.

McKinney, Wes (2011). "pandas: a Foundational Python Library for Data Analysis and Statistics". In: *Python for High Performance and Scientific Computing*, pp. 1–9.

Morsci, Natalia S., Leonard A. Haas, and Maureen M. Barr (2011). "Sperm status regulates sexual attraction in Caenorhabditis elegans". In: *Genetics* 189.4, pp. 1341–1346. ISSN: 00166731. DOI: 10.1534/genetics.111.133603.

Mortazavi, Ali et al. (2008). "Mapping and quantifying mammalian transcriptomes by RNA-Seq". In: *Nature Methods* 5.7, pp. 621–628. ISSN: 1548-7091. DOI: 10.1038/nmeth.1226.

Murphy, Coleen T. et al. (2003). "Genes that act downstream of DAF-16 to influence the lifespan of Caenorhabditis elegans." In: *Nature* 424.6946, pp. 277–283. ISSN: 00280836. DOI: 10.1038/nature01789.

Murray, John Isaac et al. (2012). "Multidimensional regulation of gene expression in the C . elegans embryo Multidimensional regulation of gene expression in the C . elegans embryo". In: pp. 1282–1294. ISSN: 1088-9051. DOI: 10.1101/gr.131920.111.

Oliphant, Travis E (2007). "SciPy: Open source scientific tools for Python". In: *Computing in Science and Engineering* 9, pp. 10–20. ISSN: 1521-9615. DOI: 10.1109/MCSE.2007.58.

Pérez, F. and B.E. Granger (2007). "IPython: A System for Interactive Scientific Computing Python: An Open and General- Purpose Environment". In: *Computing in Science and Engineering* 9.3, pp. 21–29. ISSN: 15219615. DOI: doi:10.1109/MCSE.2007.53..

Pimentel, Harold J et al. (2016). "Differential analysis of RNA-Seq incorporating quantification uncertainty". In: *bioRxiv*, p. 058164. DOI: 10.1101/058164.

Rangaraju, Sunitha et al. (2015). "Suppression of transcriptional drift extends C. elegans lifespan by postponing the onset of mortality". In: *eLife* 4.December2015, pp. 1–39. ISSN: 2050084X. DOI: 10.7554/eLife.08833.

Reece-Hoyes, John S. et al. (2005). "A compendium of Caenorhabditis elegans regulatory transcription factors: a resource for mapping transcription regulatory networks." In: *Genome biology* 6.13, R110. ISSN: 1474-760X. DOI: 10.1186/gb-2005-6-13-r110. URL: http://www.pubmedcentral.nih.gov/articlerender.fcgi?artid=1414109%7B%5C&%7Dtool=pmcentrez%7B%5C&%7Drendertype=abstract.

Schedl, Tim and Judith Kimble (1988). "fog-2, a germ-line-specific sex determination gene required for hermaphrodite spermatogenesis in Caenorhabditis elegans." In: *Genetics* 119.1, pp. 43–61. ISSN: 00166731.

Schindler, Adam J., L. Ryan Baugh, and David R. Sherwood (2014). "Identification of Late Larval Stage Developmental Checkpoints in Caenorhabditis elegans Regulated by Insulin/IGF and Steroid Hormone Signaling Pathways". In: *PLoS Genetics* 10.6, pp. 13–16. ISSN: 15537404. DOI: 10.1371/journal.pgen.1004426.

Seidel, Hannah S. and Judith Kimble (2011). "The oogenic germline starvation response in c. elegans". In: *PLoS ONE* 6.12. ISSN: 19326203. DOI: 10.1371/journal.pone.0028074.

Stroustrup, Nicholas et al. (2013). "The Caenorhabditis elegans Lifespan Machine." In: *Nature methods* 10.7, pp. 665–70. ISSN: 1548-7105. DOI: 10.1038/nmeth.2475. arXiv: NIHMS150003. URL: http://www.pubmedcentral.nih.gov/articlerender.fcgi?artid=3865717%7B%5C&%7Dtool=pmcentrez%7B%5C&%7Drendertype=abstract.

Sulston, J. E. and S. Brenner (1974). "The DNA of *Caenorhabditis elegans*." In: *Genetics* 77.1, pp. 95–104. ISSN: 00166731.

Sulston, J. E. and H. R. Horvitz (1977). "Post-embryonic cell lineages of the nematode, Caenorhabditis elegans". In: *Developmental Biology* 56.1, pp. 110–156. ISSN: 00121606. DOI: 10.1016/0012-1606(77)90158-0. URL: http://www.sciencedirect.com/science/article/pii/0012160677901580.

Sulston, J. E., E. Schierenberg, et al. (1983). "The embryonic cell lineage of the nematode Caenorhabditis elegans". In: *Developmental Biology* 100.1, pp. 64–119. ISSN: 00121606. DOI: 10.1016/0012-1606(83)90201-4. URL: http://www.ncbi.nlm.nih.gov/pubmed/6684600.

Van Der Walt, Stéfan, S. Chris Colbert, and Gaël Varoquaux (2011). "The NumPy array: A structure for efficient numerical computation". In: *Computing in Science and Engineering* 13.2, pp. 22–30. ISSN: 15219615. DOI: 10.1109/MCSE.2011.37.

Wang, Charles et al. (2014). "The concordance between RNA-seq and microarray data depends on chemical treatment and transcript abundance." In: *Nature biotechnology* 32.9, pp. 926–32. ISSN: 1546-1696. DOI: 10.1038/nbt.3001. arXiv: NIHMS150003. URL: http://www.pubmedcentral.nih.gov/articlerender.fcgi?artid=4243706%7B%5C&%7Dtool=pmcentrez%7B%5C&%7Drendertype=abstract.

Waskom, Michael et al. (2016). "seaborn: v0.7.0 (January 2016)". In: DOI: 10.5281/zenodo.45133.

Chapter 4

UNDERSTANDING THE SYNMUV PHENOTYPE FROM A TRANSCRIPTOMIC PERSPECTIVE

Chapter 5

QUALITATIVE OR QUANTITATIVE ALLELIC SERIES

Chapter 6

A STUDY OF DOSAGE RESPONSE IN *C. ELEGANS* USING TRANSCRIPTOME PROFILING

Chapter 7

STRUCTURAL GENES HAVE TRANSCRIPTIONAL CONSEQUENCES

Chapter 8

GENETIC ANALYSIS OF A PATHWAY USING TRANSCRIPTOMIC TRANS-PHENOTYPES

Chapter 9

TISSUE ENRICHMENT ANALYSIS FOR *C. ELEGANS* GENOMICS

Abstract

Background Over the last ten years, there has been explosive development in methods for measuring gene expression. These methods can identify thousands of genes altered between conditions, but understanding these datasets and forming hypotheses based on them remains challenging. One way to analyze these datasets is to associate ontologies (hierarchical, descriptive vocabularies with controlled relations between terms) with genes and to look for enrichment of specific terms. Although Gene Ontology (GO) is available for *Caenorhabditis elegans*, it does not include anatomical information.

Results We have developed a tool for identifying enrichment of *C. elegans* tissues among gene sets and generated a website GUI where users can access this tool. Since a common drawback to ontology enrichment analyses is its verbosity, we developed a very simple filtering algorithm to reduce the ontology size by an order of magnitude. We adjusted these filters and validated our tool using a set of 30 gold standards from Expression Cluster data in WormBase. We show our tool can even discriminate between embryonic and larval tissues and can even identify tissues down to the single-cell level. We used our tool to identify multiple neuronal tissues that are down-regulated due to pathogen infection in *C. elegans*.

Conclusions Our Tissue Enrichment Analysis (TEA) can be found within WormBase, and can be downloaded using Python's standard pip installer. It tests a slimmed-down *C. elegans* tissue ontology for enrichment of specific terms and provides users with a text and graphic representation of the results.

Background

RNA-seq and other high-throughput methods in biology have the ability to identify thousands of genes that are altered between conditions. These genes are often correlated in their biological characteristics or functions, but identifying these functions remains challenging. To interpret these long lists of genes, biologists need

to abstract genes into concepts that are biologically relevant to form hypotheses about what is happening in the system. One such abstraction method relies on Gene Ontology (GO). GO provides a controlled set of hierarchically ordered terms (Ashburner et al., 2000; The Gene Ontology Consortium, 2015) that provide detailed descriptions about the molecular, cellular or biochemical functions of any gene. For a given gene list, existing software programs can query whether a particular term is enriched (Mi, Dong, et al., 2009; McLean et al., 2010; Huang, Lempicki, and Brad T Sherman, 2009; Pathan et al., 2015). One area of biological significance that GO does not include is anatomy. One way to address this shortcoming is to use a 'tissue ontology' that provides a complete anatomical description for an organism (e.g.'tissue', 'organ' or 'specific cell'), in this case for *C. elegans*. Such an ontology has been described previously for this organism (R. Y. N. Lee and Sternberg, 2003). Cells and tissues are physiologically relevant units with broad, relatively well-understood functionalities amenable to hypothesis formation. The *C. elegans* database, WormBase (Howe et al., 2016), maintains a curated list of gene expression data from the literature. Here we provide a new framework that analyzes a user-input list for enrichment of specific cells and tissues.

Another problem frequently associated with GO enrichment analysis is that it is often difficult to interpret due to the large number of terms associated with a given gene (which we refer to as 'result verbosity'). DAVID, a common tool for GO enrichment analysis, clusters enriched terms into broad categories (Huang, Brad T. Sherman, et al., 2007), whereas PANTHER (Mi, Dong, et al., 2009; Mi, Muruganujan, and Thomas, 2013) attempts to solve this issue by employing a manually reduced ontology, GOslim (pers._ comm., H. Yu and P. Thomas). To reduce verbosity, we have filtered our ontology using a small set of well-defined criteria to remove terms that do not contribute additional information. To our knowledge, such filtering has not been performed in an algorithmic fashion for a biological ontology before; indeed, DAVID does not employ term trimming *a priori* of testing, but rather fuzzy clustering *post* testing to reduce the number of ontology terms. Other pruning methods do exist (see for example (J. W. Kim, Caralt, and Hilliard, 2007; Garrido and Requena, 2012)), but the pruning is query-dependent or generates a brand new 'brief ontology' which satisfies a set of logic relationships and has certain connectivity requirements. We do not propose to regenerate a new 'brief ontology', but instead we use our approach to select those nodes that have sufficient annotated evidence for statistical testing. We believe our trimming methodology strikes a good balance between detailed tissue calling and conservative testing.

We have developed a tool that tests a user-provided list of genes for term enrichment using a nematode-specific tissue ontology. This ontology, which is not a module of Gene Ontology, is verbose. We select nodes from the ontology for statistical testing using an algorithmic approach, outlined below, that reduces multiple hypothesis testing issues by limiting testing to terms that are well-annotated. The results are provided to the user in a GUI that includes a table of results and an automatically generated bar-chart. This software addresses a previously unmet need in the *C. elegans* community for a tool that reliably and specifically links gene expression with changes in specific cells, organs or tissues in the worm.

Results

Generating a Gene-Tissue Dictionary by Specific Node Selection

Reducing term redundancy through a similarity metric

For our tool, we employ a previously generated cell and tissue ontology for *C. elegans* (R. Y. N. Lee and Sternberg, 2003), which is maintained and curated by WormBase. This ontology contains thousands of anatomiy terms, but not every term is equally well-annotated. As a first step to generate our tissue enrichment software, we wished to select tissue terms that were reasonably well-annotated, yet specific enough to provide insight and not redundant with other terms. For example, nematodes have a number of neurons that are placed symmetrically along the left/right body axis, and are functionally similar. These left/right neuronal pairs (which are sisters in the ontology) have almost identical annotations, with at most one or two gene differences between them, and therefore we cannot have statistical confidence in differentiating between them. As a result, testing these sister terms provides no additional information compared with testing only the parent node to these sisters. To identify redundancy, we defined two possible similarity metrics (see *Methods* section and Figure 9) that can be used to identify ontology sisters that have very high similarity between them. Intuitively, a set of sisters can be considered very similar if they share most gene annotations. Within a given set of sisters, we can calculate a similarity score for a single node by counting the number of unique annotations it contains and dividing by the total number of unique annotations in the sister set. Having assigned to each sister a similarity score, we can identify the **average** similarity score for this set of sisters, and if this average value exceeds a threshold, these sisters are not considered testable candidates. An alternative method is check whether **any** of the scores exceeds a predetermined threshold, and if so remove this sister set from the ontology. We referred to these two scoring

criteria as '**avg**' and '**any**' respectively.

Terminal branch terms and parent terms can be safely removed in an algorithmic fashion

Another problem arises from the ontology being scarcely populated. Many nodes have 0–10 annotations, which we consider too few to accurately test. To solve this issue, we implemented another straightforward node selection strategy. For a given terminal node, we test whether the node has more than a threshold number of annotations. If it does not, the node is not used for statistical testing. The next higher node in the branch is tested and removed recursively until a node that satisfies the condition is found. At that point, no more nodes can be removed from that branch. This completion is guaranteed by the structure of the ontology: parent nodes inherit all of the annotations of all of their descendants, so the number of annotated terms monotonically increases with increasing term hierarchy (see Figure 9). In this way, we ensure that our term dictionary includes only those tissues that are considered sufficiently well annotated for statistical purposes.

Additionally, we reasoned that for any parent node if all its daughters were selected for testing, there was no additional benefit to test the parent. We removed parent nodes from the analysis if all their daughter nodes passed the annotation threshold (see Figure 9). We called this a ceiling filter. Applying these three filters reduced the number of ontology terms by an order of magnitude.

Filtering greatly reduces the number of nodes used for analysis

By itself, each of these filters can reduce the number of nodes employed for analysis, but applying the filters in different orders removes different numbers of nodes (not all the filters are commutative). We chose to always execute annotation and similarity thresholding first, followed by the ceiling filter. For validation (see below) we made a number of different dictionaries. The original ontology has almost 6,000 terms of which 1675 have at least 5 gene annotations. After filtering, dictionary sizes ranged from 21 to a maximum of 460 terms, which shows the number of terms in a scarcely annotated ontology can be reduced by an order of magnitude through the application of a few simple filters (see Table 9.1). These filters were used to compile a static dictionary that we employ for all analyses (see *Validation of the algorithm and parameter selection* section for details). Our trimming pipeline is applied as part of each new WormBase release. This ensures that the ontology database we are

using remains up-to-date with regards to both addition or removal of specific terms as well as with regard to gene expression annotations.

Tissue enrichment testing via a hypergeometric model

Having built a static dictionary, we generated a Python script that implements a significance testing algorithm based on the hypergeometric model. Briefly, the hypergeometric model tests the probability of observing n_i occurences of a tissue i in a list of size M if there are m_i labels for that tissue in a dictionary of total size N that are drawn without replacement. Mathematically, this is expressed as:

$$\mathrm{P}(n_i|N, m_i, M) = \frac{\binom{m_i}{n_i}\binom{M-m_i}{N-n_i}}{\binom{N}{n_i}}. \tag{9.1}$$

Although a user will input gene IDs, we test the number of ocurrences of a term within the gene list, so a single gene can contribute to multiple terms. Due to the discrete nature of the hypergeometric distribution, this algorithm can generate artifacts when the list is small. To avoid spurious results, a tissue is never considered significant if there are no annotations for it in the user-provided list.

Once the p-values for each term have been calculated, we apply a standard FDR correction using a Benjamini-Hochberg step-up algorithm (Benjamini and Hochberg, 1995). FDR corrected p-values are called q-values. Genes that have a q-value less than a given alpha are considered significant. Our default setting is an alpha of 0.1, which is a standard threshold broadly agreed upon by the scientific community (see for example (Love, Huber, and Anders, 2014; Pawitan et al., 2005; Storey and Tibshirani, 2003)). This threshold cannot be altered in the web GUI, but is user tunable through our command-line implementation.

Users input a gene list using any valid gene name for *C. elegans*. These names are processed into standard WormBase gene IDs (WBGene IDs). The program returns a table containing all the enriched terms and associated information such as number of terms in gene list and expected number of terms. Finally, the program can also return a bar chart of the enrichment fold change for the fifteen tissues with the lowest measured q-values. The bars in the graph are sorted in ascending order of q-value and then in descending order of fold-change. Bars are colored for ease of viewing, and color does not convey information. Our software is implemented in an

easy to use GUI (see Figure 9.2). Anatomy terms are displayed in human-readable format followed by their unique ontology ID (WBbt ID). In summary, each time the ontology annotations are updated, a new trimmed ontology is generated using our filters; in parallel, users can submit their gene lists through WormBase for testing, with results output in a number of formats (see Figure 9.3).

Validation of the algorithm and optimizing parameter selection

We wanted to select a dictionary that included enough terms to be specific beyond the most basic *C. elegans* tissues, yet would minimize the number of spurious results and which had a good dynamic range in terms of enrichment fold-change. Larger tissues are correlated with better annotation, so increasing term specificity is associated with losses in statistical power. To help us select an appropriate dictionary and validate our tool, we used a set of 30 gold standards based on microarray and RNA-seq literature which are believed to be enriched in specific tissues (Gaudet et al., 2004; Spencer et al., 2011; Cinar, Keles, and Jin, 2005; Watson et al., 2008; Pauli et al., 2006; Portman and Emmons, 2004; Fox et al., 2007; Smith et al., 2010). These data sets are annotated gene lists derived from the corresponding Expression Cluster data in WormBase. Some of these studies have been used to annotate gene expression, and so they did not constitute an independent testing set. To correct this flaw, we built a clean dictionary that specifically excluded all annotation evidence that came from these studies.

As a first attempt to select a dictionary, we generated all possible combinations of dictionaries with minimal annotations of 10, 25, 33, 50 and 100 genes and similarity cutoffs of 0.9, 0.95 and 1, using ‘avg’ or ‘any’ similarity thresholding methods (see Table 9.1). The number of remaining ontology terms was inversely correlated to the minimum annotation cutoff, and was largely insensitive to the similarity threshold in the range we explored. Next, we analyzed all 30 datasets using each dictionary. Because of the large number of results, instead of analyzing each set of terms individually, we measured the average q-value for significantly enriched terms in each dataset without regard for the perceived accuracy of the terms that tested significant. We found that the similarity threshold mattered relatively little for any dictionary. We also noticed that the ‘any’ thresholding method resulted in tighter histograms with a mode closer to 0. For this reason, we chose the ‘any’ method for dictionary generation. The average q-value increased with decreasing annotation cut-off (see Figure 9.4), which reflects the decreasing statistical power associated with fewer annotations per term, but we remained agnostic as to how significant is

the trade-off between power and term specificity. Based on these observations, we ruled out the dictionary with the 100 gene annotation cut-off: it had the fewest terms and its q-values were not low enough in our opinion to compensate for the trade-off in specificity.

To select between dictionaries generated between 50, 33 and 25 annotation cut-offs, and also to ensure the terms that are selected as enriched by our algorithm are reasonable, we looked in detail at the enrichment analysis results. Most results were comparable and expected. For some sets, all dictionaries performed well. For example, in our 'all neuron enriched sets' (Spencer et al., 2011; Watson et al., 2008) all terms were neuron-related regardless of the dictionary used (see Table 9.2). On the other hand, for a set enriched for germline precursor expression in the embryo (Spencer et al., 2011), the 50 cutoff dictionary was only able to identify 'oocyte WBbt:006797', which is not a germline precursor although it is germline related; whereas the two smaller dictionaries singled out actual germline precursor cells—at the 33 cutoff, our tool identified the larval germline precursor cells 'Z2' and 'Z3' as enriched, and at the 25 gene cutoff the embryonic germline precursor terms 'P_4','P_3' and 'P_2' were identified in addition to 'Z2' and 'Z3'. We also queried an intestine precursor set (Spencer et al., 2011). Notably, this gene set yielded no enrichment when using the 25 cutoff dictionary, nor when using the 50 cutoff dictionary. However, the 33 cutoff dictionary identified the E lineage, which is the intestinal precursor lineage in *C. elegans*, as enriched. Both of these results capture specific aspects of *C. elegans* that are well known to developmental biologists.

Not all queries worked equally well. For example, a number of intestinal sets (Spencer et al., 2011; Pauli et al., 2006) were not enriched in intestine-related terms in any dictionary, but were enriched for pharynx and hypodermis. We were surprised that intestinal gene sets performed poorly, since the intestine is a relatively well-annotated tissue.

We assessed the internal agreement of our tool by using independent gene sets that we expected to be enriched in the same tissues. We used two pan-neuronal sets (Spencer et al., 2011; Watson et al., 2008); two PVD sets (Spencer et al., 2011; Smith et al., 2010); and two GABAergic sets (Spencer et al., 2011; Cinar, Keles, and Jin, 2005). Overall, the tool has good internal agreement. On most sets, the same terms were enriched, although order was somewhat variable (see Table 9.5), and most high-scoring terms were preserved between sets. All comparisons can be found online in our Github repository (see Availability of data and materials). Overall, the

dictionary generated by a 33 gene annotation cutoff with 0.95 redundancy threshold using the 'any' criterion performed best, with a good balance between specificity, verbosity and accuracy, so we selected this parameter set to generate our static dictionary. As of this publication, the testable dictionary contains 261 terms.

Applying the tool

We applied our tool to the RNA-seq datasets developed by Engelmann et al. (Engelmann et al., 2011) to gain further understanding of their underlying biology. Engelmann et al._ exposed young adult worms to 5 different pathogenic bacteria or fungi for 24 hours, after which mRNA was extracted from the worms for sequencing. We ran TEA on the genes Engelmann *et al* identified as up- or down-regulated. Initially we noticed that genes that are down-regulated tend to be twice as better annotated on average than genes that were up-regulated, suggesting that our understanding of the worm immune system is scarce, in spite of important advances made over the last decade. Up-regulated tissues, when detected, almost always included the hypodermis and excretory duct. Three of the five samples showed enrichment of neuronal tissues or neuronal precursor tissues among the down-regulated genes. As an independent verification, we also performed GO analysis using PANTHER on the down-regulated genes for *D. coniospora*. These results also showed enrichment in terms associated with neurons (see Figure 9.6). A possible explanation for this neuronal association might be that the infected worms are sick and the neurons are beginning to shut down; an alternative hypothesis would be that the worm is down-regulating specific neuronal pathways as a behavioral response against the pathogen. Indeed, several studies (Meisel and D. H. Kim, 2014; Zhang, Lu, and Bargmann, 2005) have provided evidence that *C. elegans* uses chemosensory neurons to identify pathogens. Our results highlight the involvement of various *C. elegans* neuronal tissues in pathogen defense.

Discussion

We have presented a tissue enrichment analysis tool that employs a standard hypergeometric model to test the *C. elegans* tissue ontology. We use a hypergeometric function to test a user-provided gene list for enrichment of anatomical terms in *C. elegans*. Our hope is that the physiological relevance of anatomical terms will enable researchers to make hypotheses about high-dimensionality data. Specifically, we believe an enriched term may broadly suggest one of two hypotheses: if a list is enriched in a particular anatomical region, that anatomical region is affected by

the experimental treatment; alternatively, the anatomical regions that are enriched reflect biologically relevant interactions between tissues. We believe the first hypothesis is a reasonable one to make in the case of whole-worm RNA-seq data for example, whereas the second hypothesis may be more plausible in cases where a researcher already knows what tissues a particular gene list came from, as may be the case in single-cell RNA-seq.

Our tool relies on an annotation dictionary that is continuously updated primarily with data from single gene qualitative analyses, does not require retraining and does not require ranked genes. To our knowledge, this is the first tool that tests tissue enrichment in *C. elegans* via the hypergeometric method, but similar projects exist for humans and zebrafish (Y. S. Lee et al., 2013; Prykhozhij, Marsico, and Meijsing, 2013), highlighting the relevance of our tool for high-dimensionality biology. Chikina *et al* (Chikina et al., 2009) have previously reported a tissue enrichment model for *C. elegans* based on a Support Vector Machine classifier that has been trained on microarray studies. SVMs are powerful tools, but they require continuous retraining as more tissue expression data becomes available. Moreover, classifiers require that data be rank-ordered by some metric, something which is not possible for certain studies. Furthermore, this tissue enrichment tool provides users with enrichment results for only 6 large tissues. In contrast, our tool routinely tests a much larger number of terms, and we have shown it can even accurately identify enrichment of embryonic precursor lineages for select data sets.

We have also presented the first, to our knowledge, ontology term filtering algorithm applied to biomedical ontologies. This algorithm, which is very easy to execute, identifies terms that have specificity and statistical power for hypothesis testing. Due to the nature of all ontologies as hierarchical, acyclical graphs with term inheritance, term annotations are correlated along any given branch. This correlation reduces the benefits of including all terms for statistical analysis: for any given term along a branch, if that term passes significance, there is a high probability that many other terms along that branch will also pass significance. If the branch is enriched by random chance, error propagation along a branch means that many more false positives will follow. Thus, a researcher might be misled by the number of terms of correlated function and assign importance to this finding; the fact that the branching structure of GO amplifies false positive signals is a powerful argument for either reducing branch length or branch intracorrelation, or both. On the other hand, if a term is actually enriched, we argue that there is little benefit to presenting the user

with additional terms along that branch. Instead, a user will benefit most from testing sparsely along the tree at a suitable specificity for hypothesis formation. Related terms of the same level should only be tested when there is sufficient annotation to differentiate, with statistical confidence, whether one term is enriched above the other. Our algorithm reduces branch length by identifying and removing nodes that are insufficiently annotated and parents that are likely to include sparse information.

We endeavoured to benchmark our tool well, but our analysis cannot address problems related to spurious term enrichment. Although we were unable to determine false-positive and false-negative rates, we do not believe this should deter scientists from using our tool. Rather, we encourage researchers to use our tool as a guide, integrating evidence from multiple sources to inform the most likely hypotheses. As with any other tool based on statistical sampling, our analysis is most vulnerable to bias in the data set. For example, expression reports are negatively biased against germline expression because of the difficulties associated with expressing transgenes in this tissue (Kelly et al., 1997). As time passes, we are certain the accuracy and power of this tool will improve thanks to the continuing efforts of the worm research community; indeed, without the community reports of tissue expression in the first place, this tool would not be possible.

Conclusions

We have built a tissue enrichment tool that employs a tissue ontology previously developed by WormBase. We use a simple algorithm to identify the best ontology terms for statistical testing and in this way minimize multiple testing problems. Our tool is available within WormBase or can be downloaded for offline use via 'pip install'.

Methods

Fetching annotation terms

We used WormBase-curated gene expression data, which includes annotated descriptions of spatial-temporal expression patterns of genes, to build our dictionary. Gene lists per anatomy term were extracted from a Solr document store of gene expression data from the WS252 database provided by WormBase (Howe et al., 2016). We used the Solr document store because it provided a convenient access to expression data that included inferred annotations. That is, for each anatomy term, the expression gene list includes genes that were directly annotated to the term, as well as those that were annotated to the term's descendant terms (if there were

any). Descendant terms were those connected with the focus term by is_a/part_of relationship chains defined in the anatomy term ontology hierarchy.

Filtering nodes

Defining a Similarity Metric

To identify redundant sisters, we defined the following similarity metric:

$$s_i = \frac{|g_i|}{|\bigcup_{i=0}^{k} g_i|} \tag{9.2}$$

Where s_i is the similarity for a tissue i with k sisters; g_i refers to the set of tissues associated with tissue i and $|g|$ refers to the cardinality of set g. For a given set of sisters, we called them redundant if they exceeded a given similarity threshold. We envisioned two possible criteria and built different dictionaries using each one. Under a threshold criteron 'any' with parameter S between $(0, 1)$, a given set of sisters j was considered redundant if the condition

$$s_{i,j} > S \tag{9.3}$$

was true for any sister i in set j. Under a threshold criterion 'avg' with parameter S, a given set of sisters j was considered redundant if the condition

$$\mathrm{E}[s_i]_j > S \tag{9.4}$$

was true for the set of sisters j (see Figure 9).

Since nodes can have multiple parents (and therefore multiple sister sets), a complete set of similarity scores was calculated before trimming the ontology, and nodes were removed from the ontology if they exceeded the similarity threshold at least once in any comparison.

Implementation

All scripts were written in Python 3.5. Our software relies on the pandas, NumPy, Seaborn and SciPy modules to perform all statistical testing and data handling (McKinney, 2011; Van Der Walt, Colbert, and Varoquaux, 2011; Oliphant, 2007).

Availability of data and materials

Our web implementation is available at http://www.wormbase.org/tools/enrichment/tea/tea.cgi. Our software can also be downloaded using Python's pip installer via the command

```
pip install tissue_enrichment_analysis
```

Alternatively, our software is available for download at: http://dangeles.github.io/TissueEnrichmentAnalysis

All benchmark gene sets, benchmarking code and Figures can also be found at the same address, under the 'tests' folder.

Abbreviations

- TEA—Tissue Enrichment Analysis
- GO—Gene Ontology
- WBbt ID—A unique ID assigned to reference ontology terms
- WBgene ID—A unique ID assigned to reference nematode genes

Additional Files

Additional file 1 — TEA Tutorial

Tutorial for users interested in using our software within a python script

Additional file 2 — Folder Structure for SI files 3 and 4

A file detailing the folder structure of the zipped folders 3 and 4.

Additional file 3 — Golden Gene Sets

A list of all the genes used for our benchmarking process.

Additional file 4 — Results

A folder containing a complete version of the results we generated for this paper.

Tables

References

Ashburner, M et al. (2000). "Gene Ontology: tool for the unification of biology". In: *Nature Genetics* 25.1, pp. 25–29. ISSN: 1061-4036. DOI: 10.1038/75556.

Table 9.1: Parameter specifications and number of tissues for all dictionaries. The 'Method' column refers to the trimming criterion for the similarity metric. We used two such criteria, 'any' and 'avg'.'any': For a given sister set, if any sister had a similarity exceeding the corresponding threshold, all sisters were removed from the final dictionary. 'avg': For a given sister set, if the average similarity across all the sisters in the set was greater than the corresponding threshold, all sisters were removed from the final dictionary.

Annotation Cutoff	Similarity Threshold	Method	No. Of Terms in Dictionary
25	0.9	any	460
25	0.9	avg	461
25	0.95	any	466
25	0.95	avg	468
25	1.0	any	476
25	1.0	avg	476
33	0.9	any	261
33	0.9	avg	255
33	0.95	any	261
33	0.95	avg	262
33	1.0	any	247
33	1.0	avg	247
50	0.9	any	83
50	0.9	avg	77
50	0.95	any	82
50	0.95	avg	81
50	1.0	any	70
50	1.0	avg	70
100	0.9	any	45
100	0.9	avg	35
100	0.95	any	42
100	0.95	avg	36
100	1.0	any	21
100	1.0	avg	21

Table 9.2: Comparison of results for a GABAergic neuronal-enriched gene set from Watson (Watson et al., 2008) showing that results are similar regardless of annotation cutoff. We ran the same gene list on a dictionary with a minimum annotation cutoff of 50, similarity threshold of 0.95 and similarity method 'any' versus another with a minimum annotation cutoff of 33, similarity threshold of 0.95 and similarity method 'any'. In the table, columns are abeled with their significance value (Q-value) or enrichment fold change followed by a hyphen and a number which indicates which the cutoff for the dictionary that was used for testing. Not all tissues are present in either dictionary. Hyphens denote not-applicable values, which occurs when a particular tissue is not present in both dictionaries.

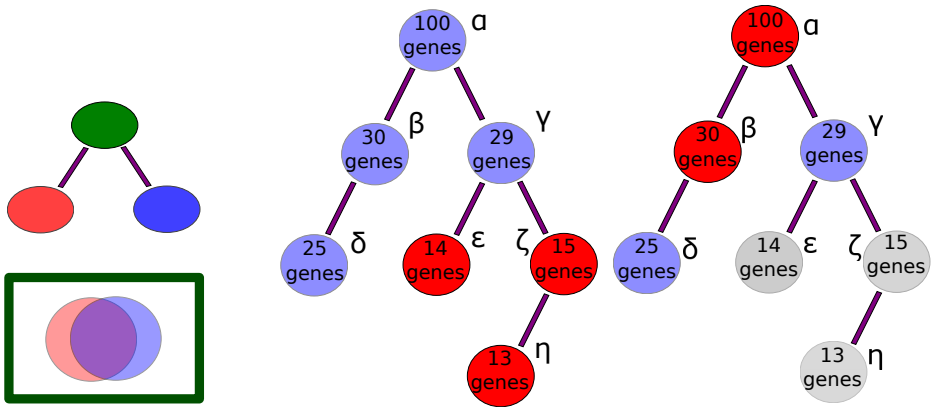

Figure 9.1: Schematic representation of trimming filters for an acyclical ontology. **a.** The parent node (green) contains at least as many annotations as the union of the two sisters. These two sisters share annotations extensively, as expressed by the overlap in the Venn diagram, so they qualify for removal. **b.** Nodes with less than a threshold number of genes are trimmed (red) and discarded from the dictionary. Here, the example threshold is 25 genes. Nodes ϵ, ζ, η, shown in red are removed. **c.** Parent nodes are removed recursively, starting from the root, if all their daughter nodes have more than the threshold number of annotations. Nodes in grey (ϵ, ζ, η) were removed in the previous step. Nodes α, β shown in red are trimmed because each one has a complete daughter set. Only nodes γ and δ will be used to generate the static dictionary.

Benjamini, Yoav and Yosef Hochberg (1995). *Controlling the False Discovery Rate: A Practical and Powerful Approach to Multiple Testing*. DOI: 10.2307/2346101. arXiv: 95/57289 [0035-9246]. URL: http://www.jstor.org/stable/2346101.

Chikina, Maria D. et al. (2009). "Global prediction of tissue-specific gene expression and context-dependent gene networks in Caenorhabditis elegans". In: *PLoS Computational Biology* 5.6. ISSN: 1553734X. DOI: 10.1371/journal.pcbi.1000417.

Cinar, Hulusi, Sunduz Keles, and Yishi Jin (2005). "Expression profiling of GABAergic motor neurons in Caenorhabditis elegans". In: *Current Biology* 15.4, pp. 340–346. ISSN: 09609822. DOI: 10.1016/j.cub.2005.02.025.

Engelmann, Ilka et al. (2011). "A comprehensive analysis of gene expression changes provoked by bacterial and fungal infection in C. elegans". In: *PLoS ONE* 6.5. ISSN: 19326203. DOI: 10.1371/journal.pone.0019055.

Fox, Rebecca M et al. (2007). "The embryonic muscle transcriptome of Caenorhabditis elegans". In: *Genome Biol* 8.9, R188. ISSN: 14656906. DOI: 10.1186/gb-2007-8-9-r188. URL: http://www.ncbi.nlm.nih.gov/pubmed/17848203.

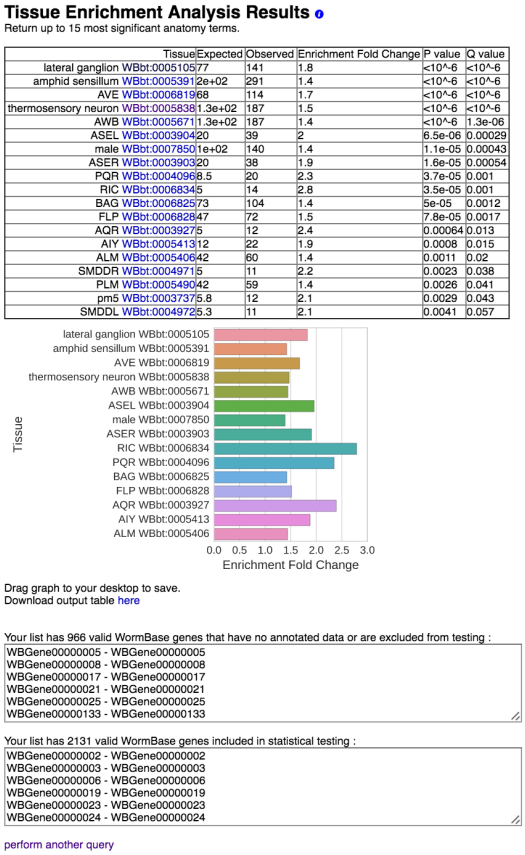

Tissue Enrichment Analysis Results

Return up to 15 most significant anatomy terms.

Tissue	Expected	Observed	Enrichment Fold Change	P value	Q value
lateral ganglion WBbt:0005105	77	141	1.8	<10^-6	<10^-6
amphid sensillum WBbt:0005391	2e+02	291	1.4	<10^-6	<10^-6
AVE WBbt:0006819	68	114	1.7	<10^-6	<10^-6
thermosensory neuron WBbt:0005838	1.3e+02	187	1.5	<10^-6	<10^-6
AWB WBbt:0005671	1.3e+02	187	1.4	<10^-6	1.3e-06
ASEL WBbt:0003904	20	39	2	6.5e-06	0.00029
male WBbt:0007850	1e+02	140	1.4	1.1e-05	0.00043
ASER WBbt:0003903	20	38	1.9	1.6e-05	0.00054
PQR WBbt:0004096	8.5	20	2.3	3.7e-05	0.001
RIC WBbt:0006834	5	14	2.8	3.5e-05	0.001
BAG WBbt:0006825	73	104	1.4	5e-05	0.0012
FLP WBbt:0006828	47	72	1.5	7.8e-05	0.0017
AQR WBbt:0003927	5	12	2.4	0.00064	0.013
AIY WBbt:0005413	12	22	1.9	0.0008	0.015
ALM WBbt:0005406	42	60	1.4	0.0011	0.02
SMDDR WBbt:0004971	5	11	2.2	0.0023	0.038
PLM WBbt:0005490	42	59	1.4	0.0026	0.041
pm5 WBbt:0003737	5.8	12	2.1	0.0029	0.043
SMDDL WBbt:0004972	5.3	11	2.1	0.0041	0.057

Drag graph to your desktop to save.
Download output table here

Your list has 966 valid WormBase genes that have no annotated data or are excluded from testing :

WBGene00000005 - WBGene00000005
WBGene00000008 - WBGene00000008
WBGene00000017 - WBGene00000017
WBGene00000021 - WBGene00000021
WBGene00000025 - WBGene00000025
WBGene00000133 - WBGene00000133

Your list has 2131 valid WormBase genes included in statistical testing :

WBGene00000002 - WBGene00000002
WBGene00000003 - WBGene00000003
WBGene00000006 - WBGene00000006
WBGene00000019 - WBGene00000019
WBGene00000023 - WBGene00000023
WBGene00000024 - WBGene00000024

perform another query

Figure 9.2: Screenshot of results from the web GUI. After inputting a gene-list, the user is provided with the results. An HTML table is output with hyperlinks to the ontology terms. A publication-ready graph is provided below, which can be saved by dragging to the desktop. The graph is colored for better visualization; color is not intended to convey information. The graph and the table show anatomy terms in human-readable format, followed by their unique WBbt ID. Finally, lists of the genes used and discarded for the analysis are also presented.

Garrido, Julián and Ignacio Requena (2012). "Towards summarizing knowledge: Brief ontologies". In: *Expert Systems with Applications* 39.3, pp. 3213–3222. ISSN: 09574174. DOI: 10.1016/j.eswa.2011.09.008.

Gaudet, Jeb et al. (2004). "Whole-genome analysis of temporal gene expression during foregut development". In: *PLoS Biology* 2.11. ISSN: 15449173. DOI: 10.1371/journal.pbio.0020352.

Howe, Kevin L et al. (2016). "WormBase 2016: expanding to enable helminth genomic research." In: *Nucleic acids research* 44.November 2015, pp. D774–D780. ISSN: 1362-4962. DOI: 10.1093/nar/gkv1217. URL: http://www.ncbi.nlm.nih.gov/pubmed/26578572.

Huang, Da Wei, Richard a Lempicki, and Brad T Sherman (2009). "Systematic and integrative analysis of large gene lists using DAVID bioinformatics resources."

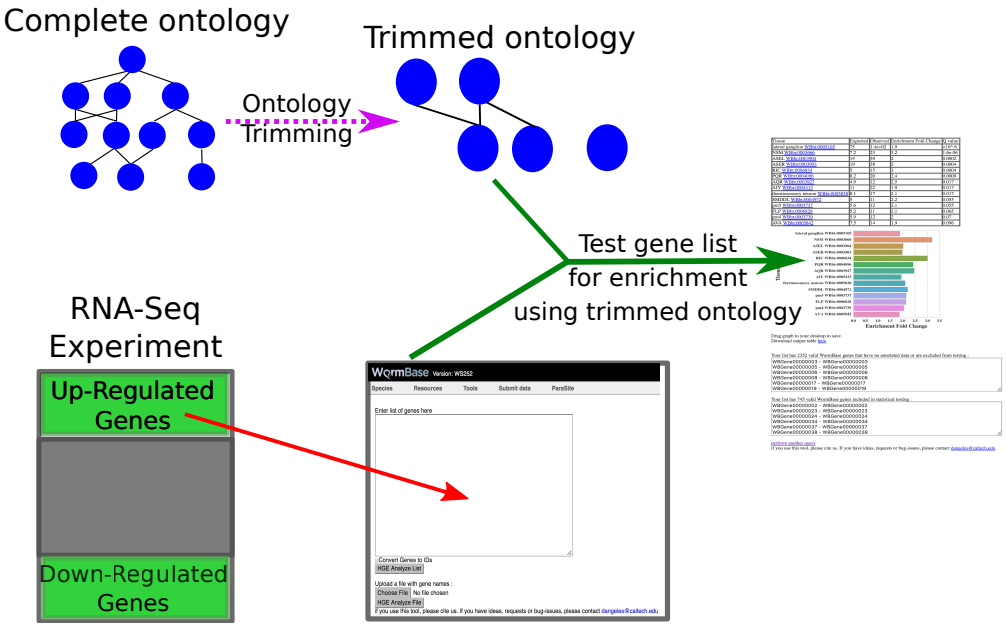

Figure 9.3: TEA Workflow. The complete ontology is annotated continuously by WormBase curators. After each update, the ontology is processed to remove uninformative terms, and the remaining terms are used for statistical testing. Users can select a gene list and input it into our tool using our WormBase portal. The gene list is tested for enrichment using the trimmed ontology, and results are output in tabular and graphic formats for analysis.

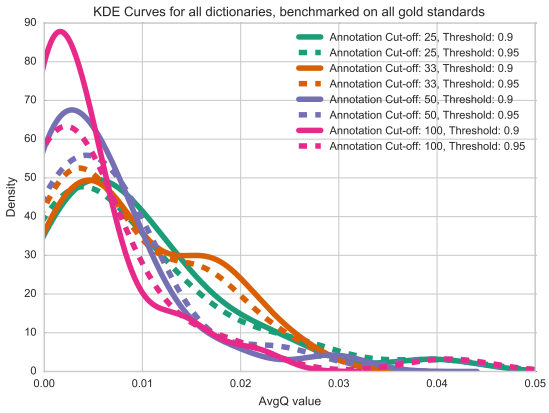

Figure 9.4: Kernel density estimates (KDE) for 30 gold standard datasets. We ran TEA on 30 datasets we believed to be enriched in particular tissues and pooled all the results to observe the distribution of q-values. The mode of the distribution for dictionaries with annotation cut-offs of 100 and 50 genes are very similar; however, when the cut-off is lowered to 25 genes, the mode of the distribution shifts to the left, potentially signalling a decrease in measurement power.

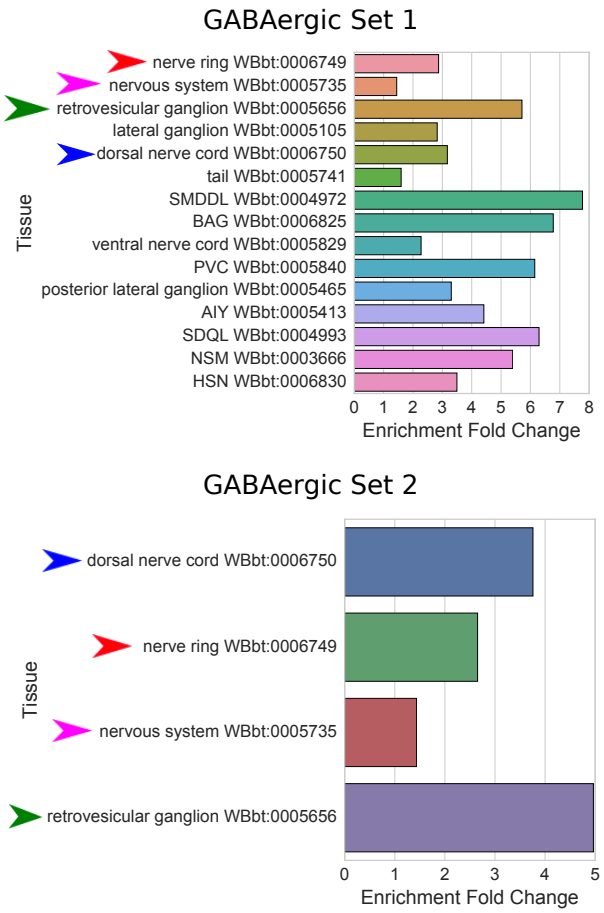

Figure 9.5: Independently derived gene sets show similar results when tested with the same dictionary. **Set 1.** GABAergic gene set from Watson (Watson et al., 2008). **Set 2.** GABAergic gene set from Spencer (Spencer et al., 2011). Arrowheads highlight identical terms between both analyses. All terms refer to neurons or neuronal tissues and are GABA-associated. Dictionary with cutoff: 33; threshold: 0.95; method: 'any'.

In: *Nature Protocols* 4.1, pp. 44–57. ISSN: 1750-2799. DOI: 10.1038/nprot.2008.211.

Huang, Da Wei, Brad T. Sherman, et al. (2007). "DAVID Bioinformatics Resources: Expanded annotation database and novel algorithms to better extract biology from large gene lists". In: *Nucleic Acids Research* 35.SUPPL.2. ISSN: 03051048. DOI: 10.1093/nar/gkm415.

Kelly, William G. et al. (1997). "Distinct requirements for somatic and germline expression of a generally expressed Caenorhabditis elegans gene". In: *Genetics* 146.1, pp. 227–238. ISSN: 00166731.

a) GO Enrichment Analysis

Displaying only results with P<0.05; click here to display all results

	Caenorhabditis elegans (REF)	Client Text Box Input (Δ Hierarchy, NEW!)				
PANTHER GO-Slim Biological Process	#	#	expected	Fold Enrichment	+/-	P value
Unclassified	12877	745	925.08	.81	-	0.00E00
translation	362	46	26.01	1.77	+	4.19E-02
└protein metabolic process	1879	246	134.99	1.82	+	1.16E-17
└primary metabolic process	4498	603	323.14	1.87	+	6.74E-58
└metabolic process	5383	697	386.71	1.80	+	6.88E-65
sensory perception	464	59	32.62	1.81	+	3.14E-03
└neurological system process	631	116	45.33	2.56	+	4.50E-17
└system process	887	183	63.72	2.87	+	4.45E-34
└single-multicellular organism process	956	196	68.68	2.85	+	2.39E-36
└multicellular organismal process	956	196	68.68	2.85	+	2.39E-36
cellular protein modification process	904	123	64.94	1.89	+	5.36E-09
regulation of transcription from RNA polymerase II promoter	695	95	49.93	1.90	+	8.54E-07
└transcription from RNA polymerase II promoter	893	115	64.15	1.79	+	5.34E-07
└transcription, DNA-dependent	928	123	66.67	1.84	+	2.64E-08
└RNA metabolic process	1258	160	90.37	1.77	+	8.08E-10
└nucleobase-containing compound metabolic process	1936	247	139.08	1.78	+	2.25E-16
└regulation of nucleobase-containing compound metabolic process	826	116	59.34	1.95	+	3.13E-09
└regulation of biological process	1619	213	116.31	1.83	+	3.53E-15
└biological regulation	2130	326	153.02	2.13	+	6.25E-37
response to stress	370	53	26.58	1.99	+	6.24E-04

b) TEA

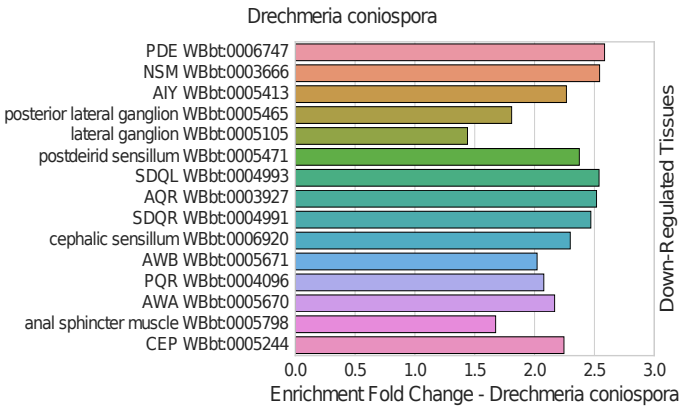

Figure 9.6: *D. coniospora* Gene Enrichment Analysis and Tissue Enrichment Analysis results. We compared and contrasted the results from a gene enrichment analysis program, pantherDB, with TEA by analyzing genes that were significantly down-regulated when *C. elegans* was exposed to *D. coniospora* in a previously published dataset by Engelmann *et al* (Engelmann et al., 2011) with both tools. **a.** pantherDB screenshot of results, sorted by p-value. Only top hits shown. **b.** TEA results, sorted by q-value (lowest on top) and fold-change. Both pantherDB and TEA identify terms associated with neurons (red square). The two analyses provide complementary, not redundant, information.

Kim, Jong Woo, Jordi Conesa Caralt, and Julia K. Hilliard (2007). "Pruning bio-ontologies". In: *Proceedings of the Annual Hawaii International Conference on System Sciences*, pp. 1–10. ISSN: 15301605. DOI: 10.1109/HICSS.2007.455.

Lee, R. Y N and Paul W. Sternberg (2003). *Building a cell and anatomy ontology of Caenorhabditis elegans*. DOI: 10.1002/cfg.248.

Lee, Young Suk et al. (2013). "Ontology-aware classification of tissue and cell-type signals in gene expression profiles across platforms and technologies". In: *Bioinformatics* 29.23, pp. 3036–3044. ISSN: 13674803. DOI: 10.1093/bioinformatics/btt529.

Love, Michael I., Wolfgang Huber, and Simon Anders (2014). "Moderated estimation of fold change and dispersion for RNA-seq data with DESeq2." In: *Genome biology* 15.12, p. 550. ISSN: 1474-760X. DOI: 10.1186/s13059-014-0550-8.

McKinney, Wes (2011). "pandas: a Foundational Python Library for Data Analysis and Statistics". In: *Python for High Performance and Scientific Computing*, pp. 1–9.

McLean, Cory Y et al. (2010). "GREAT improves functional interpretation of cis-regulatory regions." In: *Nature biotechnology* 28.5, pp. 495–501. ISSN: 1087-0156. DOI: 10.1038/nbt.1630. URL: http://dx.doi.org/10.1038/nbt.1630.

Meisel, Joshua D. and Dennis H. Kim (2014). "Behavioral avoidance of pathogenic bacteria by Caenorhabditis elegans". In: *Trends in Immunology* 35.10, pp. 465–470. ISSN: 14714981. DOI: 10.1016/j.it.2014.08.008. URL: http://dx.doi.org/10.1016/j.it.2014.08.008.

Mi, Huaiyu, Qing Dong, et al. (2009). "PANTHER version 7: Improved phylogenetic trees, orthologs and collaboration with the Gene Ontology Consortium". In: *Nucleic Acids Research* 38.SUPPL.1, pp. D204–D210. ISSN: 03051048. DOI: 10.1093/nar/gkp1019.

Mi, Huaiyu, Anushya Muruganujan, and Paul D. Thomas (2013). "PANTHER in 2013: Modeling the evolution of gene function, and other gene attributes, in the context of phylogenetic trees". In: *Nucleic Acids Research* 41.D1. ISSN: 03051048. DOI: 10.1093/nar/gks1118.

Oliphant, Travis E (2007). "SciPy: Open source scientific tools for Python". In: *Computing in Science and Engineering* 9, pp. 10–20. ISSN: 1521-9615. DOI: 10.1109/MCSE.2007.58.

Pathan, Mohashin et al. (2015). "FunRich: An open access standalone functional enrichment and interaction network analysis tool". In: *Proteomics* 15.15, pp. 2597–2601. ISSN: 16159861. DOI: 10.1002/pmic.201400515.

Pauli, Florencia et al. (2006). "Chromosomal clustering and GATA transcriptional regulation of intestine-expressed genes in C. elegans." In: *Development (Cambridge, England)* 133.2, pp. 287–295. ISSN: 0950-1991. DOI: 10.1242/dev.02185.

Pawitan, Yudi et al. (2005). "False discovery rate, sensitivity and sample size for microarray studies". In: *Bioinformatics* 21.13, pp. 3017–3024. ISSN: 13674803. DOI: 10.1093/bioinformatics/bti448.

Portman, Douglas S. and Scott W. Emmons (2004). "Identification of C. elegans sensory ray genes using whole-genome expression profiling". In: *Developmental Biology* 270.2, pp. 499–512. ISSN: 00121606. DOI: 10.1016/j.ydbio.2004.02.020.

Prykhozhij, Sergey V, Annalisa Marsico, and Sebastiaan H Meijsing (2013). "Zebrafish Expression Ontology of Gene Sets (ZEOGS): a tool to analyze enrichment of zebrafish anatomical terms in large gene sets." In: *Zebrafish* 10.3, pp. 303–15. ISSN: 1557-8542. DOI: 10.1089/zeb.2012.0865. URL: http://www.pubmedcentral.nih.gov/articlerender.fcgi?artid=3760060%7B%5C&%7Dtool=pmcentrez%7B%5C&%7Drendertype=abstract.

Smith, Cody J. et al. (2010). "Time-lapse imaging and cell-specific expression profiling reveal dynamic branching and molecular determinants of a multi-dendritic nociceptor in C. elegans". In: *Developmental Biology* 345.1, pp. 18–33. ISSN: 00121606. DOI: 10.1016/j.ydbio.2010.05.502.

Spencer, W. Clay et al. (2011). "A spatial and temporal map of C. elegans gene expression". In: *Genome Research* 21.2, pp. 325–341. ISSN: 10889051. DOI: 10.1101/gr.114595.110.

Storey, John D and Robert Tibshirani (2003). "Statistical significance for genomewide studies." In: *Proceedings of the National Academy of Sciences of the United States of America* 100.16, pp. 9440–5. ISSN: 0027-8424. DOI: 10.1073/pnas.1530509100.

The Gene Ontology Consortium (2015). "Gene Ontology Consortium: going forward". In: *Nucleic Acids Research* 43.D1, pp. D1049–D1056. ISSN: 0305-1048. DOI: 10.1093/nar/gku1179. URL: http://nar.oxfordjournals.org/lookup/doi/10.1093/nar/gku1179.

Van Der Walt, Stéfan, S. Chris Colbert, and Gaël Varoquaux (2011). "The NumPy array: A structure for efficient numerical computation". In: *Computing in Science and Engineering* 13.2, pp. 22–30. ISSN: 15219615. DOI: 10.1109/MCSE.2011.37.

Watson, Joseph D et al. (2008). "Complementary RNA amplification methods enhance microarray identification of transcripts expressed in the C. elegans nervous system". In: *BMC Genomics* 9, p. 84. ISSN: 1471-2164. DOI: 10.1186/1471-2164-9-84. URL: http://www.ncbi.nlm.nih.gov/pubmed/18284693.

Zhang, Y, H Lu, and C I Bargmann (2005). "Pathogenic bacteria induce aversive olfactory learning in Caenorhabditis elegans". In: *Nature* 438.7065, pp. 179–184. ISSN: 0028-0836. DOI: 10.1038/nature04216. URL: doi:%2010.1038/nature04216.

Chapter 10

PHENOTYPE AND GENE ONTOLOGY ENRICHMENT AS GUIDES FOR DISEASE MODELING IN *C. ELEGANS*

Abstract

Genome-wide experiments have the capacity to generate massive amounts of unbiased data about an organism. In order to interpret this data, dimensionality reduction techniques are required. One approach is to annotate genes using controlled languages and to test experimental datasets for term enrichment using probabilistic methods. Although gene, phenotype and anatomy ontologies exist for *C. elegans*, no unified software offers enrichment analyses of all the ontologies using the same methodology. Here, we present the WormBase Enrichment Suite, which offers users the ability to test all nematode ontologies simultaneously. We show that the WormBase Enrichment Suite provides valuable insight into different biological problems. Briefly, we show that phenotype enrichment analysis (PEA) can help researchers identify disease phenologs, phenotypes that are homologous across species, which can inform disease modeling in *C. elegans*. The WormBase Enrichment Suite analysis can also shed light on RNA-seq datasets by showing what molecular functions are enriched, which phenotypes these functions are implicated in and what tissues are overrepresented in the dataset. Finally, we explore the phenotype-anatomy relationship, showing that a small subset of highly specific tissues are disproportionately likely to cause an Egl phenotype, but inferring tissue expression from an Egl phenotype is limited to the largest tissues.

Introduction

The last decade has seen an explosion of techniques capable of genome-wide measurements. Some examples of genome-wide tools include RNA-seq (Mortazavi et al., 2008) to measure gene expression or CHIP-seq (Johnson, Mortazavi, and Myers, 2007) to measure protein binding to chromatin. These tools are capable of generating large quantities of data. Understanding these data, and generating hypotheses from them remains challenging. A common approach used to understand these datasets is to reduce the dimensionality of the data via enrichment analyses of ontologies (Ashburner et al., 2000), which helps researchers understand what terms

are overrepresented beyond random levels. By analyzing overrepresented terms in aggregate, researchers can better understand what biological processes were most affected in a given experiment, and form hypotheses about what is happening (Rhee et al., 2008). This approach is limited by what ontologies can be tested for enrichment. The best-known ontology for biological research is the Gene Ontology (GO), which provides a controlled language to describe molecular and cellular functions of genes (Ashburner et al., 2000). In *C. elegans*, gene, tissue and phenotype ontologies exist with which to describe *C. elegans* anatomy and phenotypes respectively (Schindelman et al., 2011; R. Y. N. Lee and Paul W. Sternberg, 2003). These ontologies are curated by professional curators at WormBase, which is a repository of all *C. elegans* data (Howe et al., 2016). However, enrichment tools only exist for gene and tissue ontologies in the community today (see for example (Chikina et al., 2009; Mi, Muruganujan, and Thomas, 2013; Angeles-Albores et al., 2016)). Another limitation is that tissue enrichment testing is not offered on the same websites as GO enrichment testing, which requires users to test their data on different websites that may or may not use different methodologies to detect enrichment.

Another way to use enrichment tools is for evolutionary comparison purposes. In molecular biology it is often useful to know when a gene is homologous between two species—that is to say, common by descent—because knowledge of homology often brings with it knowledge of function. Indeed, many important gene regulatory networks (GRNs) are conserved between organisms as highly diverged as nematodes and humans (for example, see (P W Sternberg and Han, 1998)). While genes and GRNs may be conserved between species, their outputs often differ. For example, the gene Pax6 (Eyeless in *Drosophila melanogaster*) is involved in eye formation in humans and fruit-flies (Quiring et al., 1994). Although nematodes have conserved this gene, they do not have eyes (Zhang and Emmons, 1995; Chisholm and H. Robert Horvitz, 1995). The concept of a phenolog has been put forward to explain relationships between phenotypes that have the same underlying genetic regulatory network (McGary et al., 2010; Lehner, 2013). Formally, two phenotypes are phenologs of each other if the orthologs of the genes that cause a phenotype in an organism cause a second phenotype in another.

To study a clinically relevant disease in a non-human, an appropriate model has to be established. A straightforward method towards establishing a disease model in *C. elegans* is to link a disease to a causal gene, then to identify the homologous gene in *C. elegans* and then to study the function of the genetic homolog to extrapolate

back to humans. However, this method relies on the existence of known disease genes and requires that the homolog have a phenotype that can be reliably identified and studied. A fundamentally different way to establish a disease model in *C. elegans* would be to identify the phenologs of the disease to be studied in *C. elegans* by identifying disease-associated human genes in an unbiased manner through genome-wide association studies (GWAS) and identified candidate homolog genes in *C. elegans*. The orthologs can be used to identify *C. elegans* disease phenologs, which can in turn be used as the basis for screens to identify genes that are associated with that phenolog. Approaches similar to this have been successfully used in the past to make non-obvious links between phenotypes in different species (McGary et al., 2010).

The concept of a phenolog can also be useful when applied within a species. In *C. elegans*, not all phenotypes are equally easy to study. Although genome-wide measurements can help elucidate the genetic network underlying a phenotype, devising screens to test which genes are functionally important can be difficult. A common strategy to study phenotypes that are difficult to screen is to select an easier-to-screen phenolog, and to test positive hits for the true phenotype of interest afterwards. For example, candidate genes to extend the *C. elegans* lifespan can be first screened for using heat shock survival genes involved in *C. elegans* aging sensitivity can be identified using stress assays (Kim and Sun, 2007; Mehta et al., 2009). Currently, selection of screening phenotypes is performed based on researcher experience. By formalizing phenotype enrichment analysis as a tool with which to analyze gene sets, researchers should be able to formally establish phenologs, which has consequences for screen design.

An additional problem with genome-wide queries of *C. elegans* states (be they developmental, such as L1, L2, dauer; behavioral states such as awake versus asleep; or other) is that they do not always have a straightforward interpretation in terms of phenotypes. In these situations, researchers must rely on intuition to select a phenotype for which to screen. As a result, many hits may go unexplored that would prove fruitful. The question of how to design a screen that is maximally informative is an important question that has so far not been addressed within this community.

To facilitate understanding of large datasets, and to make discovery of phenologs easier, we have completed an enrichment tool suite in WormBase that allows users to rapidly perform phenotype, tissue and gene ontology enrichment analyses (PEA,

TEA and GEA respectively) on curated *C. elegans* ontologies using the same methodology for each one. We applied our tools towards the unbiased discovery of phenologues of multigenic, complex diseases including systemic lupus erythematosus, obesity and obesity-related traits, and rheumatoid arthritis by using genes associated with these diseases via genome-wide association studies. We illustrate the utility of the complete enrichment suite for finding new relationships in complex data by analyzing a ciliary neuron transcriptome (Juan Wang et al., 2015). Finally, we show that the dictionaries generated for these enrichment analyses can help elucidate the contributions of specific tissues to specific phenotypes.

Methods

Implementing the enrichment analyses

All scripts were implemented in Python 3.5 (Rossum et al., 2011). We used pandas (McKinney, 2011) and scipy (Oliphant, 2007) to write the statistical testing framework. Matplotlib (Hunter, 2007) and Seaborn (Waskom et al., 2016) libraries are used to generate all plots. Testing was performed using the WormBase version WS256. The WormBase Enrichment suite can be installed using pip via the command:

```
pip install tissue_enrichment_analysis
```

Human disease phenolog identification

We used the GWAS EBI-NHGRI catalog (MacArthur et al., 2016) to extract information on all genome-wide association studies deposited there. We only selected traits that had > 300 associated genes. We identified 24 traits that met our criteria. Next, we used DIOPT (Hu et al., 2011) to identify candidate orthologs for the genes associated with these traits. Briefly, DIOPT combines a large number of methods for identifying orthologs and returns homolog candidates associated with a compound score. Depending on the score, orthologs can be considered ‘high’, ‘moderate’ or ‘low’ rank, reflecting confidence in the homology. Many-to-one and one-to-many homology relationships are allowed in DIOPT, reflecting a mixture of uncertainty and family expansion/reduction. For our study, we only accepted homolog candidates with ‘high’ or ‘moderate’ scores and we did not insist on a one-to-one relationship between genes.

After we identified worm orthologs for each trait, we reassessed how many traits still had > 100 gene candidates, and dropped all traits that had less than this for our analysis. We identified 18 traits that met this criteria. The gene lists for each

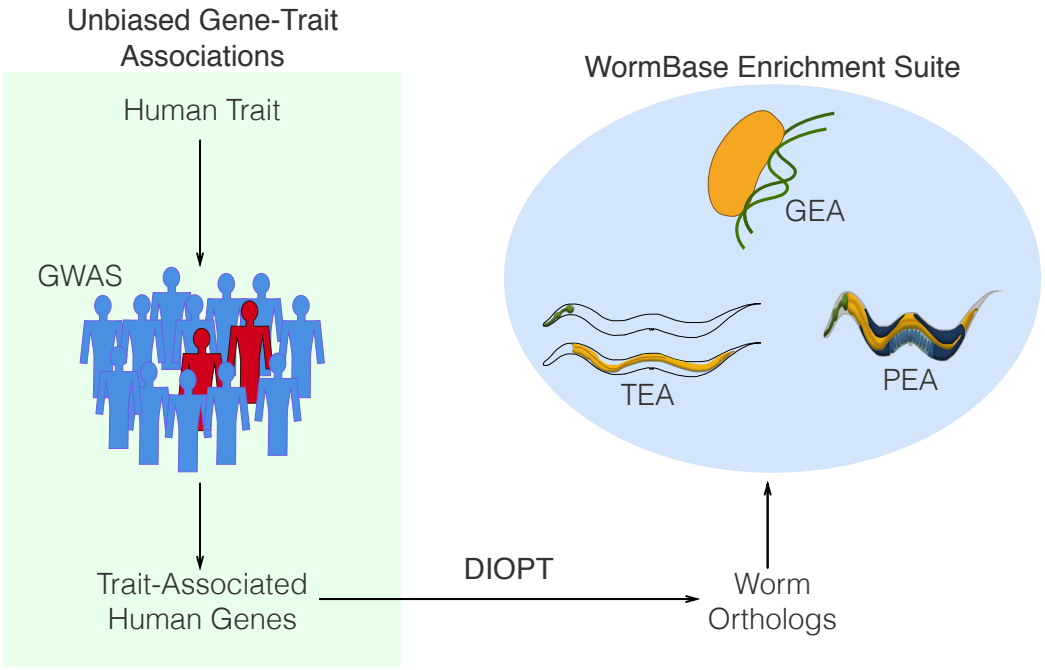

Figure 10.1: Experimental design for human-nematode phenologue identification. We used GWAS candidates from the EBI-NHGRI catalog to identify disease associated genes, then used DIOPT to identify candidate orthologs in *C. elegans*. Orthologs were used to run phenotype, gene and tissue ontology enrichment analyses to identify disease phenologues.

of these 18 traits were then analyzed for gene, tissue and phenotype enrichment (see Fig.10.1). Tissue enrichment was performed using the WormBase Tissue Enrichment Analysis (TEA) tool (Angeles-Albores et al., 2016).

Results

Developing the WormBase enrichment suite

We developed the dictionaries for PEA and GEA using the same procedure as was used for TEA (Angeles-Albores et al., 2016). We generated a dictionary that included terms with at least 50 annotating genes or more and had a similarity threshold of 0.95 for PEA (the total number of terms in the dictionary was 251, annotated by 9,169 genes for the version WS256); and we generated a dictionary that included terms with at least 50 annotating genes or more and had a similarity threshold of 0.95 for GEA (the total number of terms in this dictionary is 271, annotated by 14,636 genes for the version WS256). Next, we benchmarked the dictionaries on the same gene sets as TEA and obtained enrichment of all the expected categories (Gaudet et al., 2004; Spencer et al., 2011; Cinar, Keles, and

Jin, 2005; Watson et al., 2008; Pauli et al., 2006; Portman and Emmons, 2004; Fox et al., 2007; Smith et al., 2010). For example, on a gene set enriched for embryonic muscle genes (Watson et al., 2008), the top two enriched phenotype terms by q-value were 'muscle system morphology variant' and 'body wall muscle thick filament variant'; the top two enriched GO terms were 'myofibril' and 'striated muscle dense body'. For all the benchmarking results, see supplementary information. Having generated and validated our dictionaries, we proceeded to identify phenologs for several common human diseases.

Applying the WormBase enrichment suite

To discover phenologs, we first needed to identify genes that contribute to a disease in an unbiased manner. One way to discover gene associations in an unbiased manner is to perform GWSA in human populations. Therefore, we used the GWAS NHGRI-EBI Catalog (MacArthur et al., 2016) to identify genes associated with human diseases. We found the best nematode candidate orthologs for these genes using DIOPT (Hu et al., 2011) and applied our enrichment suite to each of these gene regulatory networks.

Systemic lupus erythematosus

Systemic lupus is an autoimmune disease that is believed to be polygenic in nature (Mohan and Putterman, 2015). It mainly affects women and is characterized by painful and swollen joints, hair loss, and fatigue (Lisnevskaia, Murphy, and Isenberg, 2014). Since worms do not have a cellular immune system, we were interested in what phenologs corresponded to this disorder in *C. elegans*. To establish phenolog candidates, we obtained 283 genes associated with the disease via GWAS studies, and found 135 homolog candidates in *C. elegans*.

Lupus-associated orthologs were reasonably well annotated. Slightly more than half of the genes had at least one phenotype annotation (76/135) and almost all genes were annotated to at least one tissue or gene ontology term (104/135 and 115/135 genes respectively). We found that Lupus-associated orthologs were enriched in 'aneuploidy' (7 genes, $q < 10^{-1}$) and 'meiotic chromosome segregation' (8 genes, $q < 10^{-1}$). 'Cell fate transformation' (6 genes, $q < 10^{-1}$), and 'excess intestinal cells' (5 genes, $q < 10^{-1}$) were also overrepresented, as was 'male tail morphology' (6 genes, $q < 10^{-1}$). Finally, the phenotype 'nonsense mRNA accumulation' was also enriched (5 genes, $q < 10^{-1}$) (see Fig. 10.2).

TEA suggested that the 'excretory duct cell' (5 genes, $q < 10^{-2}$) and the 'posterior

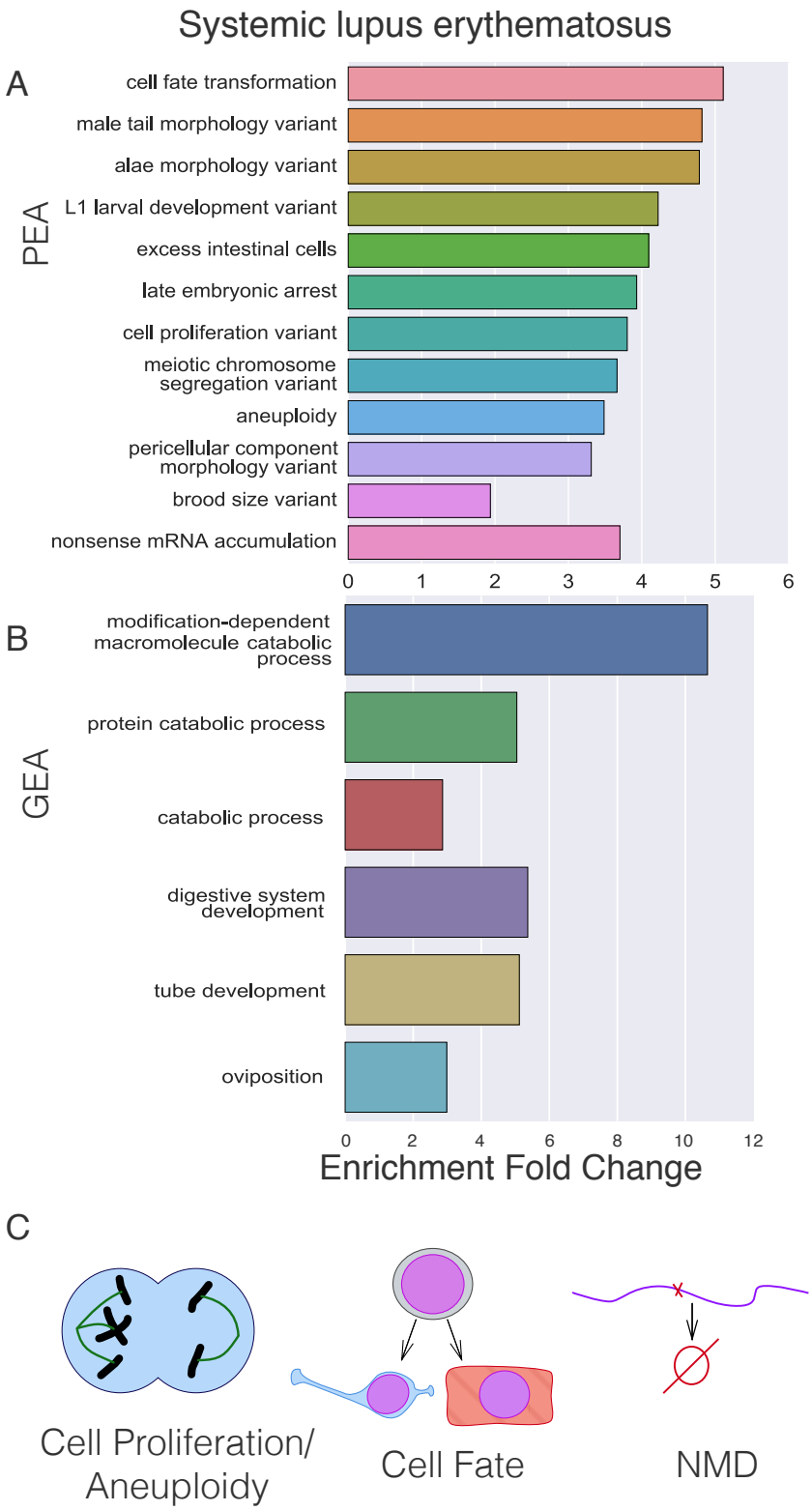

Figure 10.2: Phenologue identification for systemic lupus erythematosus. **A** Phenotype Enrichment Analysis. **B** GO Enrichment Analysis. **C** Lupus in *C. elegans* may be best represented by a combination of three phenotypes: Cell proliferation possibly accompanied by aneuploidy; cell fate transformations that may lead to dysmorphias; and a molecular phenotype involving impairment of the Nonsense-Mediated Decay (NMD) pathway.

gonad arm' are overrepresented in this dataset. We also found that the Pn.p cells P3.p through P8.p were enriched in this dataset (5 genes, $q < 10^{-1}$). GO enrichment pointed at 'modification-dependent macromolecule catabolic process' (23 genes, $q < 10^{-15}$) as a molecular function that characterizes this dataset. However, this GO term was enriched only due to a single gene family, the *skr* gene family. Almost the entire *skr* family was considered a candidate homolog to the SKP1 human gene, making the GO enrichment suspect.

Enrichment of the terms for 'aneuploidy', 'meiotic chromosome segregation', and 'excess intestinal cells' were largely driven by the same gene group, which includes *cki-1*, and several *skr* genes. On the other hand, 'cell fate transformation' and 'male tail morphology' reflected the involvement of developmental genes *let-23*, and *lin-12* among others. The term 'nonsense mRNA accumulation' was the result of *pept-3*, *smg-7*, *tsr-1*, *dhcr-7* and *F08B4.7*. Therefore, we conclude that systemic lupus erythematosus is potentially represented by a combination of three phenotypes in *C. elegans*: A cell proliferation phenotype (either increased or decreased), probably marked by increased aneuploidy; a developmental phenotype involving cell fate transformation and leading to dysmorphias; and a molecular phenotype involving impairment of the nonsense-mediated decay pathway. The results from the tissue enrichment analysis highlighted three tissues that are particularly sensitive to *lin* mutations (the gonad, the excretory duct cell and the vulval precursor cells), and the gonad arms undergo large quantities of nuclear proliferation.

Rheumatoid arthritis

Rheumatoid arthritis is an auto-immune disease that is characterized by swollen and painful joints that progressively deteriorate (Smolen, Aletaha, and McInnes, 2016). Unlike lupus, rheumatoid arthritis is not life-threatening, and comorbidity between rheumatoid arthritis and lupus has not been described in past comorbidity studies (Dougados et al., 2013), suggesting that they may have at least partially distinct genetic causes. We found 309 genes associated with rheumatoid arthritis, for which we found 124 worm homolog candidates.

The only phenotype that was enriched for these orthologs was 'short' (10 genes, $q < 10^{-4}$), even though 64 orthologs were associated with at least one phenotype term. No tissue was enriched in this dataset. Because 82 genes are annotated to have expression in at least one tissue, the lack of enrichment does not reflect ignorance about the sites of expression of these genes. GEA showed that enriched molecular

functions for these genes include ‘collagen trimer’ (22 genes, $q < 10^{-15}$). However, this term was enriched as the result of degeneracy in the homolog candidates for the SFTPD gene. Other terms included ‘glycosylation’ (10 genes, $q < 10^{-4}$) and ‘Golgi apparatus’ (11 genes, $q < 10^{-3}$), but these terms were enriched as the result of degenerate homolog candidates for the human gene B3GNT7 which encodes a beta-1,3-N-acetylgalactosaminyltransferase.

The ‘short’ phenotype was the result of the *cat-4*, *dpy-7*, *rnt-1*, *sem-4*, *unc-116*, *ocrl-1* and some genes in the *fat* family. Although these genes are bound by a common phenotype, any genetic relationships between these genes are not immediately clear. Some genes, like *sem-4* and *rnt-1* are likely transcription factors with roles in development (including hypodermal development) (Desai et al., 1988; Ji et al., 2004). Others are molecular motors (*unc-116*) that are broadly expressed throughout the body of *C. elegans*. Yet others have known roles in neuron and muscle function, such as *ocrl-1* and *cat-4*. The ‘short’ phenotype is a subset of the ‘body length variant’ phenotype. Body length in *C. elegans* can be controlled via cell size or shape(Jianjun Wang, Tokarz, and Savage-Dunn, 2002; Nakano, Nagamatsu, and Ohshima, 2004); alternatively, cuticle development can alter body shape (Cox et al., 1980; Kramer et al., 1988); finally, muscles can alter the effective body length due to their contraction state (Lewis et al., 1980).

Obesity-related traits

Obesity-related traits is a category within the GWAS NHGRI-EBI catalog that pools studies that have measured obesity and other traits associated with obesity, such as heart rate, physical activity, hormone levels, body composition and cholesterol levels. Since this category includes many parameters, we expected there would be many phenologs. GWAS studies have identified 957 genes associated with these traits. Using DIOPT, we found 614 orthologs for these genes. In total, 341/614 genes had at least one phenotype annotation; 548/614 had at least one gene ontology term annotation; and 427/614 had at least one tissue term annotation.

Top results for obesity-related traits included ‘acetylcholinesterase inhibitor response variant’ (38 genes, $q < 10^{-6}$), ‘neurite morphology variant’ (21 genes, $q < 10^{-2}$), and ‘thin’ (31 genes, $q < 10^{-2}$). Terms involving locomotion were significantly enriched, as were terms involving body shape and food consumption ($q < 10^{-1}$). Concomitant with these phenologs was a tissue enrichment in neuron-related terms. GO enrichment suggested that these genes are participating in ‘iron ion binding’ (40

genes, $q < 10^{-20}$) and 'tetrapyrrole binding' (37 genes, $q < 10^{-13}$).

Tissue and phenotype enrichment therefore suggest that obesity-related traits may be studied in *C. elegans* through neuron physiology and function, specifically with respect to acetylcholinesterase inhibitors. Moreover, GO enrichment implicates iron and tetrapyrrole binding as metabolic components of the obesity-related phenologs in *C. elegans*.

Ontology enrichment as an aid for screen design

An additional use for a tool like PEA would be as a tool to help guide and design screens to identify genes from an RNA-seq or other genome-wide experiment for further study. This would be particularly useful in cases when researchers may not know what phenotype to expect, in which case PEA can guide selection of a phenotype. Another use case is a scenario where the phenotype under study is not easy to screen for. By finding phenologs to the phenotype of interest, the researcher can design an easier screen for genes that affect the phenolog in question, then re-test genes for the original phenotype of interest.

Enrichment in the ciliary neuronal transcriptome

As an example of how ontology enrichment can improve our understanding of transcriptomes, we selected a ciliary neuron dataset (Juan Wang et al., 2015) and ran the complete WormBase Enrichment Suite on it. Ciliary neurons are present in the *C. elegans* male tail, but they are also present in the male cephalic sensillum and hermaphrodites also have ciliated neurons. PEA reveals that the ciliated neuron transcriptome is enriched for genes that are typically associated with 'meiotic chromosome segregation' (46 genes, $q < 10^{-5}$), 'aneuploidy' (42 genes, $q < 10^{-5}$) and 'spindle defective early embryos' (45 genes, $q < 10^{-2}$) (see Fig. 10.3).

In addition, TEA points at the *C. elegans* gonad primordium, the somatic gonad and early embryonic cells as the sites where genes associated with ciliary neurons are enriched. The 'male distal tip cell' is a tissue that is overrepresented in this dataset, but 'distal tip cell' is not enriched. In *C. elegans* the hermaphrodite distal tip cells (DTCs) and the male DTC are very similar to each other in their biological functions (both maintain a stem cell niche in the distal gonad). However, the male DTC is non-migratory, whereas the hermaphrodite DTCs are migratory. Therefore, the term 'male distal tip cell' may reflect cellular aspects that are correlated with the non-migratory aspects of the DTC biology, such as maintenance of proliferation.

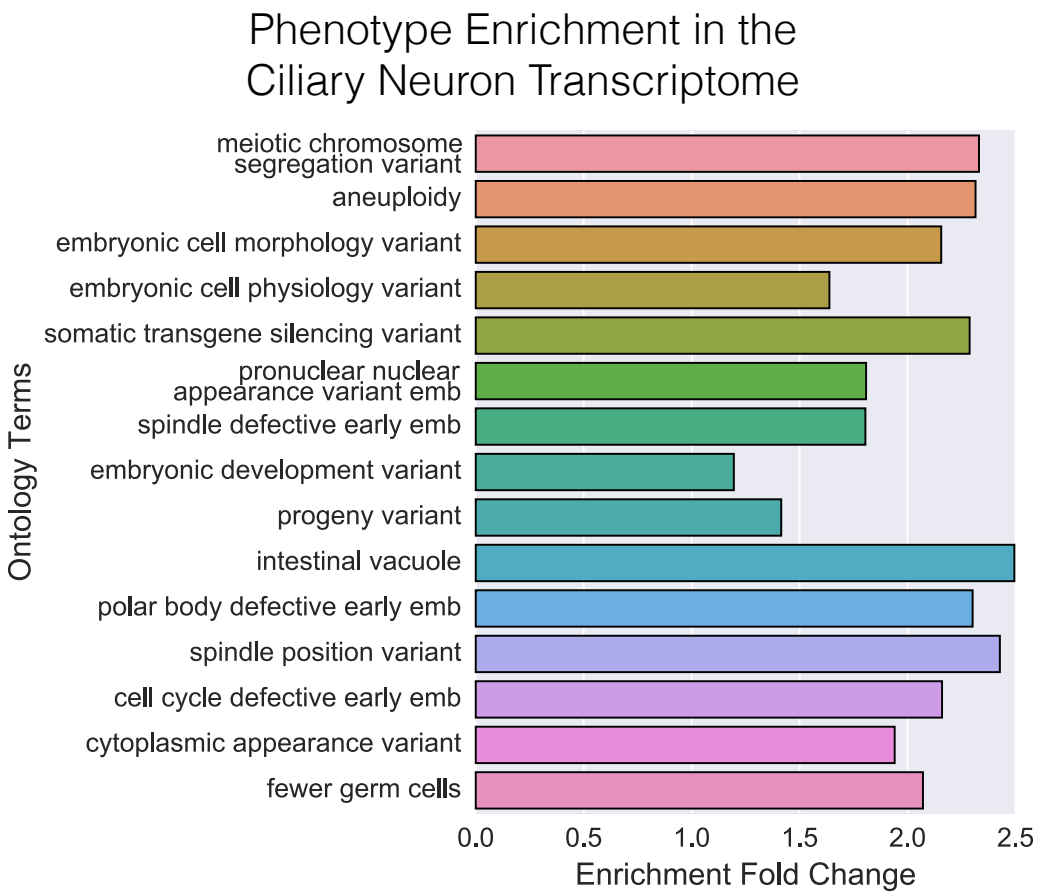

Figure 10.3: PEA shows that the ciliary transcriptome is enriched in phenotypes related to cell division. Although this could reflect enrichment of microtubules and microtubule-related genes, the enrichment is at least partially driven by cell-cycle and DNA repair genes.

Although one interpretation of the results would be that microtubule genes are driving the enrichment of these terms, another possibility is that there are cell-cycle genes that are driving the enrichment of these phenotypes and tissues. Indeed, GO enrichment shows terms such as 'DNA replication' (29 genes, $q < 10^{-5}$), and 'purine NTP-dependent helicase activity' (15 genes, $q < 10^{-1}$). Visual inspection of list in question reveals that cell-cycle and DNA replication/repair genes are abundant in this transcriptome and include genes such as *atm-1*, *dna-2*, or *hpr-17*. This analysis reveals that the ciliary neuron transcriptome is enriched in genes associated with microtubules, but includes genes that are thought to interact with DNA either via repair mechanisms or cell-cycle control (Hofmann, Milstein, and Hengartner, 2000; M. H. Lee et al., 2003; Bailly et al., 2010).

Deconstructing phenotype-tissue relationships

Tissue enrichment on the Egl gene set reveals cellular components of the phenotype

How does a phenotype emerge? We realized that with the tools that we have developed, it is possible to understand what tissues contribute to a phenotype in a probabilistic framework. In other words, we can extract all genes associated with a particular phenotype, then search for tissue terms that are enriched to understand how a phenotype arises from interactions between anatomical regions. As a test of this, we selected the egg-laying defective (Egl) phenotype. In *C. elegans*, egg-laying is a complex behavior that involves a large number of tissues (Li and Chalfie, 1990). The somatic gonad acts as a repository for the eggs, the uterine seam cells help protect the uterus, and a variety of muscles help contract the uterus and open the vulva to lay an egg (Sulston and H. R. Horvitz, 1977). The vulva must be well-formed to allow passage of an egg, and the hermaphrodite-specific neuron (HSN) is involved in the egg-laying control (Schafer, 2005). The complexity of the interactions that happen to allow egg-laying make understanding the Egl phenotype in terms of tissues a challenging task.

We extracted all of the *C. elegans* genes that have been associated with an Egl phenotype and we used TEA to understand what tissues are enriched. The HSN was enriched more than five-fold above background ($q < 10^{-7}$) as were vulD, vulC, vulE and vulF ($q < 10^{-6}$). The vulA, vulB2 and vulB1 were enriched at slightly lower levels ($q < 10^{-5}$), whereas the uterine muscles and uterine seam cells were enriched more than twice above background levels ($q < 10^{-2}$) (see Fig. 10.4). Therefore, the Egl phenotype would seem to emerge primarily from defects in the HSN, secondarily from defects in the vulva, and only sometimes from defects in the uterine seam cells or muscles. It is notable that all vulval cells were not equally enriched. Although all the 'vul' cells are annotated to a similar degree (between 50–70 genes for each cell type), the vulD and vulC cells had the largest enrichment effect size and the lowest q-values, suggesting that these cells are more likely to be associated with an Egl phenotype than the others. This may reflect the fact that vulD and vulE are the site of attachment for four vulval muscles, vm1. Perhaps this attachment is particularly fragile, and perturbations to these cells prevent adequate function of these muscles. In support of these observations, P7.pa had the largest fold-enrichment of any tissue. In *C. elegans*, P7.pa gives rise to vulD and vulC. However, vulF is also attached to a set of four additional vulval muscles, vm2. Why is vulF less associated with an

Egl phenotype?

Quantifying the anatomy-phenotype mapping via Bayesian probabilities

Another way to understand the phenotype-anatomy mapping is by considering how informative a given anatomy term is on a particular phenotype, or vice-versa. To this end, we calculated two conditional probabilities that helped us answer this question. The first conditional probability,

$$P(\text{a gene has Egl annotation}|\text{it is expressed in } X) \tag{10.1}$$

answers the question: For a gene with an expression pattern that includes the tissue term X (i.e., the gene is expressed at least in X), what is the probability that this gene has an Egl phenotype (i.e., the phenotype annotations for this gene include Egl)? For simplicity, we can re-write this equation more succintly by removing a few words. The calculation of this probability is straightforward and follows from the definition of conditional probability:

$$P(\text{Egl}|X) = \frac{N_{\text{genes annotated Egl and X}}}{N_{\text{genes annotated with X}}}. \tag{10.2}$$

Equation 10.2 measures how likely a gene is to be annotated with an Egl phenotype given that its expression pattern includes the term X. A related quantity (which is neither the inverse nor the complement) is the conditional probability that a gene which is annotated with at least the Egl phenotype is expressed in tissue X. That is to say,

$$P(X|\text{Egl}) = \frac{N_{\text{genes annotated Egl and X}}}{N_{\text{genes annotated with Egl}}}. \tag{10.3}$$

Equation 10.3 tells us how probable it is that any given gene that is annotated with an Egl phenotype includes X as a tissue term. Taken together, equations 10.2 and 10.3 help us understand how predictive anatomic expression is of phenotypes, and how predictive phenotypes are of anatomic expression.

We calculated the conditional probability that a gene has an Egl phenotype given that it's expression pattern includes a tissue term X and we searched for the tissue terms that maximized this probability. The list of terms that maximized this probability reflected the results from running TEA on the subset of genes that have an Egl

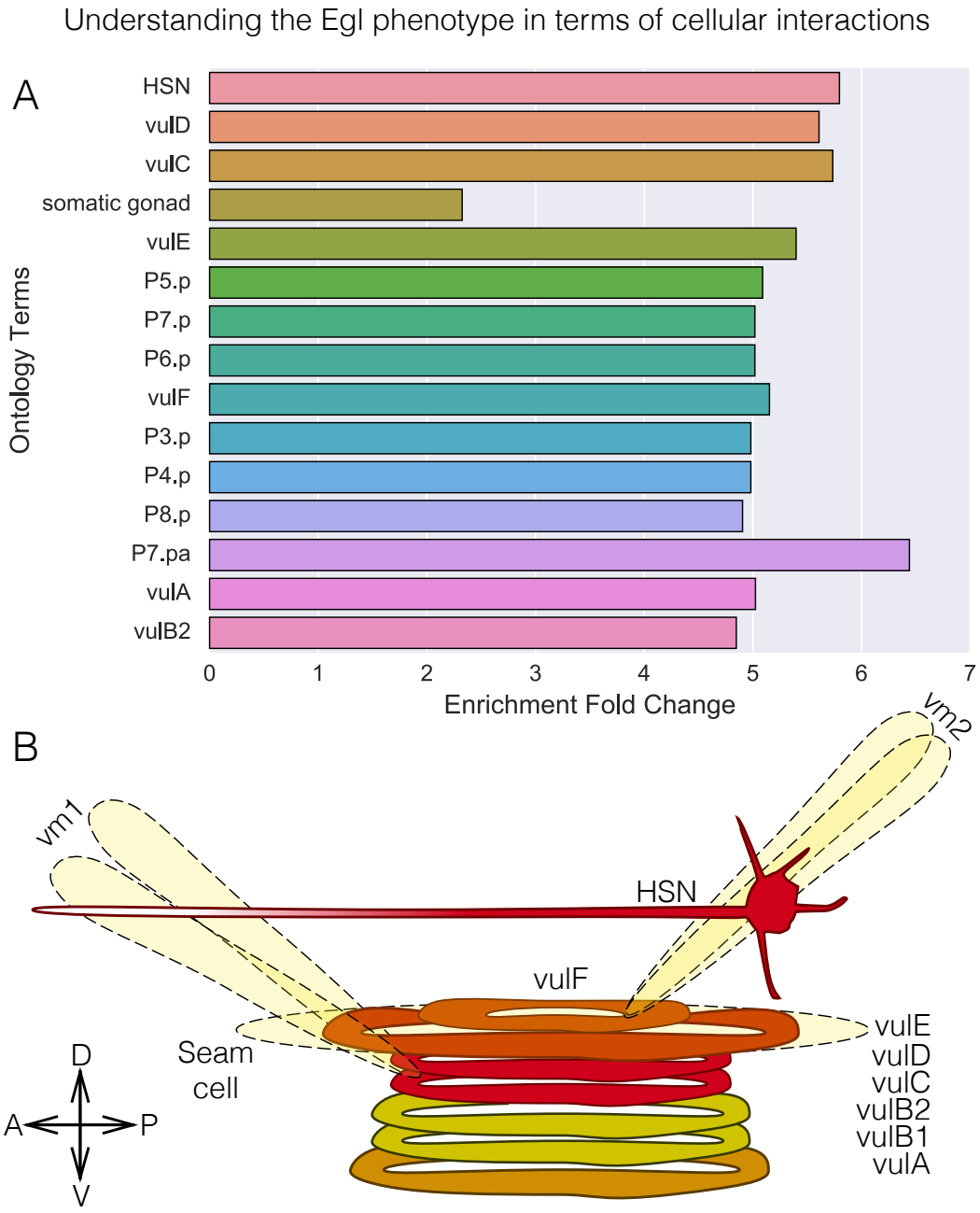

Figure 10.4: The Egl phenotype is a complex phenotype that is the result of interactions between many tissues. To dissect the contributions of individual tissues to generating an Egl phenotype, we obtained all genes annotated with with an Egl term. **A** We used TEA on the set of Egl genes to identify enriched tissues. **B** Anatomic diagram showing the tissues that are most enriched in the Egl gene set. Color coding shows the qualitative ordering of enrichment (red-Most enriched, yellow-least enriched). For clarity, not all cells are shown. All vm1 (4 cells) and vm2 (4 cells) muscles are symmetrical arranged around the vulva, but only 2 cells are shown for each. There are two seam cells on the left and right side of the vulva, but only cell on the right is shown. Only terminally differentiated cells are shown.

Table 10.1: Conditional probabilities for various tissues. The first column shows the conditional probability that a gene has an Egl phenotype given that it has expression in tissue X (given by the row). The second column shows the conditional probability that a gene has expression in the anatomy term X given that it has an Egl phenotype. The first 9 terms are the terms for which $P(\text{Egl}|X)$ is maximized. The last three terms are the terms which have the highest $P(X|\text{Egl})$. For clarity, the Pn.p cells are not shown even though $P(\text{Egl}|\text{Pn.p}) \sim 0.24$.

Tissue	$P(\text{Egl}\|X)$	$P(X\|\text{Egl})$
P7.pa	0.30	0.04
HSN	0.27	0.11
vulC	0.27	0.06
vulD	0.26	0.07
vulE	0.25	0.06
vulF	0.24	0.06
vulA	0.24	0.05
vulB2	0.23	0.05
vulB1	0.22	0.05
nervous system	0.02	0.72
pharynx	0.00	0.46
sex organ	0.07	0.41
tail	0.05	0.33

phenotype. We also calculated the conditional probability that a gene has expression in a tissue term X given that it is annotated with an Egl phenotype and we searched for terms that maximized this probability (see Table 10.1). The terms that maximized this probability were 'nervous system', 'pharynx' (a body part with a lot of neurons), 'sex organ' and 'tail' (a body part with neurons and hypodermis). In general, the terms that had a high $P(\text{Egl}|X)$ did not have a high $P(X|\text{Egl})$. Additionally, the terms that had a high $P(X|\text{Egl})$ are broad terms that include a lot of cells, whereas the terms that had a high $P(\text{Egl}|X)$ were considerably more specific. We conclude that the Egl phenotype arises from a small set of tissues. The Egl phenotype can be best predicted by genes with expression patterns that include at least one of a small number of cells (mainly vul cells, HSN). On the other hand, answering whether the

expression pattern of a gene includes a particular anatomic region or tissue given that the gene has an Egl phenotype is hard to do for small tissues or single cells. However, guesses about what functional system or broad anatomic region an Egl gene is expressed in can be answered with confidence ($\sim$ 70% of the time, an Egl mutant is expressed in the nervous system).

Conclusions

The addition of GO and Phenotype Ontology enrichment testing to WormBase marks an important step towards a unified set of analyses that can help researchers to understand genomic datasets. These enrichment analyses will allow the community to fully benefit from the data curation ongoing at WormBase. By using the same algorithms to generate enrichment dictionaries for testing and using the same model to test for term enrichment, these tools provide a coherent framework with which to analyze genomic data. In particular, it is our hope that phenotype enrichment will be of use to geneticists performing genome-wide analyses, because they are familiar with the ontological terms that are tested and with their biological meaning. Ideally, PEA could allow researchers to design better screens to maximize target gene identification by quantifying the phenotypes that are most overrepresented. An intriguing new direction of research would be to create a controlled language for screening methods. With such a language, we should be able to computationally suggest to a researcher what screens one may wish to perform given a dataset.

References

Angeles-Albores, David et al. (2016). "Tissue enrichment analysis for *C. elegans* genomics". In: *BMC Bioinformatics* 17.1, p. 366. ISSN: 1471-2105. DOI: 10.1186/s12859-016-1229-9.

Ashburner, M et al. (2000). "Gene Ontology: tool for the unification of biology". In: *Nature Genetics* 25.1, pp. 25–29. ISSN: 1061-4036. DOI: 10.1038/75556.

Bailly, Aymeric P. et al. (2010). "The *Caenorhabditis elegans* homolog of Gen1/Yen1 resolvases links DNA damage signaling to DNA double-strand break repair". In: *PLoS Genetics* 6.7, pp. 1–16. ISSN: 15537390. DOI: 10.1371/journal.pgen.1001025.

Chikina, Maria D. et al. (2009). "Global prediction of tissue-specific gene expression and context-dependent gene networks in Caenorhabditis elegans". In: *PLoS Computational Biology* 5.6. ISSN: 1553734X. DOI: 10.1371/journal.pcbi.1000417.

Chisholm, Andrew D. and H. Robert Horvitz (1995). "Patterning of the Caenorhabditis elegans head region by the Pax-6 family member vab-3". In: *Nature* 377.6544, pp. 52–55. ISSN: 0028-0836. DOI: 10.1038/377052a0. URL: http://www.nature.com/doifinder/10.1038/377052a0.

Cinar, Hulusi, Sunduz Keles, and Yishi Jin (2005). "Expression profiling of GABAergic motor neurons in Caenorhabditis elegans". In: *Current Biology* 15.4, pp. 340–346. ISSN: 09609822. DOI: 10.1016/j.cub.2005.02.025.

Cox, George N. et al. (1980). "GENETIC AND PHENOTYPIC CHARACTERIZATION OF ROLLER MUTANTS OF CAENORHABDITIS ELEGANS". In: *Genetics* 95.2.

Desai, C et al. (1988). "A genetic pathway for the development of the *Caenorhabditis elegans* HSN motor neurons." In: *Nature* 336.6200, pp. 638–646. ISSN: 0028-0836. DOI: 10.1038/336638a0.

Dougados, M. et al. (2013). "Prevalence of comorbidities in rheumatoid arthritis and evaluation of their monitoring: results of an international, cross-sectional study (COMORA)". In: *Annals of the Rheumatic Diseases* 73.1, pp. 62–68. ISSN: 0003-4967. DOI: 10.1136/annrheumdis-2013-204223. URL: http://www.pubmedcentral.nih.gov/articlerender.fcgi?artid=3888623%7B%5C&%7Dtool=pmcentrez%7B%5C&%7Drendertype=abstract.

Fox, Rebecca M et al. (2007). "The embryonic muscle transcriptome of Caenorhabditis elegans". In: *Genome Biol* 8.9, R188. ISSN: 14656906. DOI: 10.1186/gb-2007-8-9-r188. URL: http://www.ncbi.nlm.nih.gov/pubmed/17848203.

Gaudet, Jeb et al. (2004). "Whole-genome analysis of temporal gene expression during foregut development". In: *PLoS Biology* 2.11. ISSN: 15449173. DOI: 10.1371/journal.pbio.0020352.

Hofmann, E. R., S. Milstein, and M. O. Hengartner (2000). "DNA-damage-induced checkpoint pathways in the nematode Caenorhabditis elegans". In: *Cold Spring Harbor Symposia on Quantitative Biology* 65.Schedl 1997, pp. 467–473. ISSN: 00917451.

Howe, Kevin L et al. (2016). "WormBase 2016: expanding to enable helminth genomic research." In: *Nucleic acids research* 44.November 2015, pp. D774–D780. ISSN: 1362-4962. DOI: 10.1093/nar/gkv1217. URL: http://www.ncbi.nlm.nih.gov/pubmed/26578572.

Hu, Yanhui et al. (2011). "An integrative approach to ortholog prediction for disease-focused and other functional studies." In: *BMC bioinformatics* 12, p. 357. ISSN: 1471-2105. DOI: 10.1186/1471-2105-12-357. URL: http://www.pubmedcentral.nih.gov/articlerender.fcgi?artid=3179972%7B%5C&%7Dtool=pmcentrez%7B%5C&%7Drendertype=abstract.

Hunter, John D. (2007). "Matplotlib: A 2D graphics environment". In: *Computing in Science and Engineering* 9.3, pp. 99–104. ISSN: 15219615. DOI: 10.1109/MCSE.2007.55.

Ji, Yon Ju et al. (2004). "RNT-1, the C. elegans homologue of mammalian RUNX transcription factors, regulates body size and male tail development". In: *Developmental Biology* 274.2, pp. 402–412. ISSN: 00121606. DOI: 10.1016/j.ydbio.2004.07.029.

Johnson, David S, Ali Mortazavi, and Richard M Myers (2007). "Protein-DNA Interactions". In: June, pp. 1497–1503.

Kim, Yongsoon and Hong Sun (2007). "Functional genomic approach to identify novel genes involved in the regulation of oxidative stress resistance and animal lifespan". In: *Aging Cell* 6.4, pp. 489–503. ISSN: 14749718. DOI: 10.1111/j.1474-9726.2007.00302.x. URL: http://doi.wiley.com/10.1111/j.1474-9726.2007.00302.x.

Kramer, James M. et al. (1988). "The sqt-1 gene of C. elegans encodes a collagen critical for organismal morphogenesis". In: *Cell* 55.4, pp. 555–565. ISSN: 00928674. DOI: 10.1016/0092-8674(88)90214-0. URL: http://linkinghub.elsevier.com/retrieve/pii/0092867488902140.

Lee, Myon Hee et al. (2003). "Caenorhabditis elegans dna-2 is involved in DNA repair and is essential for germ-line development". In: *FEBS Letters* 555.2, pp. 250–256. ISSN: 00145793. DOI: 10.1016/S0014-5793(03)01243-2.

Lee, R. Y N and Paul W. Sternberg (2003). *Building a cell and anatomy ontology of Caenorhabditis elegans*. DOI: 10.1002/cfg.248.

Lehner, Ben (2013). "Genotype to phenotype: lessons from model organisms for human genetics." In: *Nature reviews. Genetics* 14.3, pp. 168–78. ISSN: 1471-0064. DOI: 10.1038/nrg3404. URL: http://www.ncbi.nlm.nih.gov/pubmed/23358379.

Lewis, James A. et al. (1980). "THE GENETICS OF LEVAMISOLE RESISTANCE IN THE NEMATODE CAENORHABDITIS ELEGANS". In: *Genetics* 95.4.

Li, C and M Chalfie (1990). "Organogenesis in C. elegans: positioning of neurons and muscles in the egg-laying system." In: *Neuron* 4.5, pp. 681–695. ISSN: 08966273. DOI: 10.1016/0896-6273(90)90195-L. URL: http://eutils.ncbi.nlm.nih.gov/entrez/eutils/elink.fcgi?dbfrom=pubmed%7B%5C&%7Did=2344407%7B%5C&%7Dretmode=ref%7B%5C&%7Dcmd=prlinks%7B%5C%%7D5Cnpapers2://publication/uuid/DF7BB343-CD9E-400A-8EE9-E9B02B19F1B6.

Lisnevskaia, Larissa, Grainne Murphy, and David Isenberg (2014). "Systemic lupus erythematosus". In: *The Lancet* 384.9957, pp. 1878–1888. ISSN: 1474547X. DOI: 10.1016/S0140-6736(14)60128-8. URL: http://dx.doi.org/10.1016/S0140-6736(14)60128-8.

MacArthur, Jacqueline et al. (2016). "The new NHGRI-EBI Catalog of published genome-wide association studies (GWAS Catalog)." In: *Nucleic acids research* 45.November 2016, gkw1133. ISSN: 1362-4962 (Electronic). DOI: 10.1093/nar/gkw1133. URL: http://www.ncbi.nlm.nih.gov/pubmed/27899670.

McGary, Kriston L et al. (2010). "Systematic discovery of nonobvious human disease models through orthologous phenotypes." In: *Proceedings of the National Academy of Sciences of the United States of America* 107.14, pp. 6544–6549. ISSN: 0027-8424. DOI: 10.1073/pnas.0910200107. arXiv: arXiv:1408.1149.

McKinney, Wes (2011). "pandas: a Foundational Python Library for Data Analysis and Statistics". In: *Python for High Performance and Scientific Computing*, pp. 1–9.

Mehta, Ranjana et al. (2009). "Hypoxic Response Modulates Aging in *C. elegans*". In: *Science* 324.May, pp. 1196–1198.

Mi, Huaiyu, Anushya Muruganujan, and Paul D. Thomas (2013). "PANTHER in 2013: Modeling the evolution of gene function, and other gene attributes, in the context of phylogenetic trees". In: *Nucleic Acids Research* 41.D1. ISSN: 03051048. DOI: 10.1093/nar/gks1118.

Mohan, Chandra and Chaim Putterman (2015). "Genetics and pathogenesis of systemic lupus erythematosus and lupus nephritis". In: *Nature Reviews Nephrology* 11.6, pp. 329–341. ISSN: 1759-5061. DOI: 10.1038/nrneph.2015.33. URL: http://www.nature.com/doifinder/10.1038/nrneph.2015.33.

Mortazavi, Ali et al. (2008). "Mapping and quantifying mammalian transcriptomes by RNA-Seq". In: *Nature Methods* 5.7, pp. 621–628. ISSN: 1548-7091. DOI: 10.1038/nmeth.1226.

Nakano, Yoshiya, Yasuko Nagamatsu, and Yasumi Ohshima (2004). "cGMP and a germ-line signal control body size in C. elegans through cGMP-dependent protein kinase EGL-4". In: *Genes to Cells* 9.9, pp. 773–779. ISSN: 1356-9597. DOI: 10.1111/j.1365-2443.2004.00771.x. URL: http://doi.wiley.com/10.1111/j.1365-2443.2004.00771.x.

Oliphant, Travis E (2007). "SciPy: Open source scientific tools for Python". In: *Computing in Science and Engineering* 9, pp. 10–20. ISSN: 1521-9615. DOI: 10.1109/MCSE.2007.58.

Pauli, Florencia et al. (2006). "Chromosomal clustering and GATA transcriptional regulation of intestine-expressed genes in C. elegans." In: *Development (Cambridge, England)* 133.2, pp. 287–295. ISSN: 0950-1991. DOI: 10.1242/dev.02185.

Portman, Douglas S. and Scott W. Emmons (2004). "Identification of C. elegans sensory ray genes using whole-genome expression profiling". In: *Developmental Biology* 270.2, pp. 499–512. ISSN: 00121606. DOI: 10.1016/j.ydbio.2004.02.020.

Quiring, R et al. (1994). “Homology of the eyeless gene of Drosophila to the Small eye gene in mice and Aniridia in humans”. In: *Science* 265.5173.

Rhee, Seung Yon et al. (2008). “Use and misuse of the gene ontology annotations.” In: *Nature reviews. Genetics* 9.7, pp. 509–15. ISSN: 1471-0064. DOI: 10.1038/nrg2363. arXiv: NIHMS150003. URL: http://www.ncbi.nlm.nih.gov/pubmed/18475267.

Rossum, Guido Van et al. (2011). “Python (programming language)”. In: *Flying*, pp. 1–14.

Schafer, William R (2005). *Egg-laying*. WormBook.

Schindelman, Gary et al. (2011). “Worm Phenotype Ontology: integrating phenotype data within and beyond the C. elegans community.” In: *BMC bioinformatics* 12, p. 32. ISSN: 1471-2105. DOI: 10.1186/1471-2105-12-32. URL: http://www.pubmedcentral.nih.gov/articlerender.fcgi?artid=3039574%7B%5C&%7Dtool=pmcentrez%7B%5C&%7Drendertype=abstract.

Smith, Cody J. et al. (2010). “Time-lapse imaging and cell-specific expression profiling reveal dynamic branching and molecular determinants of a multi-dendritic nociceptor in C. elegans”. In: *Developmental Biology* 345.1, pp. 18–33. ISSN: 00121606. DOI: 10.1016/j.ydbio.2010.05.502.

Smolen, Josef S., Daniel Aletaha, and Iain B. McInnes (2016). “Rheumatoid arthritis”. In: *The Lancet* 388.10055, pp. 2023–2038. ISSN: 1474547X. DOI: 10.1016/S0140-6736(16)30173-8. URL: http://dx.doi.org/10.1016/S0140-6736(16)30173-8.

Spencer, W. Clay et al. (2011). “A spatial and temporal map of C. elegans gene expression”. In: *Genome Research* 21.2, pp. 325–341. ISSN: 10889051. DOI: 10.1101/gr.114595.110.

Sternberg, P W and M Han (1998). “Genetics of RAS signaling in *C. elegans*”. In: *Trends in Genetics* 14.11, pp. 466–472. DOI: 10.1016/s0168-9525(98)01592-3.

Sulston, J. E. and H. R. Horvitz (1977). “Post-embryonic cell lineages of the nematode, Caenorhabditis elegans”. In: *Developmental Biology* 56.1, pp. 110–156. ISSN: 00121606. DOI: 10.1016/0012-1606(77)90158-0. URL: http://www.sciencedirect.com/science/article/pii/0012160677901580.

Wang, Jianjun, Rafal Tokarz, and Cathy Savage-Dunn (2002). “The expression of TGFβ signal transducers in the hypodermis regulates body size in C. elegans”. In: *Development* 129.21.

Wang, Juan et al. (2015). “Cell-Specific Transcriptional Profiling of Ciliated Sensory Neurons Reveals Regulators of Behavior and Extracellular Vesicle Biogenesis”. In: *Current Biology* 25.24, pp. 3232–3238. ISSN: 09609822. DOI: 10.1016/j.cub.2015.10.057. URL: http://dx.doi.org/10.1016/j.cub.2015.10.057.

Waskom, Michael et al. (2016). "seaborn: v0.7.0 (January 2016)". In: DOI: 10.5281/zenodo.45133.

Watson, Joseph D et al. (2008). "Complementary RNA amplification methods enhance microarray identification of transcripts expressed in the C. elegans nervous system". In: *BMC Genomics* 9, p. 84. ISSN: 1471-2164. DOI: 10.1186/1471-2164-9-84. URL: http://www.ncbi.nlm.nih.gov/pubmed/18284693.

Zhang, Yinhua and Scott W. Emmons (1995). "Specification of sense-organ identity by a Caenorhabditis elegans Pax-6 homologue". In: *Nature* 377.6544, pp. 55–59. ISSN: 0028-0836. DOI: 10.1038/377055a0. URL: http://www.nature.com/doifinder/10.1038/377055a0.

Chapter 11

AN AUTOMATED FRAMEWORK FOR TRANSCRIPTIONAL PROFILING

Appendix A

QUESTIONNAIRE

Appendix B

CONSENT FORM

[1]Endnotes are notes that you can use to explain text in a document.